Grant Agreement:	**247223**
Project Title:	**A**dvanced **R**adio In**T**erface Technolog**I**es for 4G **S**ys**T**ems ARTIST4G
Document Type:	PU (Public)

Document Identifier:	**D1.2**
Document Title:	**Innovative advanced signal processing algorithms for interference avoidance**
Source Activity:	WP1
Editors:	Valeria D'Amico and Hardy Halbauer
Authors:	Daniel Aronsson, Carmen Botella, Stefan Brueck, Cristina Ciochina, Valeria D'Amico, Thomas Eriksson, Richard Fritzsche, David Gesbert, Jochen Giese, Nicolas Gresset, Hardy Halbauer, Tilak Rajesh Lakshmana, Behrooz Makki, Bruno Melis, Rikke Abildgaard Olesen, María Luz Pablo, Dinh Thuy Phan Huy, Stephan Saur, Mikael Sternad, Tommy Svensson, Randa Zakhour, Wolfgang Zirwas
Status / Version:	Final / Version 1.0
Date Last changes:	31.12.10
File Name:	D1.2.doc

Abstract:	This document provides an overview of the proposed innovations and activities in Task 1.1 of Work Package 1 (WP1) of the ARTIST4G project, related to interference avoidance. Focus is on the technical approaches applicable at the physical layer, which are grouped into four different classes of innovations related to single-cell multi-user MIMO schemes, multi-cell multi-user MIMO schemes, advanced 3D beamforming and enabling functionalities. Descriptions of the proposed innovations are given including basic ideas, potential of performance, simulation results, realization options and possible implementation restrictions.

Keywords:	Interference avoidance, Multi User MIMO, Coordinated Multi Point, Coordinated Beamforming, Joint Processing, Channel Estimation, Channel Prediction, Feedback, Robust design, ARTIST4G

Document History:	
31.12.2010	Version 1.0 of document released.

Table of Contents

Authors

Name	Beneficiary	E-mail address
Daniel Aronsson	Uppsala University	Daniel.Aronsson@signal.uu.se
Carmen Botella	Chalmers University of Technology	carmenb@chalmers.se
Stefan Brueck	Qualcomm	sbrueck@qualcomm.com
Cristina Ciochina	Mitsubishi Electric R&D Centre Europe	c.ciochina@fr.merce.mee.com
Valeria D'Amico	Telecom Italia	valeria1.damico@telecomitalia.it
Thomas Eriksson	Chalmers University of Technology	thomase@chalmers.se
Richard Fritzsche	TU Dresden	Richard.fritzsche@ifn.et.tu-dresden.de
David Gesbert	EURECOM	gesbert@eurecom.fr
Jochen Giese	Qualcomm	jgiese@qualcomm.com
Nicolas Gresset	Mitsubishi Electric R&D Centre Europe	n.gresset@fr.merce.mee.com
Hardy Halbauer	Alcatel-Lucent	Hardy.Halbauer@alcatel-lucent.com
Tilak Rajesh Lakshmana	Chalmers University of Technology	tilak@chalmers.se
Behrooz Makki	Chalmers University of Technology	behrooz.makki@chalmers.se
Bruno Melis	Telecom Italia	bruno1.melis@telecomitalia.it
Rikke Abildgaard Olesen	Uppsala University	Rikke.Abildgaard@signal.uu.se
María Luz Pablo	Telefónica I+D	mlpg@tid.es
Dinh Thuy Phan Huy	France Telecom	dinhthuy.phanhuy@orange-ftgroup.com
Stephan Saur	Alcatel-Lucent	Stephan.Saur@alcatel-lucent.com
Mikael Sternad	Uppsala University	Mikael.Sternad@signal.uu.se
Tommy Svensson	Chalmers University of Technology	tommy.svensson@chalmers.se
Randa Zakhour	EURECOM	zakhour@eurecom.fr
Wolfgang Zirwas	Nokia Siemens Networks	wolfgang.zirwas@nsn.com

1 - Executive Summary

This document provides an overview of the proposed innovations and activities in Task 1.1 of Work Package 1 (WP1) of the ARTIST4G project, related to interference avoidance schemes applied at Layer 1. The motivation for interference avoidance is based on the fact that the performance of cellular mobile communication systems is limited by the interference caused by neighbouring cells or due to reuse of radio resources within the same cell. Reduction or avoidance of interference is therefore a promising strategy to improve performance.

After a short introduction of the targets of Task 1.1 in section 2, some generic Layer 1 aspects with respect to different interference avoidance schemes and scenarios are discussed and key performance indicators are highlighted in section 3.

The main activities of this task are then described in section 4, structured into four main classes of innovation:

- **Single-cell MU-MIMO schemes**

Improved pairing methods and feedback mechanisms for optimized single cell Multi User Multiple-Input Multiple-Output schemes are investigated. Innovations achieving interference reduction through specific design and optimization of transmit and receive filtering and precoding are considered. Also specific approaches for indoor and femto scenarios, like the “Time Reversal” method, and uplink schemes relying on Single Carrier Space-Frequency Block Codes are addressed.

- **Multi-cell MU-MIMO schemes**

Different innovative methods of coordinated beamforming, joint processing, precoding and data sharing are analyzed in a multi-cell scenario. The majority of these techniques are based on joint processing, where the data is transmitted to the user simultaneously from multiple sites. For joint processing centralized and distributed approaches are proposed to enable dynamic joint processing modes to optimally serve the users. Among the precoding and data sharing topics the potential and impact of centralized versus distributed control is investigated. Strategies for design of increased robustness of precoding, zero-forcing cooperative transmission and multi-cell layer 1 interference control schemes are presented.

- **Advanced 3D Beamforming**

Beamforming and beam coordination already have shown their potential to reduce the interference impact in neighbouring cells. The performance can be improved if, in addition, also beamsteering in vertical direction is applied. This will further reduce interference in adjacent cells when serving users close to the base stations with a larger downtilt, providing an additional degree of freedom for beam coordination. Different realization options, impact on system design, and the potential of performance improvement are analyzed.

- **Enablers: channel estimation & feedback design**

Enabling functionalities related to channel estimation and feedback design are analyzed. The considered topics are advanced channel estimation and prediction methods for Multiple-Input Multiple-Output channels together with advanced feedback design approaches, such as hierarchical feedback for multi-cell cooperation or different feedback compression schemes. Some of these schemes are related to the generic innovations described in the other classes of innovation.

Finally, in section 5 some general conclusions on the assessment of the WP1 major sets of innovations and an outlook on the focus of the upcoming work within the project are given. Particularly the relationships of these innovations with the ARTIST4G trial activities are addressed.

2 - Introduction

The main objective of the ARTIST4G Work Package 1 (WP1) is to build forward on the 3GPP Long Term Evolution (LTE) Release 8 and upcoming releases, proposing a novel fair mobile broadband technological framework in which to design innovative, practical, scalable and cost-effective interference avoidance solutions. Such an approach will enable the identification of optimal strategies also taking into account the practical implications on the real system.

In particular, as specified in the ARTIST4G Description of Work, the specific aim of Task 1.1 of WP1 is:

- to propose and to define innovative signal processing algorithms to be applied at the transmitter end of a communication system, in which a certain level of coordination/cooperation is introduced among different points for downlink (DL) transmission and/or for uplink (UL) transmission, in order to achieve interference avoidance;
- to take advantage, in the definition of these techniques, of all the degrees of freedom offered by optimized multiple antenna processing.

Therefore, in this Task 1.1 physical layer techniques for interference avoidance are investigated, which will allow performance improvements at cell edge as well as increase in the mean cell throughput.

This deliverable D1.2 presents the technical approaches applicable at the physical layer, which are under investigation within the scope of Task 1.1 of WP1. In an earlier ARTIST4G deliverable D1.1 [ARTD11] these innovations have been analyzed with respect to their requirements and expected impacts on the Radio Access Network (RAN) architecture. In this document a more detailed technical description of these innovations is provided, including basic ideas, potential improvements of performance, simulation results, realization options and possible implementation restrictions.

Deliverable D1.2 is complemented by deliverable D1.3 [ARTD13], which covers advanced scheduling and cross-layer solutions for interference avoidance, to support and enhance the physical layer techniques so as to make optimum use of the interference avoidance potential.

The D1.2 document is organized as follows. In section 3 the basic physical layer aspects relevant for interference avoidance are shortly explored. First, the main features of Coordinated MultiPoint (CoMP) transmission schemes, comprising Coordinated Scheduling / Coordinated Beamforming (CS/CB) and Joint Processing (JP) schemes, are analyzed. The specific properties of centralized and decentralized approaches are taken into account. A more detailed definition of the terms “centralized”, “decentralized” and “distributed” as considered within ARTIST4G is given in section 3.2. The benefits and drawbacks of both are highlighted. Then the generic aspects of the uplink and downlink direction of the transmission systems are described, indicating the applicability and feasibility of different interference control principles. The impact of the used duplexing mode, time division or frequency division duplex, on channel state information acquisition and on system operation is discussed. Finally, reference to the relevant Key Performance Indicators (KPI) and system performance metrics is given.

The technical topics analyzed in Task 1.1 can be sorted mainly into four classes of innovations, which are addressed separately in section 4. The grouping of the schemes is chosen in the order of increasing complexity, starting with the single cell scenario and extending towards multicell scenarios. Then advanced beamforming is considered, which can be applied in both of the previous scenarios. Finally, the last class of innovations covers enabling functionalities, which are needed to enhance the considered schemes. Among the investigated schemes the focus is more on downlink rather than on uplink. This is due to the WP1 focus on interference avoidance. In downlink the interference diversity, i.e. the number of different interference sources and the variation of their activity over time and frequency, is less than in uplink, so that higher gains with coordination schemes are expected. In addition, the possibility to use larger antenna arrays at the base station than on User Equipment (UE) side further increases the potential of interference avoidance schemes in downlink.

The first class of innovations covers the **single-cell MU-MIMO schemes**. Here enhancements of the 3GPP Single User Multiple-Input Multiple-Output (SU-MIMO) schemes with improved pairing methods and feedback mechanisms for enabling optimized Multi User Multiple-Input Multiple-Output (MU-MIMO) operation are investigated. Other innovations deal with optimization of transmit and receive filter design. Prefiltering for the time reversal method to be applied in all-femto scenarios and an enhanced uplink method relying on Single Carrier Space-Frequency Block Code (SC-SFBC) are also addressed.

The second class of innovations is focussed on **Multi-cell MU-MIMO schemes**. Within this class, different innovative methods of coordinated beamforming, joint processing, precoding and data sharing are investigated. For joint processing centralized and distributed approaches are proposed. Among the precoding and data sharing topics, advanced distributed precoding and partial data sharing schemes, methods for increased robustness of precoding, zero-forcing cooperative transmission and multicell layer 1 interference control schemes are presented.

In a third class of innovations the focus is on **advanced 3D beamforming**, where the vertical dimension of beamforming, in addition to horizontal beamforming, is exploited. Realization options, impact on system design, and the potential of performance improvement are discussed.

The fourth class of innovations finally comprises various **enabling functions related to channel estimation and feedback design**. The considered topics are advanced channel estimation and prediction methods for Multiple Input Multiple Output (MIMO) channels. Also advanced feedback design approaches like hierarchical feedback for multicell cooperation or different feedback compression schemes are addressed. Some of these schemes are related to the generic innovations described in the other classes of innovation.

In section 5 a general assessment of the innovations is given and relationships to planned trials [ARTD61] are indicated. Next steps of the work on these innovations within ARTIST4G are pointed out.

3 - Generic aspects of interference avoidance schemes

A common approach to achieve the high spectral efficiency targets of future mobile communication networks is the reuse of the total available transmission resources in every cell of the system (frequency reuse factor one). While increasing the spectrum availability, this premise leads to eminently increasing inter-cell interference, especially for users close to the cell edge. The deployment of denser systems to serve a higher number of users also increases the amount of inter-cell interference.

CoMP transmission or reception is a promising concept to employ dense frequency reuse and suppress inter-cell interference at the same time [3GPP36814]. This is enabled by the exchange of information about channel quality - Channel Quality Indicator (CQI) - or Channel State Information (CSI) among multiple coordinated enhanced Node Bs (eNBs). Considering downlink transmission, further improvements can be achieved by also sharing user data among the involved eNBs. Depending on the type of exchanged information, different cooperation schemes are applicable. Sharing only control data like CQI or CSI, eNBs are able to adjust their scheduling decisions or beamforming weights in a coordinated manner, to reduce interference to users in adjacent cells, applying CS/CB. Furthermore, if eNBs share user data, JP can be applied, where coordinated eNBs form a virtual MIMO system together with the users that are assigned to the same transmission resources.

This section provides an overview description of the generic Layer 1 (L1) aspects of the specific signal processing algorithms introduced in section 4 for interference avoidance.

Section 3.1 describes some of the main L1 aspects of CoMP schemes (CS/CB and JP). Section 3.2 introduces the concepts of centralized, decentralized and distributed CoMP interference avoidance schemes in the framework of ARTIST4G. In sections 3.3 and 3.4, the impact of duplexing modes and downlink and uplink specific aspects over the schemes presented in section 4 is summarized, respectively. Finally, key performance indicators for the assessment of the performance, together with system performance metrics, are outlined in section 3.5.

3.1 - Coordinated MultiPoint Schemes

Coordinated Scheduling/ Coordinated Beamforming (CS/CB)

The basic intention of CS/CB is the avoidance of interference by an appropriate choice of the scheduling decisions or the beamforming weights. In contrast to JP, CS/CB does not require the exchange of user data among collaborating base stations, since there is only one transmission point for the user data. However, an exchange of control information is still needed in order to coordinate the scheduling decisions or the beamforming weights, but with significantly reduced backhaul requirements compared to JP. We distinguish several approaches of CS/CB with different demands on the backhaul capacity.

Open-loop beamforming is a transmission mode without Precoding Matrix Index (PMI) feedback from the UE. The base station radiates the signal in the direction of the UE by exploiting statistical CSI, i.e. long-term channel knowledge like the Direction of Arrival (DoA) of the uplink signal that changes only slowly over time. Appropriate beamforming weights can be derived from the estimated DoA. However, this requires calibrated antennas with correlated elements, e.g. a linear array of closely spaced antenna elements.

Generally, a high expected Signal to Interference plus Noise Ratio (SINR) is achieved if both the desired signal strength is maximized and the interference from adjacent cells is minimized. Open-loop beamforming without coordination always fulfils the first requirement. However, significant mutual interference occurs if two beams are directed towards the same location at the border between two neighbouring cells. This unfavourable case is shown in Figure 3.1 top right. With CS/CB both conditions can be fulfilled. In this case, the radio resources are allocated based on the statistical CSI of both desired signal and interfering signals as illustrated in Figure 3.1 bottom. This information has to be exchanged among collaborating base stations. From the perspective of the UE, the beamformed receive signal seems to originate from one single

antenna port. In consequence, in addition to the cell-specific reference signals also UE-specific reference signals have to be transmitted. They are beamformed in the same way as the user data and are needed to enable channel estimation.

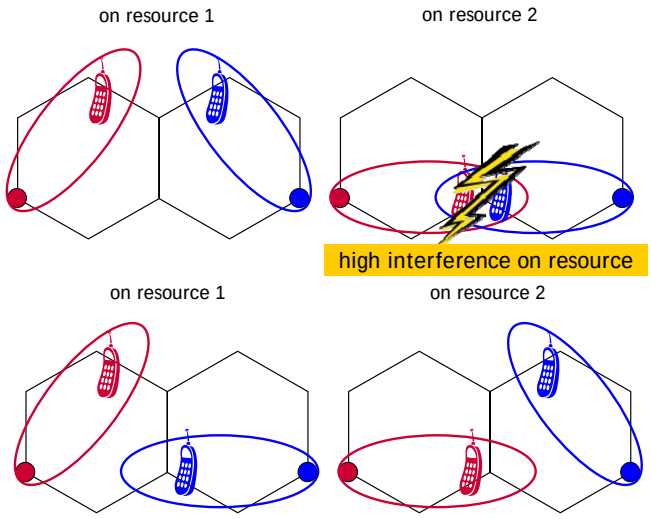

Figure 3.1: Unfavourable scheduling decisions lead to high interference (top). This can be mitigated by coordinating scheduling decisions among base stations (bottom).

Alternatively, *rank 1 closed-loop precoding* can be applied. Actually, it is a special case of MIMO spatial multiplexing with only one transmitted layer per user. For LTE Release 8, PMI feedback is assumed. For coordination, the terminals have to measure the channels of their main interfering signals additionally. Besides its own desired PMI, each UE reports one PMI value per neighbour cell that would cause the worst interference when this PMI would be applied in the neighbour cell on the considered radio resources. Alternatively, also the best possible PMI value per neighbour cell can be fed back [3GPP-R1090777]. The base stations exchange this information and can therefore coordinate their scheduling decisions. Again the effect shown in Figure 3.1 is achieved, i.e. the SINR is maximized. In case of MU-MIMO, this Space Division Multiple Access (SDMA) like principle is applied for intra-cell beam coordination. In contrast to open-loop beamforming, rank 1 closed-loop precoding does not require correlated and calibrated antenna elements. Furthermore, cell-specific reference signals are sufficient. However, since the achievable beam shape depends on the antenna type, also the capability of interference avoidance with beam coordination depends on the type of antenna in combination with the deployment scenario.

In CS/CB, the base stations need a prediction of the interference caused by the envisaged scheduling decisions. In downlink, this requires knowledge of the channels between the base station and the UEs in the neighbouring cells. This information can be given either explicitly in form of CSI of interfering signals, or as additional PMI feedback. Therefore the UEs would have to take additional measurements of these inter-cell channels. Appropriate measurement procedures would be needed. In uplink, the channels between UE and the adjacent base stations need to be measured. In a Time Division Duplex (TDD) system the reciprocity of the channel might be exploited and eNB measurements could to some extent be used for downlink, too, saving UE to eNB reporting overhead in uplink. Dynamic vertical beamforming, as one possible enhancement for CS/CB, offers an additional degree of freedom. If we assume that different downtilt angles can be applied, the PMI values also depend on the respective downtilt of the interfering signals.

Joint Processing (JP)

JP promises the largest performance gains, but comes at the cost of the highest signalling requirements with respect to the single-point user data transmission case. For the purpose of

interference avoidance, the downlink case is more challenging and relevant than the uplink, where interference exploitation techniques are commonly discussed. In the remainder of this text, we focus on the downlink case, if not mentioned otherwise.

Regarding dedicated precoding methods, a further challenge introduced by JP is the per base station power constraint, i.e. limited transmit power per group of antennas. In practical cellular systems the transmit power per base station (summed power from all antennas) is restricted due to electromagnetic compatibility aspects. In addition there are per antenna power constraints due to limitations of the power amplifier. The applied precoding has to fulfil these restrictions, which leads to constraint optimization problems. The introduction of multiple coordinated eNBs inserts additional constraints into the optimization problem.

Achieving optimality of a certain target function leads to more complicated optimization problems. A popular target function is based on the Minimum Mean Square Error (MMSE), where an optimal solution was formulated in [SSV+08]. Quality of service aspects were regarded in [TCJ07] and [MF08], for example.

In JP, the achievable performance is very sensitive to CSI uncertainties, like channel estimation errors, interpolation between pilot positions, feedback quantization and delays. Assuming Frequency Division Duplex (FDD) systems and frequency selective channels, downlink CSI cannot be estimated from the uplink channel and has to be fed back to the base stations using limited uplink transmission resources. CSI of the links of all collaborating base stations to a single terminal is commonly only fed back to the base station to which the terminal is assigned. However, for applying joint processing, CSI from all coordinated base stations has to be available and thus needs to be exchanged between the cooperating base stations.

For the JP, two strategies can be differentiated (see section 3.2). In the centralized approach, the CSI collected at all base stations is forwarded to a central unit, where the joint processing is carried out. The results of the processing are then sent back to the base stations in a second step. Less signalling is needed for the decentralized approach, where CSI is exchanged directly between base stations and every base station performs its own precoding. The performance of decentralized precoding only differs from the centralized approach in the case where a limited backhaul capacity requires further CSI compression. In that case, a different version of the compound channel matrix is available at each base station, which therefore leads to different precoding results. In general, due to the required signalling, JP suffers from additional delays that degrade the CSI quality.

3.2 - Centralized versus decentralized approaches

As it appears clearly from the above descriptions of categories (coordinated scheduling, coordinated beamforming, and joint processing), the gain in interference avoidance arising from multi-cell cooperation goes at the expense of information gathering across the several cell users to allow for the joint optimization of scheduling and beamforming decisions. In particular the Channel State Information at the Transmitter (CSIT) for each user must be obtained through a feedback channel, typically by the serving eNB. How this information is then shared among cooperating cells and exploited in view of a suitable scheduling and beamforming design is however left to be specified. In particular several degrees of decentralized-ness of the architecture and several degrees of distributed-ness of the algorithms may be envisioned, each having a specific consequence on system performance and design. Some brief examples and definitions now follow allowing to clarify the terminology in use in the ARTIST4G project.

Architectures for multi-cell processing and coordination

In a centralized architecture of multi-cell processing or coordination, the CSI needed to compute the optimal transmission decisions is collected to a single central physical entity (which could be co-located with one of the eNBs or possibly implemented in a separate location of the network). This physical entity is referred to in the following as the Central Coordination Node (CCN). The CCN processes the channel/user information and computes the final decisions which are then distributed to the eNBs involved in the coordination cluster or set of collaborating eNBs. For instance, in Coordinated Beamforming, the CCN collects all CSI and computes all the

beamforming weights required to pre-code the data from each of the eNBs. The beamforming coefficients pertaining to a given eNB are then sent to this eNB alone, which exploits them to perform the local beamforming operation.

In the example of Joint Processing a similar centralized architecture can be used. However another variant of a centralized architecture can be envisioned in which the CCN does not limit itself to computing the beamforming coefficients but collects as well the user data to perform the actual beamforming operation on the data. In this case, the CCN sends the final precoded data to the eNBs. The eNBs can then map the precoded data to the transmit antennas and launch it over the air after some standard upconversion and filtering operations.

In the decentralized architecture of coordinated scheduling, beamforming or joint processing, there is no CCN. Rather, the computation of the coordinated scheduling or beamforming decisions are carried out individually by each one of the eNBs and implemented locally as well.

Although the above description mentions two extreme options for centralized and decentralized architectures, one may also envision other levels of decentralization where a subset of calculations are implemented in a CCN while other remaining calculations are physically located in intermediate nodes or locally at each eNB.

Importantly, note that although some transmission decisions are derived locally at the eNBs in decentralized architectures, the computations of such decision may rely on global or partial CSI. In the case of decisions made on the basis of global CSI, the CSI for all users and cells has to be acquired at the level of the eNBs and fully exchanged across all of them. In the case that global CSI is somehow not available at all eNBs, a distributed optimization algorithm must be used in order to arrive at the final transmission decisions. This point is explicated below.

Distributed optimization algorithms

A distributed optimization of a coordination or CoMP scheme refers to the capability of computing the transmission decisions (beamforming coefficient, power level, subcarrier usage, scheduler user index, etc.) based on non complete CSI data. Therefore this relates to the mathematical nature of the employed technique rather than where it is physically implemented (in this latter case one will refer to above described centralized vs decentralized architecture).

An example of distributed coordination is illustrated by distributed coordinated scheduling where each eNB makes a scheduling decision primarily based on the link quality and interference information reported by its own cell users, in the absence of link quality information reported by other cell users.

Also, a distributed Joint Processing CoMP scheme refers to a scenario where a eNB computes the beamforming matrix to be used at this eNB alone, based on partial CSI only.

Partial Channel State Information (CSI)

There are various forms and definitions of partial CSI. The three most important ones are described below:

- **Partial CSI based on incomplete information**: each eNB acquires only a subset of the coefficients for the global CSI matrix. For instance, the eNB in cell i obtains CSI for users served by cell i but not for other users. In another example, the eNB obtains CSI related to the direct channel gains (to their eNBs) for all network users, but no information related to the channel from a user and the interfering eNBs.
- **Partial CSI based on statistical information**: this scenario is similar to the one above, but some statistical information (mean, variance, correlation coefficients) is added to the partial instantaneous CSI for some of the missing CSI matrix elements. This extra information helps the eNB refine its optimization of the transmission parameters.
- **Partial CSI based on imperfect information**: in this case, the eNB acquires all or a subset of the CSI matrix coefficients, however the coefficients are only imperfectly represented, due either to channel estimation errors or to quantization effects over the feedback channel.

More generally, a distributed optimization refers to the use of an algorithm capable of determining transmission parameters (scheduling slot, subcarrier usage, power level, beamforming coefficients, etc.) on the basis of any combination of the three above forms of partial CSI.

The advantage of distributed techniques over non distributed ones is the reduction of the CSI exchange overhead required for interference mitigation. Clearly, according to the above definitions, although a distributed algorithm only makes sense for a decentralized architecture, a decentralized architecture does not imply necessarily the use of a distributed algorithm (e.g. in the case where all nodes involved in the calculations rely on the same complete CSI).

3.3 - Downlink and uplink specific aspects

Most of the schemes proposed in section 4 for interference avoidance focus on the downlink of a single-cell or multi-cell system. Uplink and downlink directions have different constraints and require different solutions. In this section, we analyse the impact of the following aspects on the selection of an appropriate interference avoidance scheme.

Uplink and downlink traffic loads

Traffic load is asymmetric: downlink traffic load is higher than the uplink. Thus, spatial multiplexing and MU-MIMO techniques to increase the cell throughput are more important for the downlink direction than for the uplink direction. Identically, CoMP techniques to increase the cell edge throughput provide more gains for downlink than for uplink.

Equipment complexity, power consumption and size

At the network side, eNB complexity, power consumption and size can be much larger than for the UE, especially when the UE is a handset which has a limited battery life. As a consequence, the number of transmit antennas and power amplifiers is lower for the uplink (up to 4 antennas at the UE in Release 10 LTE-A) than at the downlink (up to 8 antennas at the eNB in Release 10 LTE-A). Thus the beamforming gain is larger in the downlink direction, as it benefits from larger antenna arrays. If the power per antenna element is maintained, with increasing number of elements also a power gain can be exploited, as long as regulatory constraints are respected. On the other hand, receivers with higher complexity can be implemented at the eNBs and more complex Multi-User Detection algorithms can be implemented in the uplink direction. Regarding amplifier complexity, UEs can only support low Peak to Average Power Ratio (PAPR), this is one of the reasons why Single Carrier Frequency Division Multiple Access (SC-FDMA) was selected for LTE Release 8 for the uplink, while Orthogonal Frequency Division Multiple Access (OFDMA) is used for the downlink.

Interference Control in Single User MIMO

In SU-MIMO, power control and load control is mandatory for the uplink direction while full transmit power is often assumed in downlink. In the uplink, the interference received by one eNB is variable in both frequency and time directions, mainly because of uplink interferers' variability. Indeed, in the uplink, the UE from a neighbouring cell, creating interference in one particular resource in frequency, can change from one frame to the other due to scheduling. This interferer diversity is not present in downlink systems with full power transmission, where the source of the interference is always the same neighbouring eNB.

To control and limit the uplink interference, schemes such as uplink schedulers monitoring uplink noise rise or uplink fractional power control [UVR+08] can be used. To control and limit the downlink interference, schemes such as Soft Frequency Reuse (SFR) or CB can be used. To conclude, downlink interference can be controlled more tightly than uplink interference, because of the uplink interferers diversity.

Interference Control in Multi-User MIMO

MU-MIMO schemes spatially multiplex streams of several UEs. They can be applied in both uplink and downlink directions. For both directions, the performance depends on the level of CSI availability at the transmitter, and the Multi-User Detection receiver complexity. Spatial multiplexing introduces intra-cell interference, which did not exist originally in Orthogonal Frequency Division Multiplexing (OFDM) based systems.

As a consequence, the near-far problem arises in both downlink and uplink directions. Near-Far problem in uplink arises when a UE near the eNB is multiplexed with a UE far from the eNB. In this case the interference created by the nearest UE can be very damaging to the other UE and uplink power control is in this case important.

Scheduling for MU-MIMO schemes and switching between SU-MIMO and MU-MIMO is a critical issue. Indeed, the MAC scheduler should switch to MU-MIMO only if the cumulated throughput of the spatially multiplexed UEs is expected to exceed the one of one single UE. Only UEs which are not interference limited can be spatially multiplexed. For both uplink and downlink directions, UEs that can be spatially multiplexed are thus near the centre of the cell.

3.4 - Impact of duplexing modes

The use of duplexing modes clearly impacts the design and performance of interference avoidance schemes. In general, interference avoidance schemes rely on the availability of some level of CSI. How to obtain this CSI, especially in the downlink, is a fundamental difference between FDD and TDD duplexing modes. Therefore, the mechanism for CSI acquisition is going to indirectly determine several aspects of interference avoidance schemes, such as the complexity or the robustness with respect to CSI impairments. Although most of the schemes presented in section 4 consider a FDD duplexing mode, in the following section the impacts on L1 aspects caused by the choice of either FDD or TDD are highlighted.

CSI acquisition

Interference avoidance schemes are based on the availability of some level of CSI. Then, the performance bounds of the schemes and the robustness with respect to CSI impairments are determined by the choice of the duplexing mode and the related CSI acquisition mechanism.

In TDD systems, CSI can be estimated using the reciprocity of the channel, but it should be noted that the interference distribution is not reciprocal. In the downlink of FDD systems, CSI cannot be estimated from the uplink, and the user needs to feed back the estimated channel to the serving eNB. In centralized CoMP systems, the CSI received at the serving eNB needs to be transmitted via the backhaul towards the central unit.

Interference avoidance schemes in TDD systems should be designed considering that, in general, higher synchronization requirements between cells are needed. In addition, guard times and discontinuous transmission due to the frame division into uplink and downlink slots may influence the delay requirements for some type of users, e.g. real time. These requirements are even more challenging in the case of CoMP systems.

In FDD, interference avoidance schemes should consider that some level of imperfect CSI is available at the eNBs. Here, imperfect CSI includes channel estimation errors, feedback errors or quantization losses and impact of delayed or outdated CSI.

Scheme complexity and performance

In TDD systems, CSI can be available at the eNBs to design interference avoidance schemes without the quantization losses and the feedback delays. Then, it is possible to design advanced interference avoidance schemes being able to dynamically adapt to the changes in the system. This is particularly important for JP schemes, where the performance of the schemes is highly influenced by the availability of accurate CSI.

The availability of some level of imperfect CSI in FDD systems constraints the performance of the schemes. JP schemes suffer from performance degradation, especially due to delayed CSI. Single-cell and CB/CS algorithms are more robust in this sense.

3.5 - Key Performance Indicators

Guidelines for the evaluation of concepts developed within the ARTIST4G project were presented in [ARTD51]. Moreover, a set of new performance indicators, evaluation scenarios and methodologies were also provided.

The specific signal processing algorithms for interference avoidance presented in section 4 are mainly considered for macro-cell related deployments (although one all-femto indoor deployment is also included). In the following, we identify possible impacts of these innovations in the field of single-cell MU-MIMO, CoMP transmission and advanced beamforming, and point out important system level performance metrics. Note that this information is a subset of the one included in the ARTIST4G document [ARTD51].

The basis for the performance evaluation of CoMP transmission and advanced beamforming schemes could be “3GPP case 1” (c.f. Table A.2.1.1-1 of [3GPP36814], see also [3GPP25996] and [BSG+05]).

The performance of interference management concepts to be investigated depends on several aspects as described in the previous sections. These aspects should be taken into consideration and clearly described when defining the scenario to be used for the assessment by means of numerical simulations.

One of the main features is the number of transmission points, i.e., the serving cell is the only transmission point or multiple cells including the serving cell serve simultaneously as transmission points (i.e. applying CS/CB techniques or JP techniques). Related to this we have the question whether the cells participating in the interference management operations belong to the same site or to different sites. Intra-site interference management relaxes the constraint of limited capacity on the X2-interface because data and control information can be exchanged via the backplane of the eNBs located at one site. Intra or inter-site interference management assumptions directly impact other aspects such as the backhaul capacity and latency, or the delay related to the information exchange between the participating cells.

Regarding CSI aspects, assumptions on uplink sounding and channel reciprocity (depending on FDD or TDD operation) should be also highlighted. FDD or TDD operation modes also impact on the availability, accuracy and nature of CSI measurements within a cluster of cooperating sites.

In the case of JP, the performance further depends on whether the transmissions from different cells are coherent (adding amplitudes at the Rx) or non-coherent (adding powers). In advanced beamforming schemes, the related antenna model solely is not sufficient to evaluate the performance of dynamic vertical beam steering adequately. In addition to the existing model, optionally also the support of sampled radiation patterns derived from antenna measurements may be provided.

System performance metrics

According to [3GPP36814], the following KPIs are to be considered as possible metrics to assess the performance in the presence of advanced interference avoidance schemes.

For evaluations with full-buffer traffic model, the following KPIs need to be considered:

- Mean user throughput
- Throughput Cumulative Distribution Function (CDF)
- Median and 5% worst user throughput

An important objective of the project is to reduce discrepancies of the quality of service throughout the entire network. Therefore special care is taken to improve cell-edge performances and especially the cell-edge over cell-average performance ratio. The

performances in cellular networks depend on the location of the user. For example, the spectral efficiency is generally larger in the cell centre than at the cell border. A possible way to measure this variability is to consider the ratio between the cell-edge spectral efficiency and the average spectral efficiency. However, in ARTIST4G, as specified in [ARTD51], special attention will be given to the Jain Index as a parameter to measure these disparities.

In section 4, the first results of the specific signal processing algorithms for interference avoidance are presented. Although the use of ARTIST4G KPI is in the scope of these results, further work is needed to fully characterize the algorithms based on the proposed KPI. Currently, KPI such as the mean user throughput are already being used to assess the performance of the algorithms. Note that enablers such as channel estimation and feedback design cannot be directly evaluated using ARTIST4G KPI.

4 - Description of specific signal processing algorithms for interference avoidance

In the following sections, the technical topics addressed in Task 1.1 of WP1 have been sorted into four classes of innovations. The grouping of the schemes is chosen in the order of increasing complexity, starting with the single cell scenario and extending towards multicell scenarios. Subsequently, advanced beamforming is considered, which can be applied in both of the previous scenarios. Finally, the last class of innovations covers enabling functionalities, which are needed to enhance the considered schemes. Among the investigated schemes the focus is more on downlink rather than on uplink.

Given the diverse nature of the contributions made in the above areas, choices will be made in the next phase of the project to determine the innovations that show promise and those which are suitable for a real-life implementation test. The challenge ahead lies in the construction of a complete interference avoidance scheme which will combine the above progress in basic beamforming design with some of the new approaches in the MU-MIMO and multi-cell coordination/ JP CoMP, together with the selection of a suitable feedback architecture.

The aim of this construction will be to show good performance, robustness, ability for distributed implementation when possible, and reasonable feedback overhead.

4.1 - Single-cell MU-MIMO schemes

As recently investigated, SDMA has strong advantages compared to other access strategies in terms of spectral efficiency especially in the high SINR range [JG04]. To apply this strategy, multiple antennas have to be available at the eNB. Depending on the number of eNB antennas, multiple data streams can be transmitted in parallel using the same radio resource. The transmitted streams can be assigned to multiple UEs, where a certain UE can decode at most as much data streams as UE antennas are available. SDMA with multiple UE antennas (MU-MIMO) provide significant performance improvements in comparison with single antenna UEs as in Multi User Multiple-Input Single-Output (MU-MISO) [Jin06]. This section takes a look at scenarios where interference from other cells (inter-cell interference) is neglected or regarded as Gaussian noise. In terms of interference avoidance the principal challenge of single-cell MU-MIMO is to repress intra-cell interference by pre-processing the transmit signals.

Under the precondition of CSIT various beamforming schemes in combination with power control (precoding) can be applied to separate the data streams in the spatial domain [JUN05], [SSJ+05], [Cos83].

An important issue according to the performance of MU-MIMO schemes is the impact of the CSI quality at the UE and the eNB [CS03]. In practical systems, CSI is impaired by several impacts as e.g. channel estimation. Furthermore, TDD systems suffer from non-perfectly reciprocal channels, while feedback channels of FDD systems possess delays and rate restrictions.

In this section, MU-MIMO based on CSI designed for SU-MIMO in 3GPP LTE Release 8 is analyzed, regarding the requirements to the codebook. LTE SU-MIMO Modulation and Coding Schemes (MCS) adaptation based on CQI will be expanded to MU-MIMO adaptation. Then, several improvements to the MU-MIMO scheme in 3GPP LTE Release 8 are introduced and evaluated.

Schemes for designing the precoding matrix and the linear receive filters are analyzed with respect to the control data exchange. Three general schemes are compared. In the first approach precoding matrix and receive filters are jointly computed at the eNB based on CSIT, and receive filters are forwarded to the UEs. In the second approach the receive filters are directly computed at the UEs, where additional precoded pilots are required. At the third scheme, receive filters are computed at the UEs without knowing the precoding matrix, where CSIT consists of the channel and the receive filters.

Furthermore, combined Spatial Multiplexing (SM) / Space Frequency Block Coding (SFBC) schemes in a SC-SFBC / SC-FDMA context are addressed. Double Alamouti schemes based on SC-SFBC are introduced and evaluated in a SU-MIMO scenario, in comparison with rate one transmit diversity techniques, for a particular spectral efficiency. This analysis opens the door for MU-MIMO specific joint scheduling and resource allocation for a pair of UEs using SC-SFBC.

Finally, time reversal precoding is analyzed. In contrast with the aforementioned innovations, time reversal is considered in TDD mode where reference signals are transmitted in the uplink and measured from the eNB to estimate CSI. Here, the channel is assumed to be perfectly reciprocal.

4.1.1 - Design and link adaptation for single-cell MU-MIMO systems

In LTE Release 8 SU-MIMO is already supported for the downlink direction. According to [3GPP36211-R8] and [3GPP36213-R8] the separation of the streams being sent to a mobile station is done by means of precoding matrices whose columns are orthogonal to each user. The precoding matrices are addressed by pre-defined precoding matrix indices, so-called PMI. The mobile stations feed back the desired PMI based on channel measurements. The CQI/PMI/Rank Indicator (RI) feedback of the mobile station reflects the channel conditions. The individual streams sent to a single user are precoded with the orthogonal columns of the precoding matrices.

In addition to SU-MIMO, a basic version of single cell MU-MIMO is already supported in LTE Release 8 for the downlink direction. It allows configuring a terminal for MU-MIMO semi-statically, the so-called transmission mode 5 in [3GPP36213-R8] and relies on the Release 8 codebook optimized for SU-MIMO. Transmission to a UE is performed on only one spatial layer in the MU-MIMO mode, i.e. fast rank adaptation between rank 1 and rank 2 is not possible, which does not allow exploiting potential gains by spatial multiplexing. Another drawback of Release 8 MU-MIMO is that the uplink feedback only supports wideband PMI precoding reports [3GPP36213-R8].

Extension of proportional fair scheduling to MU-MIMO

Before the MU-MIMO design is presented it shall be briefly outlined how the existing proportional fair scheduler is updated to support MU-MIMO. It is well known, that proportional fair scheduling for SU-MIMO maximizes the utility function given by

$$\text{SU-MIMO}: \max_{\delta_i} \sum_{i=1}^{N} \frac{\delta_i \sum_{j=1}^{M} r_{ij}(t)}{R_i(t)}, \ \delta_i \in \{0,1\}$$

where $R_i(t)$ denotes the average throughput of user i at time t and N indicates the number of active users in the current TTI. M is the number of available streams, $r_{ij}(t)$ denotes the achievable rate for each of the M streams. In LTE a resource corresponds to a physical resource block. The task of the scheduler is to allocate the resources per TTI, i.e. to choose the indices $\delta_i \in \{0,1\}$. For SU-MIMO the resource allocation indicator δ_i depends on the user index i, but not on the stream index j, which means that all of the M streams are used for one user. This resource allocation rule can now be generalized to MU-MIMO:

$$\text{MU-MIMO}: \max_{\delta_{ij}} \sum_{i=1}^{N} \frac{\sum_{j=1}^{M} \delta_{ij} r_{ij}(t)}{R_i(t)}, \ \delta_{ij} \in \{0,1\}$$

In case of MU-MIMO, however, the resource allocation indicator δ_{ij} depends also on the stream index j since the individual streams are allocated to different users. The task of the scheduler now is to maximize the above expression. In case of two available streams the scheduler has to find users $i_1, i_2 \in \{1,\ldots, N\}$ such that:

$$\max_{i_1, i_2 \in \{1,\ldots N\}} \left(\max\left(\frac{r_{i_1 1}(t)}{R_{i_1}(t)} + \frac{r_{i_2 2}(t)}{R_{i_2}(t)} \right), \frac{r_{i_1 2}(t)}{R_{i_1}(t)} + \frac{r_{i_2 1}(t)}{R_{i_2}(t)} \right)$$

SU-MIMO appears then as special case of MU-MIMO if the user indices are equal, i.e. $i_1 = i_2$.

System description of the innovation

Because of these drawbacks mentioned in the introduction the applicability of MU-MIMO in Release 8 is limited. Therefore extensions to the existing MU-MIMO transmission mode 5 were considered. The investigated MU-MIMO approach relies on the Release 8 SU-MIMO precoding matrices and re-uses the already existing SU-MIMO scheduler.

The scheduling of the resources is done in two stages. The first stage entirely re-uses the Release 8 SU-MIMO scheduler and allocates each PRB uniquely to a user. A user i_1 being scheduled in the first stage is called resident user. Only two users are allowed to be paired in the current analysis. In the second stage all users i_2 that have not been scheduled yet, are candidates to be paired with the resident users of the first stage, for each PRB, if they fulfill the following criteria:

1. Null Space Criterion: $(B_1)^H \cdot B_2 = 0$
2. Sum Utility Criterion: $U(i_1;P/2) + U(i_2;P/2) > U(i_1;P)$

B_1 and B_2 denote the precoding matrices of the resident user i_1 and the candidate user i_2, respectively. Note that the null space criterion does not pose restrictions to the number of streams allocated to a user in the sense that only one layer can be allocated to a mobile station. $U(i;P)$ denotes the utility of the applied scheduler. In case of proportional fair scheduling it is $U(i;P) = r_i(t)/R_i(t)$ as outlined above. P in the utility indicates the dependency of the achievable rate $r_i(t)$ on the allocated Tx power P.

In order to keep the interference between the resident user and the additionally allocated user low, the desired precoding matrix B_2 of the candidate user should be in the null space of the precoding matrix B_1 of the resident user, i.e. $(B_1)^H \cdot B_2 = 0$. The candidate user with the highest value of the proportional fair utility metric in this PRB is paired with the resident user, if the resulting proportional fair metric exceeds the original metric of the resident user.

In case of user pairing, the transmit power is equally split up between the paired users which results in a power reduction of 3 dB. This power reduction needs to be taken into account for the link adaptation since it is not reflected in the CQI report of the terminal. Although the precoding matrix of the paired user is orthogonal to that of the resident user, intra cell inter user interference may occur since B_2 may not necessarily be in the null space of the channel matrix of the resident user. However, these impacts of inter-user interference are not yet taken into account for the link adaptation.

If no candidate user can be found that increases the utility metric, no user pairing takes place and the decision of the first stage of the SU-MIMO scheduler is maintained. Then it is better to allocate all available streams to one user, i.e. to choose $i_1 = i_2$.

It is further proposed that the described user pairing takes place for each PRB separately. This requires an enhanced uplink feedback that supports frequency selective PMI reporting in the MU-MIMO transmission mode. Additionally, for the downlink transmission it is assumed that, per PRB, a different precoding matrix can be applied. This is not supported in Release 8 since only one precoding matrix can be applied for all allocated PRBs, which is signaled in the PDCCH to the UE.

This restriction to one precoding matrix for all allocated PRBs is mainly due to the fact that demodulation is based on cell-specific reference signals, which requires explicit signaling of the precoding matrix to the UE. This means that frequency-selective precoding requires additional signaling overhead. Therefore UE-specific RSs that are precoded in the same way as the data symbols themselves are proposed. This avoids the need to signal the precoding matrix explicitly to the terminal. The advantage of such an approach is that frequency-selective precoding can be applied for downlink transmission.

The last proposal for MU-MIMO enhancements is the support of subframe switching between SU-MIMO and MU-MIMO. This is not possible in LTE Release 8 since the MU-MIMO transmission mode 5 only allows rank 1 transmission to a UE. In order to serve a UE with more

than one stream, it is required that a RRC reconfiguration takes place. This is associated with a delay that does not allow subframe switching between SU-MIMO and MU-MIMO.

Table 4.1 lists the downlink MU-MIMO enhancements proposed to improve the existing Release 8 MU-MIMO transmission mode 5.

Table 4.1: Proposed MU-MIMO Enhancements

Feature	Release 8 MU-MIMO	MU-MIMO Enhancements
PMI reporting	Wideband PMI	Frequency-selective PMI
PMI precoding	Wideband precoding	Frequency-selective precoding
Demodulation RS	Cell-specific RS only	UE-specific RS
SU/MU-MIMO Switching	Based on RRC signaling	Subframe switching
Rank adaptation	Rank 1 transmission only	Fast L1 rank adaptation

Similar enhancements are meanwhile supported in LTE Release 9 by the new transmission mode 8 for dual layer transmission with two antenna ports [3GPP36213]. This transmission mode introduces dual layer transmission to a single UE applying UE-specific RS as defined in [3GPP36211]. If only one antenna port is used for a transmission to a single UE, the standard principally allows using the second antenna port for transmission to a second UE [3GPP36213]. Transmission mode 8 could thus be used for MU-MIMO as well. However, only two users with one stream per user only can be paired.

Performance results and future steps

The performance of MU-MIMO with the proposed enhancements was evaluated by means of system level simulations with the assumptions defined in Table 4.2. Additionally, ideal MSC selection is applied. Hereby it is understood that the MCS is ideally selected at the UE based on the instantaneously received SINR. This ideal assumption neglects the CQI reporting delay and the impact of changes of precoding matrices in neighbor cells. First we compare system level performance gains over Release 8 SU-MIMO based on the following assumptions as described in Table 4.2.

Table 4.2: System Level Simulation Assumptions

Simulation Parameter	Value
Channel Model	3GPP Case 1 3D (ISD 500m), v = 3 km/h, 10 MHz bandwidth, 2 GHz carrier frequency
Power Amplifier	46 dBm
Antenna Configuration	4x2 vertically polarized antennas with 0.5λ antenna spacing at UE and eNB
Scheduling	Proportional fair, MU-MIMO scheduling
Maximal Number of Users/PRB	2
Maximal Number of Streams/User	2
UE Receiver	MMSE
Noise Figure	7 dB
CQI Quantization	5 bits addressing 5 consecutive PRBs for Release 8 and MU-MIMO
CQI/PMI/RI Feedback Delay	6ms
Reporting Periodicity	One CQI/PMI/RI report per subframe
Channel Estimation	Non-ideal
Control Channel Overhead	L = 3 OFDM symbols/subframe for PDCCH

Feedback and Control Channel Errors	None

Figure 4.1 shows the relative gains of 4x2 MU-MIMO over Release 8 4x2 SU-MIMO under the above assumptions for a specific user throughput quantile. The indication '1 Layer' in the legend means that only users that report a rank-1 channel are considered for user pairing. In this case two users are paired with one stream per user according to the restriction of Release 9 transmission mode 8.

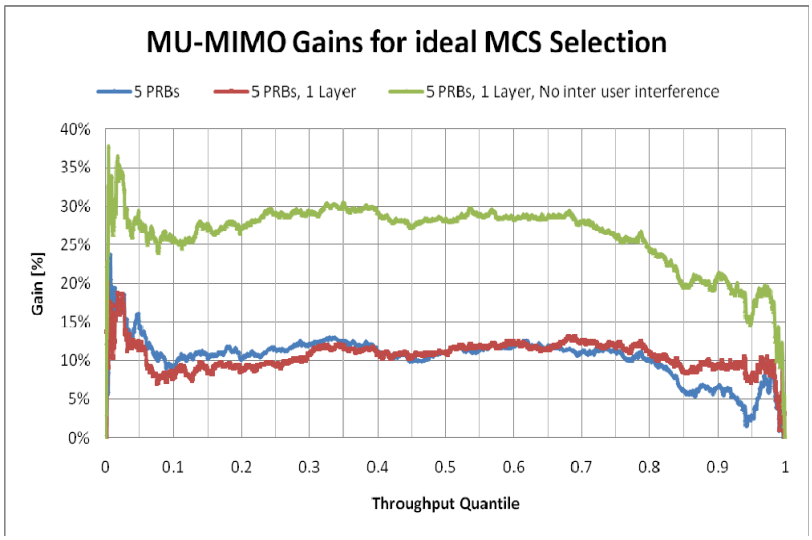

Figure 4.1: MU-MIMO Gains under ideal Assumptions

It can be seen that under the assumption of ideal MCS selection, the designed MU-MIMO approach improves the performance by about 10% compared to SU-MIMO. This is roughly true both with and without the restriction of one stream per user. From this result it can be concluded that Release 8 PMI-based MU-MIMO including Release 9 transmission mode 8 results in gains over Release 8 SU-MIMO, but they are limited to roughly 10% under the chosen assumptions. Allocating more than one layer per user offers only small gains at lower quantiles, compared to the case when transmission is restricted to one layer only. At very high quantiles this restriction even offers better performance.

In a second step it was investigated how much improvement can be expected by MU-MIMO in case no inter user interference is present. The gains over LTE Release 8 SU-MIMO increase to almost 30%. This result indicates that inter user interference has a significant impact on the performance. This also means that the transmission modes 8 in LTE Release 8/9 can potentially be enhanced further if additional information is provided to the base stations to improve the user pairing and reduce the inter user interference.

Two options on how to improve the user pairing can be identified. In case of MU-MIMO based on the unitary precoding matrices introduced in Release 8, additional information can be reported by a UE in form of best matching precoding vectors (matrices) for candidate UEs. This candidate precoder can be sent together with a CQI/PMI/RI report. Similar approaches are currently under discussion for LTE Release 10. Secondly, explicit CSI reporting by the UE can be introduced. In that case, an appropriate design criterion is Signal to Leakage Ratio (SLR) introduced in [STS07] since it achieves a good balance between maximizing the power of the received signal and minimizing interference. Conditioned on a specific UE pairing, the precoding vectors w_0 and w_1 are chosen such that the SLR is optimized. Denoting the channel matrices to users i_0, i_1 by H_0 and H_1, the SLR criterion can be written as

$$w_i = \arg\max_{\|w_i\|=1} \frac{\lambda_i^2 \left| v_i^* w_i \right|^2}{\mu + \lambda_{1-i}^2 \left| v_{1-i}^* w_i \right|^2}$$

where λ_i and v_i denote the dominant singular value and eigenvector of H_i. The scalar μ denotes interference and noise power stemming from thermal noise and other cell interference. It is easy to show that the precoding vector is then given by

$$w_i \sim \left(\mu I + \lambda_{1-i}^2 v_{1-i} v_{1-i}^* \right)^{-1} v_i$$

This computation of the precoding vectors can be done on a per subband basis. For the scheduling the same extended proportional fair approach as previously outlined is chosen. Again, at most two users are allocated to one PRB, each with one stream transmission. The future investigations will address how the quantization of the feedback of the dominant singular value and the eigenvector impacts the system performance.

The LTE Release 8 transmission mode 5 MU-MIMO has been analysed and some drawbacks have been identified that result in limited applicability. Enhancements like UE-specific RS, frequency-selective precoding, subframe switching between SU/MU-MIMO and fast L1 rank adaptation have been identified. Similar enhancements are meanwhile addressed in LTE Release 9 transmission mode 8 'Dual Layer Transmission'. System level analysis showed that the gains of these enhancements are in the order of 10% compared to Release 8 SU-MIMO. The simulations also revealed that further gains are achievable if the inter user interference could be controlled in a better way as it is the case with the implicit CQI/PMI/RI reporting defined in [3GPP36213]. In order to better eliminate the inter user interference, CSI based feedback together with SLR based precoding is currently under investigation. The next steps will be to investigate the impact of the feedback quantization on the performance.

4.1.2 - Transmit and receive filter design with limited signalling information

In single-cell MU-MIMO downlink transmission, linear transmit filtering at the eNB and linear receive filtering at the UEs is a low complexity solution for spatial multiplexing data streams to multiple UEs using a shared radio resource. In this contribution, three basic concepts for transmit and receive filter design steps are compared in terms of performance, signalling overhead and applicability.

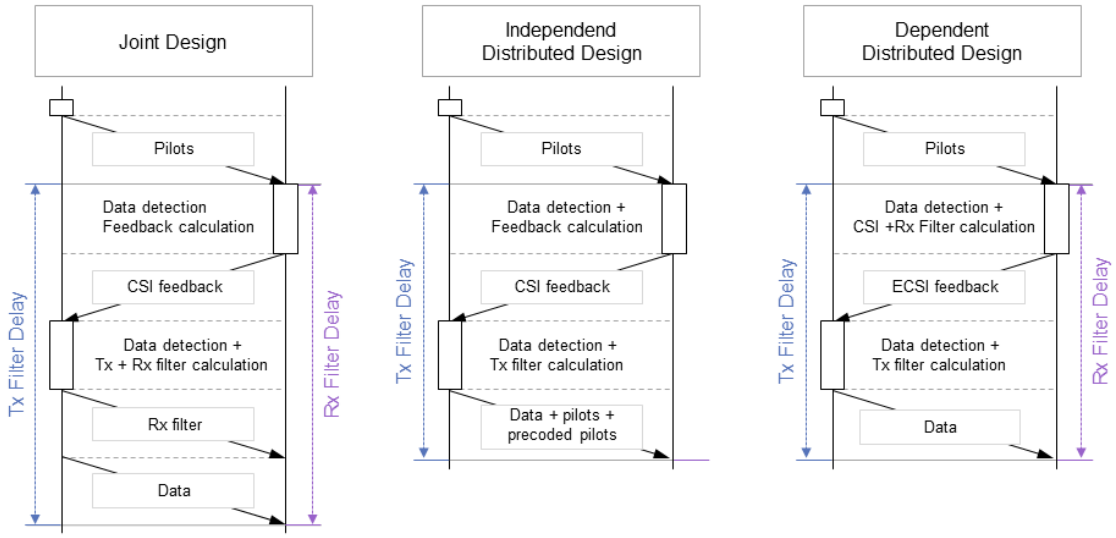

Figure 4.2: Flow chart of the three presented design schemes, where the left-hand side represents the transmitter, while the right-hand side is the receiver

The Joint Design (JD) approach is the most common method to jointly calculate transmit and receive filters at the eNB based on CSIT [JUN05], [ZL06]. The eNB feeds forward the receive filters to the intended UEs. A major disadvantage of JD is that CSIT usually suffers from quantization and compression, compared to Channel State Information at the Receiver (CSIR). Furthermore, forwarding the receive filters to the UEs requires quantization and compression, which introduces a trade-off between performance and signalling overhead.
To relax the sensitivity of receive filter inaccuracy a Distributed Design (DD) can be applied. Here, two concepts are distinguished. In the Independent Distributed Design (IDD) the receive filters are directly computed at the UEs based on the knowledge of the UE specific channels and on the inter-user interference. To obtain interference information, precoded pilots can be placed onto orthogonal resources. However, compared to JD the performance suffers from less information quantity (not the whole channel matrix is available), which might be compensated by better information quality (higher quantization resolution and smaller delays). In the Dependent Distributed Design (DDD) the receive filters are directly computed at the UEs, only based on the actual available channel (non-precoded pilots). Afterwards the product of the channel and the receive filter (effective receive channel) is fed back to the eNB. Based on that effective CSI (ECSI) the transmit filters are calculated. Since no precoded pilots are required, the signalling overhead can be drastically reduced.
Regarding time varying channels, the delay between channel observation and the application of a filter calculated based on that observation can eminently impact the data transmission performance. As it is shown in Figure 4.2 the joint design comes with the largest delay for both, transmit and receive filter. Because no forwarding is required for DD, the delay between channel observation for the transmit filter design and the actual data transmission can be reduced. Furthermore, for IDD the receive filter can be calculated directly based on the pilots inserted into the transmission block the filter is used for. Hence, no delay impact on the receive filter design is obtained by this scheme. For DDD the receive filter could also be calculated directly from the pilots of the resource block where the inherent data transmission takes place. However, for that scheme the transmit filter is adapted to the receive filter, where changing the receive filter may not lead to performance enhancements compared to just applying the outdated version. Hence, the receive filter delay can be evaluated as the delay for the transmit filter (see Figure 4.2).

System description of the innovation

The MU-MIMO downlink transmission to UE k is described by the equation

$$\hat{\mathbf{s}}_k = \mathbf{U}_k \left(\mathbf{H}_k \mathbf{W}_k \mathbf{P}_k^{1/2} \mathbf{s}_k + \sum_{l \neq k} \mathbf{H}_k \mathbf{W}_l \mathbf{P}_l^{1/2} \mathbf{s}_l + \mathbf{n} \right),$$

where $\mathbf{s}_k$, $\hat{\mathbf{s}}_k$, $\mathbf{H}_k \in C^{[M \times N]}$, $\mathbf{W}_k \in C^{[N \times L]}$, $\mathbf{P}_k \in C^{[L \times L]}$ and $\mathbf{U}_k \in C^{[L \times M]}$ is the user symbol vector, the estimated symbol vector, the MIMO coupling matrix, the unit column beamforming matrix, the power allocation matrix and the receive filter associated with UE k, respectively. Furthermore, $\mathbf{n}$ denotes the additive white Gaussian noise vector due to receiver noise. The eNB is equipped with N antennas, while the number of antennas at UE side is denoted by M. The number of data layers assigned to a single UE is $L \leq M$. A very simple scheme, for designing $\mathbf{W}_k$, $\mathbf{P}_k$ and $\mathbf{U}_k$ is the Transmit Wiener Filter (TxWF) approach, which minimizes the SMSE (Sum Mean Square Error) assuming unitary scalar receive filters [JUN05].
Because of that property, the receive filter can be calculated centralized at the eNB and broadcasted to the UEs, resulting in low signalling information. For JD the performance of post equalizing highly depends on the quantization resoltution of the receive filters for feed forward to the UEs. Obviously, this degree of freedom also scales the signalling overhead. However, the performance can be increased by UE specific receive filters elevating the signalling overhead.
Since the quality of the receive filters suffers from CSIT uncertainty and feed forward quantization, receive filters can be calculated directly at the UE side. The simplest approach is to just separate the user data streams without taking care of other-user interference. For IDD, however, additional precoded pilots have to be introduced to estimate the effective transmit channel $\mathbf{H}_k \mathbf{W}_k \mathbf{P}_k^{1/2}$. Based on this estimation the receive filter can be designed for separating multiple streams of user k. This approach can be extended by including knowledge of the noise

variance and other-user interference into the filter scheme. To obtain knowledge of the interference from other UEs symbols, the pilot overhead has to be increased by using orthogonal pilot resources for every UE. This enables the possibility of interference estimation. Note that in this case the choice of the pilot structure can eminently influence the performance. Assuming an OFDM system based on the LTE standard, pilots can be scattered over a time-frequency resource block. The direct knowledge of other-user interference can be used for interference cancellation. Directing zeros to the direction of interference results in

$$\mathbf{U}_k \mathbf{H}_k \mathbf{W}_l \mathbf{P}_l^{1/2} = \mathbf{0}\,.$$

Of course, this only works if $\mathbf{P}_l^{1/2}\mathbf{W}_l^H \mathbf{H}_k^H$ have a non-trivial null space, i.e. $L < M$ if the effective transmit channel offers independent rows. Further schemes based on this approach can be found in the field of interference rejection combining (e.g. [KO02]).

To reduce the signaling overhead precoded pilots can be disclaimed by introducing DDD. Tracing just a data stream separation at the UE side, the preliminary receive filter can be calculated based on the actual UE specific channel matrix $\mathbf{H}_k$. The ECSI obtained from UE k results in

$$\tilde{\mathbf{H}}_k = \tilde{\mathbf{U}}_k \mathbf{H}_k\,,$$

where the ECSI quality suffers from channel prediction and quantization as for JD and IDD. Based on $\tilde{\mathbf{H}} = \left[\tilde{\mathbf{H}}_1^T, ..., \tilde{\mathbf{H}}_K^T\right]^T$ the precoding matrix is calculated by handling the ECSI like the actual channel matrix. For the actual receive filtering, the preliminary receive filters are downscaled by the transmit power to $\mathbf{U}_k = \tilde{\mathbf{U}}_k / \rho$. In accordance with these considerations, a DDD scheme based on other-user interference cancelation was presented in [MK10].

Performance results and future steps

For comparison of the results the achievable rate of UE k can be calculated with

$$R_k = \sum_{l=1}^{L} \log_2\left(1+\gamma_{k,l}\right),$$

where

$$\gamma_{k,l} = \frac{\left|\left[\mathbf{U}_k \mathbf{H}_k \mathbf{W}_k \mathbf{P}_k^{1/2}\right]_{l,l}\right|^2}{\sum_{i=1;i\neq l}^{L}\left|\left[\mathbf{U}_k \mathbf{H}_k \mathbf{W}_k \mathbf{P}_k^{1/2}\right]_{l,i}\right|^2 + \sum_{j=1;j\neq k}^{K}\sum_{i=1}^{L}\left|\left[\mathbf{U}_k \mathbf{H}_k \mathbf{W}_j \mathbf{P}_j^{1/2}\right]_{l,i}\right|^2 + \left[\mathbf{U}_k \mathbf{U}_k^H\right]_{l,l}\sigma_n^2}$$

denotes the SINR of UE k and layer l. The presented schemes were simulated assuming CSIR corruptions due to channel estimation and CSIT and Effective Channel State Information at the Transmitter (ECSIT) corruptions due to additional quantization effects. The results are presented in Figure 4.3, where the achievable rate is plotted over the number of feedback bits per resource block. Indeed, JD clearly outperforms the distributed schemes, but no quantization was assumed for feed forward the receive filter matrices. The difference between IDD and DDD is small compared to the JD. Creating an adequate metric by taking the signaling overhead as cost factor into account, JD will suffer from feed forward transmission, while for IDD precoded pilots have to be considered. Under this consideration it can be assumed, that DDD outperforms IDD and the gap between JD and the distributed approaches will be drastically decreased.

Table 4.3: Simulation parameters

Simulation Parameter	Value
Number of eNB antennas	$N = 4$
Number of UEs	$K = 2$
Number of UE antennas	$M = 2$
Max delay spread	$\tau = 2\mu s$
User velocity	$v = 5\,km/h$
SNR	$\rho/\sigma_n^2 = 10dB$

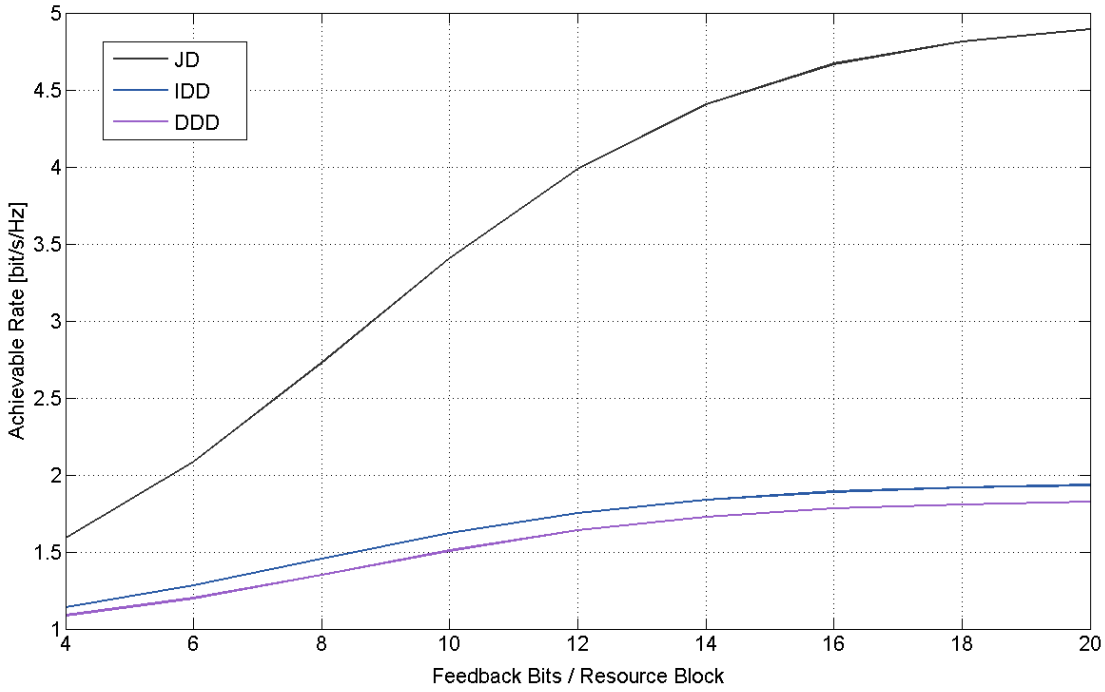

Figure 4.3: Averaged achievable user rate over the SNR for the three presented schemes

We showed the achievable rate averaged over the users as a function of feedback bits per resource block. By increasing the number of feedback bits a joint design outperforms both distributed design schemes, where saturation in dedicated bits can be observed, that depends on the channel properties in time and frequency. In these analyses the number of pilots and the overhead for feed forward the receive filters is not taken into account. A further step will be to create a metric, including performance and the complete signalling overhead. For simple filter schemes we will try to find analytical expressions or approximations for such a metric, where a performance metric for data transmission as well as the impairment model are considered. If no direct analytical expression can be found, the approximation will be compared with simulation results.

4.1.3 - Time reversal pre-filtering for interference avoidance in HeNBs networks

Time reversal is the matched filter at the transmission side. More precisely, considering a target point in space and a given source, if $h(t)$ is the channel impulse response between the target

and the source, the source will send data in time reversal manner, by pre-filtering its data flow by $h^*(-t)$, where * is the complex conjugate. Time Reversal is a beam-forming technique that has the interesting property to provide space focusing and time compression at the target point [EVH+04]. In this section, another property of time reversal, in indoor environment, which is the creation of minima of received power around the target point at a specific distance from the target, is exploited to perform multi-stream transmission with low complexity receivers.

System description of the innovation

Considering omni-directional mono-chromatic sources of wavelength λ regularly deployed over a circle with a radius $R >> \lambda$ centered on a target at position $(x=0, y=0)$, and focusing on this target using time reversal, the signal $S(x,y,t)$ at a position (x,y) near the target is given by:

$$S(x,y,t) = \sum_{k=1}^{N} \frac{A}{\sqrt{(x-x_k)^2+(y-y_k)^2}} \cos\left(2\pi(ft - \frac{\sqrt{(x-x_k)^2+(y-y_k)^2}}{\lambda} + \frac{\sqrt{x_k^{\,2}+y_k^{\,2}}}{\lambda})\right).$$

The averaged power at position (x,y) is given by: $P(x,y) = f\sum_{k=1}^{N}\int_{t=0}^{1/f} S(x,y,t)^2\,dt$. This spatial function is plotted in Figure 4.5 for 32 sources and $R/\lambda = 10/0.15$, it has a circular geometry and is minimal for positions on circles centered on the target with a radius R_k such that $R_k/\alpha \approx 3/8 + k/2$, where k is an integer. Thus, $R_k/\lambda \approx 3/8; 7/8; ...$ It can be easily shown that the zeros of $P(x, y=0)$ are the zeros of $J_0(2\pi x/\lambda)$ where $J_0(u)$ is the Bessel Function of order zero.

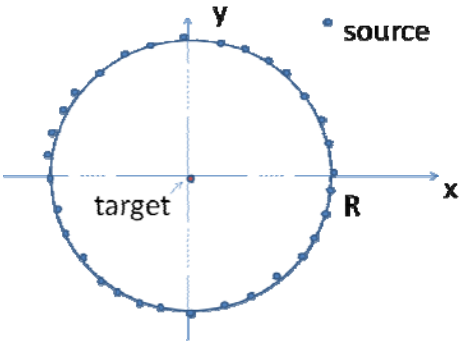

Figure 4.4: source and target positions

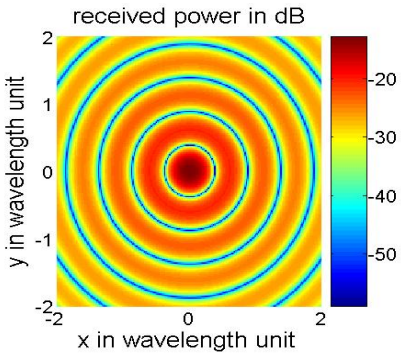

Figure 4.5: P(x,y) in dB

In indoor environment, the angular spread is high, thus the same kind of $P(x,y,t)$ may be obtained when time reversal is used, with minima at specific distances from the target. We therefore propose to exploit this particular property of $P(x,y,t)$ in indoor to build a MIMO scheme with basic multi-antenna receiver without interference cancellation. We consider 1 UE with $N_r = 2$ receive antennas spaced by Δ in lambda unit and 1 Home eNB (HeNB) with a linear array of N_t transmit antennas. We propose to use $\Delta = 7/8 = 0.875$ instead of the usual value of $\Delta = 0.5$. We consider the downlink direction and assume an OFDM system with N sub-carriers and a sampling frequency F_S. The HeNB has two transmission modes and dynamically switches between them. In dual stream mode, stream 1, intended to antenna 1, and stream 2, intended to antenna 2, are transmitted simultaneously, and with half transmit power each. In mono-stream mode, a single stream in sent to antenna 1 with full transmit power. To focus a stream on its target antenna, we use time reversal at the transmission side. It is applied

in the frequency domain, on the OFDM equivalent channel. For each sub-carrier f_k the signal is multiplied by $h^*_{i,j}(f_k)$, where $h_{i,j}(f_k)$ is the Fourier transform of the channel impulse response between transmit antenna i and receive antenna j on sub-carrier f_k and * is the complex conjugate. Hence, assuming a receiver noise spectrum density N_0 and noise figure F the received SIR $w_{k,j}$ on sub-carrier f_k at receive antenna j is given by:

$$w_{k,j} = \frac{\frac{1}{\frac{1}{N}\sum_{i=1}^{N_t}\left|h_{i,j}(f_k)\right|^2}\frac{P_{\max}}{2F_s}\left|\sum_{i=1}^{N_t}\left|h_{i,j}(f_k)\right|^2\right|^2}{\frac{1}{\frac{1}{N}\sum_{i=1}^{N_t}\left|h_{i,l\neq j}(f_k)\right|^2}\frac{P_{\max}}{2F_s}\left|\sum_{i=1}^{N_t}h^*_{i,l\neq j}(f_k)h_{i,j}(f_k)\right|^2 + N_0F}$$

A dynamic switch selects single stream transmission when it outperforms double stream transmission in terms of achievable spectral efficiency. In the case of single stream transmission, the receive antenna 1 and the receive SIR $w_{k,1}$ at antenna 1 is given by:

$$w_{k,1} = \frac{1}{N_0F}\frac{1}{\frac{1}{N}\sum_{i=1}^{N_t}\left|h_{i,1}(f_k)\right|^2}\frac{P_{\max}}{2F_s}\left|\sum_{i=1}^{N_t}\left|h_{i,1}(f_k)\right|^2\right|^2$$

Based on a perfect Channel State Information the HeNB estimates the effective received SINR per stream and each MCS using the Mutual Information formula and above SIRs per sub-carrier formulas. Then, for each stream, the HeNB selects the best MCS in terms of spectral efficiency with 10% BLER, using pre-computed AWGN link layer curves. To perform dynamic switch, the HeNB compares the spectral efficiency in mono-stream mode with the summed spectrum efficiencies in dual stream mode.

Performance results and future steps

The proposed system has been simulated for various antenna separations at the receiver, in one floor of a particular building. The system bandwidth is 10MHz.The Winner II channel model has been implemented. More precisely, for the large scale parameters, the path loss laws have been implemented using the Winner II formulas in table 4-4 of [WIN2D112], and take into account whether the propagation is Room-To-Room, Room-To-Corridor, Corridor-To-Room, LOS or NLOS. For the small scale parameters, the Cluster Delay Line model for LOS and NLOS in indoor specified in tables 6-1 and 6-2 of [WIN2D112] has been used. In LOS the angle of departure/arrival of multi-path components are much less spread than in NLOS. Finally, the spatial correlation of the small scale parameters is modelled, i.e. the channel received at the receive antenna 1 is correlated with the channel received at antenna 2, and this correlation depends on the separation Δ between antennas, and also on the angles of departure and angle of arrivals, thus it is lower for NLOS and higher for LOS.

The simulations assumptions are summarised in Table 4.4 below.

Table 4.4: Simulation parameters

Parameter	Value
Duplex Mode	TDD
Receiver type	MRC
N_{UE}	1

N_{HENB}	1
N_t	16
N_r	2 or 1
Δ	0.5/0.6/0.7/0.8/0.85/0.875/0.9/1.0 in λ unit
$P_{\max}$	21dBm
N_0	-174dBm/Hz
F	9dB
F_0	2GHz
λ	15cm
N	1024sub-carriers

The performance metric is the average achieved spectral efficiency $SE(x,y)$ for UE position (x,y) in the building. This metric is assessed through N simulation runs. For each run, the small scale parameters are drawn for each UE position (x,y) in the building; the achieved spectral efficiency at (x,y) is computed as explained, and stored. Finally, the spectral efficiency at (x,y) is averaged over runs and stored into $SE(x,y)$. $SE(x,y)$ is plotted as a function of (x,y). A Cumulative Distribution Function of this metric is also computed: $f(u)$ = % of UE positions (x,y) such that $SE(x,y) < u$. $SE(x,y)$ is assessed for several scenarios: MISO (mono-stream only); and MIMO (dynamic switch between dual stream and mono stream) with various Δ values.

We consider M different MCSs and m_k the spectral efficiency associated with MCS k. The spectral efficiency m_k of MCS k is defined as the coding rate multiplied by the number of modulation bits. For QPSK, the number of modulation bits is 2, for 16QAM it is 4 and for 64QAM is 6. The values of m_k range between 0.33 and 4.8 bps/Hz with a high granularity. The highest MCS achieves 4.8bps/Hz with 64QAM and 8/10 as a coding rate. Our simulations do not take into account Layer1&2 control overhead, TDD DL/UL sub-frame structure, ARQ or H-ARQ.

From the CDF of $SE(x,y)$ plotted in Figure 4.7 below, we can conclude that a MISO system with $P_{\max} = 21dBm$ is limited by the highest MCS (4.8bps/Hz) and not by the HeNB transmit power. For all positions where 4.8bps/Hz is reached, a second stream could be added without increasing the power. We can also confirm that the optimum receive antenna separation is $\Delta = 7/8 = 0.875$ for all positions in the building.

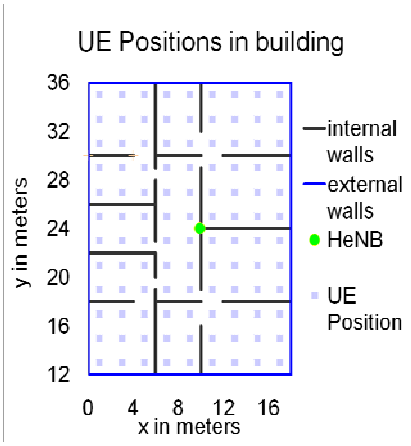

Figure 4.6: UE positions in building

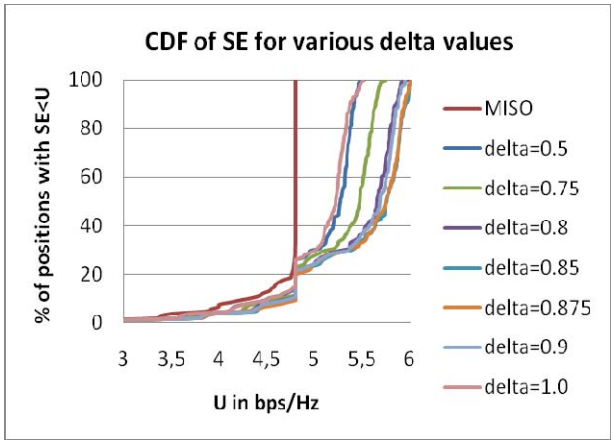

Figure 4.7: CDF of SE

In Figure 4.8 and Figure 4.9 the achieved $SE(x,y)$ is represented as a function of UE position (x,y) for the MISO case and the MIMO case with $\Delta = 0.875$. In MISO, the maximum MCS (4.8bps/Hz) can be reached in every position in the building except at the corners, which are far from the HeNB. In MIMO mode, thanks to spatial multiplexing, the spectral efficiency is enhanced in most positions in the building.

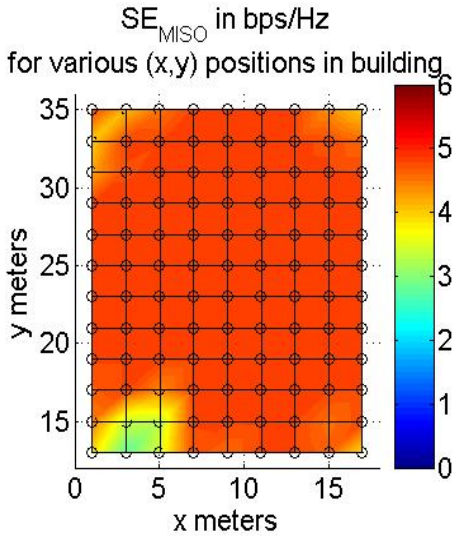

Figure 4.8: MISO

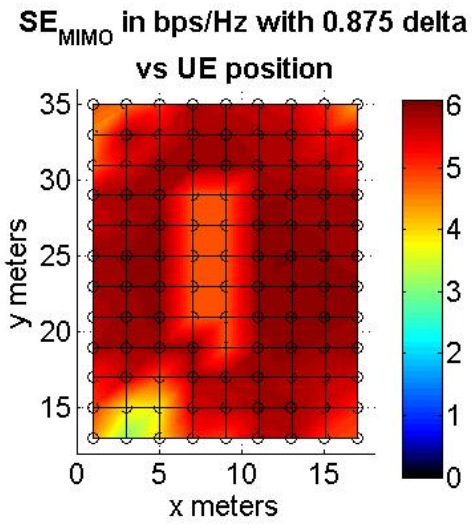

Figure 4.9: MIMO with Delta=7/8

In Figure 4.10 and Figure 4.11 the gain in spectral efficiency due to MIMO instead of MISO is plotted, as a function of UE position, for $\Delta = 0.5$ and $\Delta = 0.875$ respectively. For both values, MIMO brings a gain only in the rooms which are in NLOS of the HeNB and not in the corridor which is in LOS with the HeNB. This is due to the very low angular spread of LOS which creates highly correlated channels. The MIMO to MISO gain lies between 3 and 12% for $\Delta = 0.5$, and between 10 and 26% for $\Delta = 0.875$.

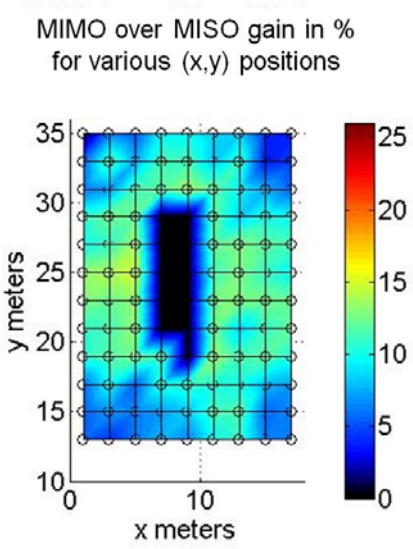

Figure 4.10: 0.5 lambda

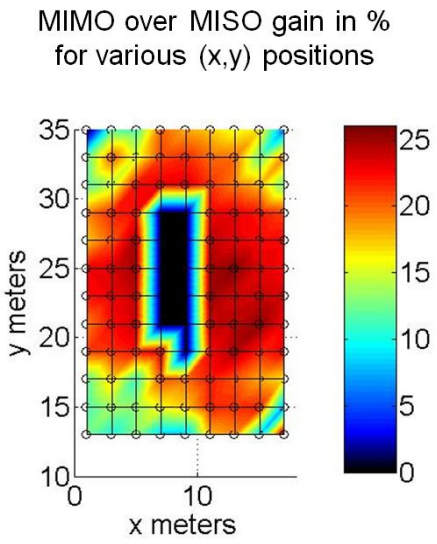

Figure 4.11: 0.875lambda

We have studied a simple MIMO scheme for HeNBs that relies on Time Reversal and does not require an interference canceller at the receiver. We have found that in a building where the HeNB is deployed in the corridor and transmits at full power, due to the high angular spread in rooms around the corridor, MIMO brings a gain in spectral efficiency, and that this gain is maximum when receive antenna separation is $\Delta = 7/8 = 0.875$ in wavelength unit. The next steps include a comparison of the proposed scheme with Zero Forcing (ZF) and Singular Value Decomposition (SVD), in terms of spectral efficiency, complexity, robustness and the extension to Multi-User and Multi-Cell transmission with coordinated femtos.

4.1.4 - SC-SFBC principles: applications for SU-MIMO

OFDMA and OFDMA-based multi-carrier (MC) transmission schemes have undeniably become one of the main references in modern communications systems. Almost all recent communication standards rely on an OFDMA downlink air interface and implement MIMO techniques [WWRF08]. Such is the case in IEEE 802.11n for Wireless Local Area Networks (WLAN), IEEE 802.16e-2005 for mobile WiMAX, LTE of UMTS (Universal Mobile Telecommunications System), and also in the future LTE-Advanced standard.

The general acceptance of OFDMA as a good option for the downlink of recent communications systems is motivated by its well-known advantages: good spectral efficiency, good coverage, flexible dynamic frequency allocation, simple equalization at tone level [SKJ94]. Even though there is a large consensus on OFDMA for the downlink, its use in the uplink is hampered by the high peak to average power ratio (PAPR) it displays. The PAPR problem, common for all MC transmission schemes, induces numerous performance issues such as reduced power efficiency, spectral regrowth and in-band distortion when using nonlinear High Power Amplifiers (HPA). Many efforts were directed to efficiently alleviating the PAPR problem [Tel00], [LX08] but because of either some standard-compatibility issues or some practical system limitations the problem is not yet considered as completely solved [CBS06].

While the PAPR problem, inevitable in the downlink, can be coped with by using highly linear (and thus expensive) HPAs for example, this is a much more sensitive issue in the uplink. Mobile users strive for good coverage, good autonomy handsets, but do not neglect the associated costs. Backing-off the uplink signal level to the linear region of the HPA would reduce the coverage and using highly linear HPAs would increase the handset cost.

For these reasons, the uplink physical layer of LTE [3GPP36211] was chosen to be a precoded OFDMA air interface, called SC-FDMA. The precoder is a Discrete Fourier Transform (DFT),

which restores the low envelope fluctuations of single-carrier (SC) systems. But SC-FDMA may lose its low-PAPR property in MIMO systems if no precaution is taken.

A PAPR-preserving transmit diversity technique for SC-FDMA, coined SC-SFBC, was already introduced for a user with two transmit antennas in [CCM+09], and some extensions to users with four transmit antennas were also presented. SC-SFBC makes use of an innovative subcarrier mapping in order to apply the well-known Alamouti scheme [Ala98] in an SC-FDMA system at subcarrier level in the frequency domain without degrading the PAPR.

The purpose of this contribution is to extend the SC-SFBC concept to the MU-MIMO SC-FDMA scenario.

System description of the innovation

Low-PAPR MIMO Techniques for SC-FDMA

Future mobile terminals will be equipped with typically two or even four transmit antennas and several radio frequency chains. It is therefore natural to try and apply MIMO techniques for the uplink of future wireless communications systems, since terminals will be able to use their multiple transmit antennas in order to increase throughput, increase link quality, mitigate interference, or perform a trade-off among the above [TV05]. More particularly, transmit diversity techniques are interesting to be applied for example for users at cell edge benefiting of poor propagation conditions, for high mobility users not disposing of a reliable channel state information, or more generally for the transmission of sensitive data such as control information where a good reliability is required despite the absence of feedback information.

SC-FDMA combines a SC signal with an OFDMA-like multiple access in order to achieve both the low PAPR specific to SC signals and the flexible dynamic frequency allocation specific to OFDMA. In its frequency domain implementation [3GPP36211], [MLG06], SC-FDMA is a precoded OFDMA transmission scheme, where precoding is done by means of a DFT. As in all cyclic-prefixed OFDMA-based systems, the system in the frequency domain (before passing through the Inverse Discrete Fourier Transform (IDFT)) experiences an equivalent diagonal channel. Therefore, it is after the DFT precoding that a transmit diversity precoding module must be inserted, in order to be able to correctly apply at subcarrier level space-time (ST) or space-frequency (SF) block codes (BC) that were originally designed for narrowband channels.

This is shown in Figure 4.12. At time t, data block vector $\mathbf{x}^{(t)}$, which is composed of M modulation symbols $x_k^{(t)}$ (k=0…M-1), e.g., Quadrature Phase Shift Keying (QPSK) symbols, is DFT-precoded by means of a M-sized DFT $\mathbf{F}_M$. M-sized vectors $\mathbf{s}^{(t)}$ thus obtained undergo ST/SF precoding, resulting in M-sized vectors $\mathbf{s}^{\mathrm{Tx}_n,(t)}$, $n = 0...N_{\mathrm{Tx}} - 1$ where N_{Tx} is the number of transmit antennas. These vectors are then mapped on M out of N inputs of the IDFT $\mathbf{F}_N^{\mathrm{H}}$ (the superscript $(.)^{\mathrm{H}}$ stands for the Hermitian of a vector or matrix) according to the subcarrier mapping strategy in order to be transmitted on antennas Tx_n. In this paper, we will consider that the mapping matrix $\mathbf{Q}$ corresponds to localized subcarrier mapping. To combat the effect of the frequency selective channel, a Cyclic Prefix (CP) is inserted in front of each N-sized block thus obtained.

Classically applying transmit diversity in SC-FDMA systems raises several issues. Let us suppose that $N_{\mathrm{Tx}} = 2$. The choice of an Alamouti code [Ala98] is natural for scenarios with two transmit antennas, since it has full rate, full diversity and is easily decodable.

If trying to apply an Alamouti-based STBC (i.e. precoding in the time domain between time-consecutive frequency samples $s_{k_0}^{(t_0)}$ and $s_{k_0}^{(t_1=t_0+1)}$ carried by the same k_0th subcarrier), we increase the granularity of the system. All transmission bursts would need to be composed of an even number of SC-FDMA symbols, which is difficult to guarantee into practice.

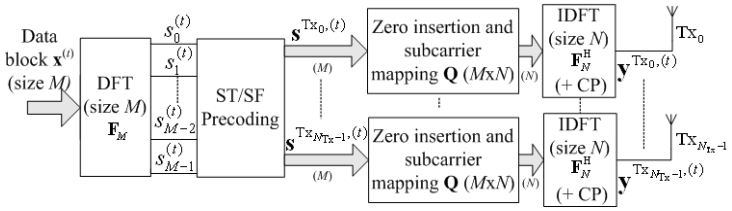

Figure 4.12: SC-FDMA transmitter with ST/SF precoding (*M* out of *N* allocated subcarriers, N_{Tx} transmit antennas).

In the LTE-Advanced system for example, for certain formats of the uplink control channel, only 5 SC-FDMA symbols will be present in a slot. This makes it impossible to use STBC. The advantage of STBC is that it preserves the SC-like PAPR of SC-FDMA.

On the other hand, if trying to apply an Alamouti-based SFBC (i.e. precoding in the frequency domain between frequency-adjacent frequency samples $s_{k_0}^{(t_0)}$ and $s_{k_1=k_0+1}^{(t_0)}$ belonging to the same SC-FDMA symbol), this would increase the PAPR of the resulting signal, as shown in [3GPP-R1063179], [CCM+09]. The main advantage of SC-FDMA, which is its SC-like PAPR, would be lost. However, the advantage of SFBC is its flexibility, since it can be applied to any number of SC-FDMA symbols in a transmission burst.

SC-SFBC is an innovative mapping scheme suitable for implementing transmit diversity in SC-FDMA systems, since it conserves both the flexibility of SFBC and the good PAPR of STBC. Just as classical SFBC, SC-SFBC performs Alamouti-based precoding in the frequency domain between frequency samples belonging to the same SC-FDMA symbol. The main difference with respect to classical SFBC is that SC-SFBC precodes between non-adjacent frequency samples $s_{k_0}^{(t_0)}$ and $s_{k_1=(p-1-k_0)\bmod M}^{(t_0)}$, where M is the number of subcarriers allocated to a user and p is an even integer satisfying $0 \le p < M-1$. In the following, the superscripts (t_0) will be omitted. SC-SFBC is constructed such as:

$$\begin{cases} \mathbf{s}^{\mathrm{Tx}_0} = \mathbf{s} \\ \mathbf{s}^{\mathrm{Tx}_1} = \mathrm{SC}_p^M(\mathbf{s}) \end{cases}$$

The SC_p^M operation consists in taking the complex conjugates of vector **s** in reversed order, applying alternative sign changes and then cyclically shifting down its elements by p positions. This is depicted in Figure 4.13. Alamouti-precoded pairs appear on couples of non-adjacent subcarriers (k_0, k_1) with:

$$k_1 = (p-1-k_0) \bmod M$$

Intuitively, based on the properties of the Fourier transform, the SC_p^M operation applied in the frequency domain is equivalent to complex conjugation and phase shifts in the time domain, but no amplitude modification is performed. It is fully proven in [CCM+09] that SC-SFBC does not increase the PAPR of the resulting signal and that the signals on both transmit antennas have the same PAPR as the original SC-FDMA signal.

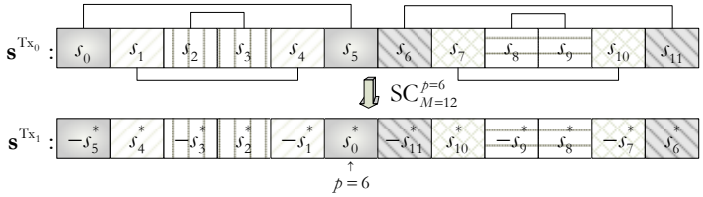

Figure 4.13: SC-SFBC precoding; example for *M*=12, *p*=6.

The maximum separation between subcarriers carrying frequency samples precoded together is max(*p*,*M*-*p*) and is thus controlled by the parameter *p*. Distant subcarriers might experience

different or even uncorrelated channel realizations, which generates some interference within the Alamouti-precoded pair. Some slight performance degradation can therefore occur on very selective channels and/or when the precoding distance is rather large. The optimum value of p, minimizing the maximum distance between subcarriers carrying Alamouti pairs is the even integer closest to $M/2$:

$$p_{\text{opt}} = 2\text{floor}\left(M/4\right)$$

SC-SFBC can benefit from low-complexity frequency-domain decoding. Indeed, couples of subcarriers (k_0,k_1) carrying Alamouti pairs can be identified and separately decoded. To minimize the impact of the interference created within the Alamouti pair by precoding onto distant subcarriers, MMSE is employed instead of the Maximum Ratio Combinig (MRC) usually employed in Alamouti decoding. MMSE decoding remains low-complexity (inversion of one order-2 matrix for each of the $M/2$ Alamouti pairs in one SC-FDMA symbol).

Double SC-SFBC for double-codeword SU-MIMO/collocated MU-MIMO

So far, the work reviewed in the previous subsection concentrated on transmit diversity techniques for SU-MIMO transmission, where each Mobile Station (MS) uses its transmit antennas to improve the performance at a given throughput, making use of the diversity gain. Let us now introduce the principles of SC-SFBC in a double-codeword SU-MIMO/collocated MU-MIMO scenario.

Space-time block codes, like the Alamouti orthogonal design for example, were conceived to ensure full spatial diversity, $N_{\text{Tx}} \times N_{\text{Rx}}$, with very low complexity separate decoding. In this case, the multiple antennas are used to improve the performance at a given throughput, making use of the diversity gain. The drawback of such schemes is their low (SISO-like) maximum transmission rate.

On another hand, the use of multiple antennas can be translated in increasing the capacity of MIMO channels. The aim is to increase the throughput with respect to SISO channels for the same target performance, measured, *e.g.*, by means of Frame Error Rate (FER). The maximum transmission rate which can be achieved is $\min(N_{\text{Tx}},N_{\text{Rx}})$ symbols per channel use. Assuming in uplink a number of antennas larger at the base station than at the terminal, this means a maximum transmission rate N_{Tx} times higher than the SISO data rate. The simplest approach to achieve this maximum throughput is to demultiplex the data stream into N_{Tx} parallel streams, and transmit one independent stream per transmit antenna. This technique is called spatial multiplexing. Many space-time architectures based on this idea were developed, as for example V-BLAST (Vertical Bell Labs Layered Space-Time architecture), D-BLAST (Diagonal BLAST) or Turbo-BLAST. Obviously, this extra throughput is obtained at the expense of sacrificing some diversity. Generally, these types of systems achieve a diversity gain in the order of N_{Rx}.

To combine transmit diversity techniques with spatial multiplexing, the main idea consists in splitting the N_{Tx} transmit antennas into K groups. The input data stream will be divided into K parallel data sub-streams, each sub-stream being encoded according to a transmit diversity technique (*e.g.*, SC-SFBC) in order to achieve the maximum diversity for each group of antennas. The transmission of the K transmit-diversity codes is done simultaneously, each code representing therefore interference for the other K-1 codes. The receiver should be able to decode each sub-stream, while minimizing the effects of the other interfering sub-streams.

We will treat here a case where an MS is equipped with $N_{\text{Tx}} = 4$ transmit antennas, split in $K = 2$ groups of 2 antennas each. The transmit diversity technique employed by each group of 2 antennas is an orthogonal block code, as, for example, Alamouti-based SFBC. The generator matrix of this code can be expressed as:

$$\mathcal{A}^{\text{dA}} = \begin{pmatrix} a_0 & -a_1^* & a_2 & -a_3^* \\ a_1 & a_0^* & a_3 & a_2^* \end{pmatrix} \begin{matrix} \leftarrow t_0 \text{ or } f_{k_0} \\ \leftarrow t_1 \text{ or } f_{k_1} \end{matrix}$$
$$\begin{matrix} \uparrow & \uparrow & \uparrow & \uparrow \\ \text{Tx}_0 & \text{Tx}_1 & \text{Tx}_2 & \text{Tx}_3 \end{matrix}$$

This type of code is sometimes called double Space Time Transmit Diversity (STTD) [Hot03], or product STBC [TJC99], when applied in the time domain. Since we also treat here of codes

implemented in the frequency domain, we will employ the generic term of double Alamouti, which can take the form of double STBC, double SFBC or double SC-SFBC respectively.

When employed in an SC-FDMA transmitter, the double Alamouti scheme is implemented as in Figure 4.14. In a Double Codeword (DCW) SU-MIMO/MU-MIMO scenario, sub-streams $\mathbf{x}$ and $\mathbf{x}'$ would contain modulation symbols generated from separate Forward Error Correction code (FEC) codewords.

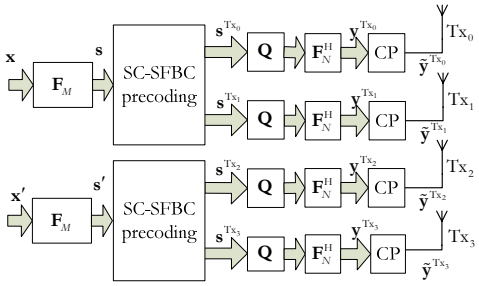

Figure 4.14: Block diagram of a DCW SU-MIMO/MU-MIMO SC-FDMA transmitter employing combined spatial multiplexing and SC-SFBC block coding.

To implement double SC-SFBC, we will need to choose the indeterminates in the generator matrix of the code as being:

$$a_m = \begin{cases} s_{k_m}, \text{ if } m = 0,1 \\ s'_{k_{m \bmod 2}}, \text{ if } m = 2,3 \end{cases}.$$

(k_0, k_1) are chosen according to $k_1 = (p - 1 - k_0) \bmod M$, so as to correspond to SC-SFBC transmit diversity scheme, as explained in the previous subsection.

If two users with the same spectral allocation wish to share the same band, using SC-SFBC each, this can be simply done as schematically shown in Figure 4.15. The only restriction is for them to use the same *p* parameter, which results in a MU double SC-SFBC scheme, as in Figure 4.15.

Let us now investigate the performance of such a scheme. Let us consider a SC-FDMA system with *N* = 512 subcarriers, among which 300 are active data carriers, to fit a bandwidth of 5 MHz. To retrieve frequency diversity, groups of 12 SC-FDMA symbols with Quaternary Phase Shift Keying (QPSK) or 16 Quadrature Amplitude Modulation (16QAM) signal mapping are encoded together with a rate-1/2 or rate 1/3 turbo code using the LTE interleaving pattern [3GPP36211]. A cyclic prefix with a length of 36 samples is employed. We consider an uncorrelated Vehicular A MIMO channel with 6 taps and a maximum delay spread of 2.51 μs [3GPP25996]. Localized subcarrier mapping and ideal channel estimation are assumed. We employ MMSE detection.

MMSE detection with low complexity can be used in this case. Indeed, we can identify pairs of subcarriers of index (k_0, k_1) carrying double Alamouti pairs. If we consider $\mathbf{H}_k = \left[H_{n_{\mathrm{Rx}}, n_{\mathrm{Tx}}, k} \right]$, with $n_{\mathrm{Rx}} = 0 \ldots N_{\mathrm{Rx}} - 1$ and $n_{\mathrm{Tx}} = 0 \ldots 3$, and:

$$\mathbf{H}_{(k_0,k_1)} = \begin{bmatrix} & \mathbf{H}_{k_0} & \\ \mathbf{H}^*_{k_1} & \begin{bmatrix} 0 & -1 \\ 1 & 0 \end{bmatrix} & \mathbf{0}_2 \\ & \mathbf{0}_2 & \begin{bmatrix} 0 & -1 \\ 1 & 0 \end{bmatrix} \end{bmatrix},$$

we can state that the estimates of the transmitted frequency samples can be written as:

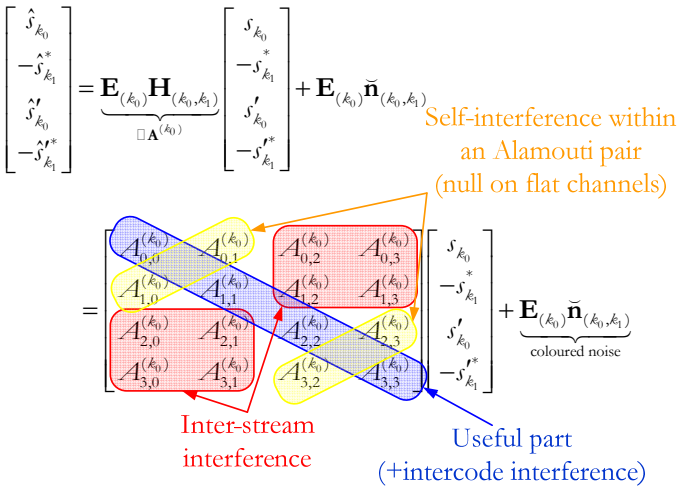

The MMSE equalizing matrix $\mathbf{E}_{(k_0,k_1)}$ can be expressed as:

$$\mathbf{E}_{(k_0,k_1)} = \left(\mathbf{H}^{\mathrm{H}}_{(k_0,k_1)}\mathbf{H}_{(k_0,k_1)} + \sigma^2\mathbf{I}_4\right)^{-1}\mathbf{H}^{\mathrm{H}}_{(k_0,k_1)}.$$

After splitting the two Alamouti streams, the decoding process can continue as in normal SC-FDMA detection. The diagonal (blue) term, stressing out the interference composants, gives rise to the useful signal and (after per-subcarrier equalization and size-*M* IDFT deprecoding) to an intercode interference term. A self-interference term due to precoding onto different subcarriers (yellow) also appears, which becomes null on flat channels (or for STBC with stationary channel). A third term appears (red), representing the inter-stream interference between the two Alamouti pairs sent in parallel. This term has the most important part in the interference balance, since each Alamouti stream represents for the other an interference with the same power as the useful signal.

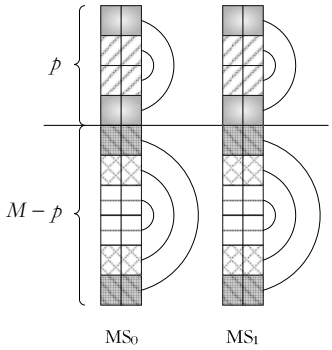

Figure 4.15: Double SC-SFBC with the same spectral allocation.

Performance results and future steps

A simple MMSE detector is able to decode the double Alamouti stream, but the MU case experiences performance degradation with respect to the Single User (SU) Single Codeword (SCW) case, as shown in Figure 4.16. The KPI used here is the Frame Error Rate (FER) as defined in [ARTD51].

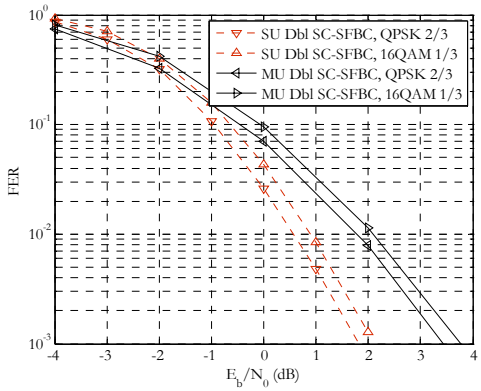

Figure 4.16: SCW SU and DCW SU/MU double SC-SFBC, 4x4; 1RB, 120kmph, ideal channel estimation.

Simulation parameters are summarized in the Table 4.5 below:

Table 4.5: Simulation parameters

Simulation Parameter	Value
Transmission bandwidth	5MHz
Number of subcarriers (N_{FFT})	512
Maximum number of data subcarriers (M_{max})	300
Number of allocated subcarriers (M)	12
Signal mapping	QPSK, 16QAM
FEC coding	Turbo code 1/3, 2/3
Number of transmit antennas (N_{Tx})	4
Number of receive antennas (N_{Rx})	4
Channel type	3GPP Typical Urban
Channel estimation	Ideal
Velocity	120kmph

For simplification, SU SCW is simply denoted by SU, while SU DCW/MU is simply denoted by MU in the legend. MMSE detection is suboptimal in reducing the interference between the two Alamouti streams. While in the SU case the outer turbo code manages to significantly reduce the residual interference after MMSE detection, the MU scheme does not benefit from any joint coding. To improve the MU performance, more complex detectors are needed.

In practice different users might have different communication needs and thus be allocated different bandwidths. This will result in a mismatch between the structures of their respective SC-SFBCs and an interference problem will arise. This will be treated in [ARTD13].

4.2 - Multi-cell MU-MIMO schemes

In this section, we consider some proposed joint processing methods across eNBs, in which a set of cooperating base stations is identified. In addition, also a coordinated beamforming scheme is considered, where the cooperating base stations need fast exchange of the CSIT but not of the user data. In the downlink of JP CoMP, the cooperating bases share the CSI as well as the user data. In doing so, joint processing schemes mimic MIMO methods and can help alleviate interference. Although the strong analogy with MIMO techniques provides us with a good understanding of the possible precoding methods, such as: linear beamforming, ZF, MMSE, non linear approaches based on Dirty Paper Coding (DPC), a number of important issues should be tackled. These issues include specifically:

- The system level evaluation and comparison of state of the art CoMP schemes.
- The development of distributed techniques allowing to reduce the need for information exchange. This problem is addressed in several different ways
    - Use of thresholding methods to dynamically reduce the size of the cooperating cluster.
    - Use of hierarchical feedback design in order to allow for multi-level decoding of the CSIT.
    - Design of beamforming schemes which adapt to partial levels of sharing of the user data.
- Robustness with respect to CSI feedback errors and tracking. Several robust schemes are developed exploiting the knowledge of the estimation and feedback error statistics.
- Development of beamforming methods which are able to cope with independent CSI at the cooperating eNBs, i.e. distributed processing.
- Power control for the JP CoMP schemes, subject to per base power constraint, for the frequency selective channels based on OFDM.

4.2.1 - Dynamic Joint Processing

Joint processing between different base stations, or inter-site JP, promises high spectral efficiency under idealized assumptions. How much of these gains remain in more realistic scenarios is still an open question. The main challenges to bring inter-site JP to reality, particularly in DL, are the following:

- How to obtain the CSI from the users. JP can be implemented using centralized or distributed approaches, with CSI requirements ranging from global CSI to local CSI with proper granularity to be available at each base station (see section 3.2). Centralized schemes, though theoretically optimal for a certain performance metric (e.g., spectral efficiency), require global and perfect CSI to be made available at a CCN for the design of joint multi-cell multi-user MIMO schemes. In this framework, the total overhead introduced may decrease the overall gains perceived. Distributed approaches alleviate the overhead requirements, but they suffer from CSI impairments, e.g., the estimates of CSI may differ amongst base stations.
- How to distribute the CSI, scheduling information and user data between base stations. The design and capacity of the backhaul network is crucial, along with the design of the distribution and buffering scheme of the user data.
- Sensitivity to impairments: schemes requiring coherent reception at the UE are highly sensitive to impairments (outdated or delayed CSI, partial CSI, non-ideal synchronization, etc).

Clustering techniques, which define subsets of base stations for cooperation, and thus reduce the range where information should be exchanged, have been recently proposed to mitigate the above problems without compromising the performance. JP is then performed within each cluster and the overhead requirements are reduced with respect to a globally coordinated network. However, backhauling and signalling requirements can be decreased further by exploring the potential of *dynamic joint processing schemes*.

In general, current JP schemes are designed assuming static environments, i.e., a scheme remains fixed for a given cluster area and a set of CoMP *served* users. In a real scenario, the mobility of the users directly impacts the statistics of the interference in the cluster, and hence, the cluster of base stations should be able to dynamically adapt the JP scheme to fulfil each user requirements, with minimum use of available resources, e.g., backhaul or feedback load. In addition, user grouping should be used to serve with JP only those users that benefit from the scheme, depending on their current location and required services. Dynamic modes are defined to achieve this goal. In our case, the modes considered are: fully centralized, partial, distributed JP or the conventional single-cell transmission [BSX+10].

System description of the innovation

Under the assumption of a centralized coordination, JP in the DL can be seen as an extension to multi-cell of a MU-MIMO DL system, where the antennas at the transmitter are spatially distributed between several transmitting points or cells. From this point of view, well-known MU-MIMO techniques can be applied, e.g. DPC, block diagonalization, etc. One of the main differences between JP and MU-MIMO is the fact that the power constraint is applied separately in each cell, which can be thought of as applying per-antenna (in an array) power constraints in the MU-MIMO case. This change in the power constraint highly influences the design of the algorithms or schemes. In addition, the channels from several base stations present different properties when compared to channels from the antennas of a single antenna array.

In this activity, the objective is to design a dynamic JP scheme, based on three basic approaches, centralized, partial and distributed JP, including also the case of no JP or conventional single-base transmission. We consider a static cluster of K base stations, each one equipped with Nt antennas, where M single-antenna users are using a particular orthogonal dimension. The centralized, partial and distributed JP schemes establish different degrees or stages of JP between the base stations in the cluster. A linear precoder based on zero-forcing is considered. The available transmission power at each base station is assumed to be limited by a maximum value $P_{\max}$. For simplicity, intercluster interference is not included in the system model and simulations. Under these assumptions, the received signals at the M users can be expressed in vector notation as

$$\mathbf{y} = \mathbf{HW}\sqrt{\mathbf{P}}\mathbf{s} + \mathbf{n},$$

where the matrix $\mathbf{W} \in C^{K \cdot Nt \times M}$ includes the beamformers designed for each of the users, $\mathbf{w}_m \in C^{K \cdot Nt \times 1}$, and the matrix $\mathbf{H} \in C^{M \times K \cdot Nt}$ includes the channels between each user and all the base stations in the cluster, $\mathbf{h}_m \in C^{1 \times K \cdot Nt}$. Note that $C^{m \times n}$ denotes the set of $m \times n$ complex matrices. Matrix $\sqrt{\mathbf{P}}$ is a diagonal matrix given by [ZD04]

$$\sqrt{\mathbf{P}} = \left\{ \min_{k=1,\ldots,K} \sqrt{\frac{P_{\max}}{\left\| \mathbf{W}^{(k)} \right\|_F^2}} \right\} \cdot \mathbf{I}_{[M \times M]},$$

where $\mathbf{W}^{(k)}$ are the rows of matrix $\mathbf{W}$ related to the *k*th base station, and $\|\cdot\|_F$ stands for the Frobenius norm. This power allocation is suboptimal, since it typically results in only one base station meeting the maximum transmitted power requirement with equality. Vector $\mathbf{s}$ includes the user information symbols s_m, $m = 1,\ldots,M$, and $\mathbf{n}$ is the receiver noise. Assuming coherent reception at the user, the average sum-rate per cell is given by

$$SR = \frac{1}{K} E_H \left[\sum_{m=1}^{M} \log_2 \left(1 + \mathrm{SINR}_m \right) \right].$$

Centralized Joint Processing (CJP)

In the Centralized Joint Processing (CJP) scheme, global CSI is available at the transmitter side, and the base stations included in the cluster jointly perform the power allocation and the

design of the transmit beamformers. This scheme relies on a CCN, which could be located in one of the base stations or in a dedicated network node. The drawback with the CJP scheme is that a large overhead is introduced due to the required feedback from the users (each user feeds back the estimated CSI related to all the base stations in the cluster to its serving base station) and the information exchange between the base stations/CCN (which includes CSI, user data and precoding weights). Assuming that $K \cdot Nt \geq M$, the intra-cluster interference is completely removed with a joint zero-forcing beamforming design

$$\mathbf{W}_{CJP} = \mathbf{H}^H \left(\mathbf{H}\mathbf{H}^H \right)^{-1},$$

which is the pseudo-inverse of the channel matrix.

Partial Joint Processing (PJP)

The Partial Joint Processing (PJP) scheme is a particular case of the CJP scheme, which allows different degrees or stages of JP between base stations. The PJP scheme dynamically defines active sets or *subclusters* of base stations for each user in the cluster area. Hence, it results in the formation of M overlapping subclusters inside the static cluster of K base stations, one per user. Note that the M subclusters can be formed by different number of base stations.

To form the serving subcluster for a given user, a threshold-based approach is used [PBG+04]. The user estimates the average gain of the received channels, one from each base station, and defines its reference link or strongest channel, associated to a given base station (usually the serving base station). Then, the user compares the channel gains related to the remaining base stations with the reference link, and includes these base stations in its active set/subcluster only if their channel gains are above a relative threshold, with respect to the strongest channel. The threshold value is specified by the cluster (at CCN level).

The outcome of the PJP scheme for a given active set threshold value can be represented using a thresholding matrix $\mathbf{T}$, of dimensions $[M \times K]$. The *(m,k)-th* element of this matrix is set to '1' if the link between user *m* and base station *k* is active (falls within the active set threshold), and to '0' if the link is inactive. Then, each user only feeds back the CSI information related to the active channels, reducing the amount of feedback load of the cluster. Note that a similar approach has been proposed in [PBG+10].

The PJP scheme introduces multi-user interference in the system, since less CSI is available at the CCN for the design of the transmit beamformers, and no specific techniques to mitigate the interference between the overlapping subclusters are currently used. The joint partial zero-forcing beamformer is designed as follows [LBS+10]

$$\mathbf{W}_{PJP} = \mathbf{S}^H \left(\mathbf{G} + \overline{\mathbf{R}} \right)^{-1},$$

where matrix $\mathbf{S} \in C^{M \times K \cdot Nt}$ is the useful channel matrix, $\mathbf{G} \in R^{M \times M}$ is a diagonal channel scaling matrix and $\overline{\mathbf{R}}$ stands for the off-diagonal elements of the channel correlation matrix, $\mathbf{R} \in C^{M \times M}$. This expression for the joint partial zero-forcing beamformer, based on [WWK+09], is built over the concepts of useful channels and significant interference channels, given in this case by the active and inactive links of matrix $\mathbf{T}$. Matrix $\mathbf{S}$ is defined as

$$\mathbf{S} = \left[\mathbf{T} \otimes \mathbf{1}_{Nt} \right] \bullet \mathbf{H},$$

where $\otimes$ stands for the Kronecker product, $\mathbf{1}_{Nt}$ is an all ones Nt row vector and $\bullet$ is the element-wise multiplication operation. The channel scaling matrix $\mathbf{G}$ is a diagonal matrix, where each element in the main diagonal is given by

$$\mathbf{G}_{(m,m)} = \left(\mathbf{S}\mathbf{S}^H \right)_{(m,m)}.$$

The channel correlation matrix $\mathbf{R} \in C^{M \times M}$ is formed using the useful channel matrix $\mathbf{S}$ and the interference channel matrices $\mathbf{V}_m \in C^{M \times K \cdot Nt}$ ($m = 1, \ldots, M$)

$$\mathbf{R} = \left(\mathbf{V}_1 \mathbf{S}^H_{(1,:)} \quad \cdots \quad \mathbf{V}_M \mathbf{S}^H_{(\mathrm{M},:)} \right),$$

where $\mathbf{S}_{(m,:)}$ stands for the *m*th row of matrix $\mathbf{S}$. The interference channel matrices $\mathbf{V}_m$ represent the amount of interference caused due to the transmission to the *m*th user in the cluster

$$\mathbf{V}_m = \left[\mathbf{T}_m \otimes \mathbf{1}_{Nt}\right] \bullet \mathbf{H}.$$

In the above expression, matrix $\mathbf{T}_m$ is built for the *m*th user taking as a reference the matrix of active links $\mathbf{T}$. In a first step, $\mathbf{T}_m = \mathbf{T}$. Then, the elements that do not have any significance from an interference-sense, are set to zero [WWK+09]. These are the elements in the *m*th row of the matrix $\mathbf{T}_m$, $\left(\mathbf{T}_m\right)_{(m,:)} = \mathbf{0}_K$ (since the transmission to the *m*th user does not introduce interference to the user itself), and the elements of the column in $\mathbf{T}_m$ where you can find an inactive link in the *m*th row of matrix $\mathbf{T}$, that is, $\left(\mathbf{T}_m\right)_{(:,k)} = \mathbf{0}_M$, when $\mathbf{T}_{(m,k)} = 0$.

The expression of the joint partial zero-forcing beamformer, $\mathbf{W}_{PJP}$, may seem similar as computing the pseudo-inverse of the useful channel matrix $\mathbf{S}$. However, the joint partial zero-forcing beamformer gives slightly better performance, since it is explicitly designed to remove the interference of the 'significant' channels.

As pointed out in [PBG+10], when computing the pseudo-inverse of a sparse matrix (for example, matrix $\mathbf{S}$ for a conventional joint zero-forcing beamformer based on the actual fed back CSI information), it is difficult to predict a priori the positions of the elements that will be equal to zero. For a given user, non-zero elements in the beamforming matrix may imply that a user data needs to be available in base stations whose links were marked as inactive, i.e., outside the active set of base stations of the user. In other words, the reduction in the backhaul exchange in terms of exchange of user data is not equal to the reduction achieved in the feedback, and some additional mechanisms are required to meet this constraint. In the case of the PJP scheme, once $\mathbf{W}_{PJP}$ is computed, we explicitly null the weights of the base stations that are outside the active set or subcluster of the user. This suboptimal approach gives a lower bound in the sum-rate achieved with the PJP scheme.

Distributed Joint Processing (DJP)

In the Distributed Joint Processing (DJP) scheme, base stations are only aware of their local CSI. The transmit beamformer and power allocation are locally implemented at each base station, and then, the cardinality of the set of spatially separated users that can be served by each base station in the cluster is reduced to Nt. In this framework, the problem of assigning users to base stations under a JP assumption arises [SGH08]. In this case, each base station serves the Nt users with the highest channel gain, and a user may be scheduled for transmission in more than one base station (joint processing) depending on its given channel conditions. With this approach, a certain number of users in the cluster may remain without service and some fairness mechanism would be additionally required. However, this can be easily solved by exploiting many parallel channels in the case of multicarrier systems. The zero-forcing beamformer is obtained in each base station *k* as

$$\mathbf{W}_{DJP}^{k} = \mathbf{H}_k^H \left(\mathbf{H}_k \mathbf{H}_k^H\right)^{-1},$$

where $\mathbf{H}_k \in C^{M \times Nt}$ includes the local channels between base station *k* and the served users. The power available at the base station is equally assigned to the served users. Note that the allocation of users to base stations can be performed assuming a CCN or in a decentralized manner (exchanging the local CSI between base stations), resulting in different robustness capabilities when facing imperfect CSI.

Performance results and future steps

The simulations are based on the WINNER II channel model [WIN2D112], scenario B1. We consider a static cluster of 3 base stations, with 3 antennas each, and with a cell radius of 500 m (see Figure 4.17). To cover all the cluster area, 6 single-antenna users are dropped at 54 predefined positions over the cluster layout, along a uniform distribution following an ellipse around each position. 500 independent channel realizations are evaluated in each predefined

position over the cluster, and the cell edge SNR is set to 15 dB. In these simulations, we do not take advantage of the frequency diversity. Thus, the active sets or subclusters of base stations are defined based on an average over all the resource blocks (256 resource blocks are defined). As we are concerned with an interference limited system, all the users are scheduled in every resource block.

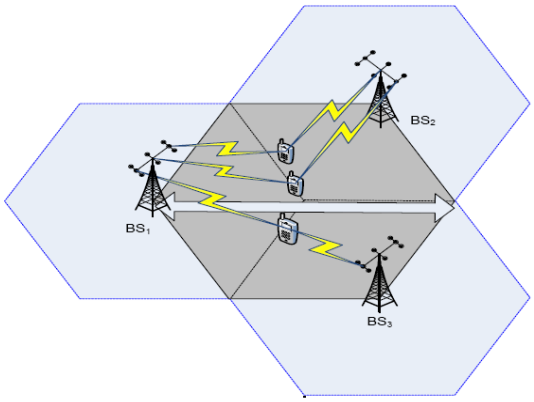

Figure 4.17: Cluster layout.

Table 4.6: Simulation parameters

Simulation Parameter	Value
Number of base stations	3
Number of users	6
Number of antennas at each base station	3
Number of antennas at each user	1
Antenna type at the base station	Uniform Linear Array
Antenna spacing	4λ
Number of channel realizations at each position	500
Centre frequency	2 GHz
Channel Model	Winner II, scenario B1
Cell radius	500 m
Number of resource blocks	256

The performance of the CJP, PJP and DJP schemes as independent and stand-alone operation modes has been previously evaluated for flat and frequency selective fading channels ([BSX+10] and [LBS+10], respectively). Figure 4.18 shows the average sum-rate per cell per resource block achieved by the different schemes under the simulation assumptions of Table 4.6. In the PJP scheme, four values of the active set threshold are considered, 5, 10, 20 and 40 dB. The case in which the best 2 base stations (BS) transmit to each user is included for comparison and denoted as '2BSs'. We consider a subset of the predefined positions that forms a line from base station 1 towards the cluster centre and towards the cell edge of base station 2 and 3 (see Figure 4.17). Note that the main difference of this plot with respect to the one in [LBS+10] is that in this case, we explicitly null the weights of the PJP scheme related to base stations outside the active set of a user (in case they are not equal to zero). In addition, all the schemes are simulated fixing a common total transmitted power per base station.

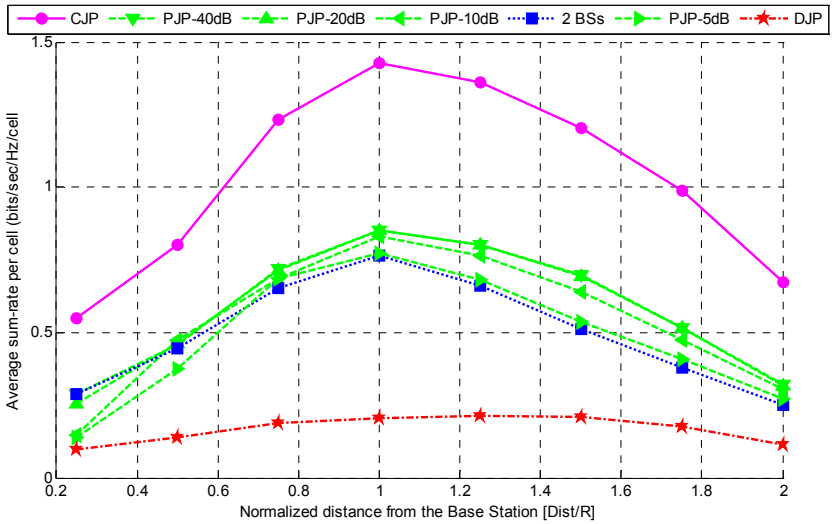

Figure 4.18: Average sum-rate per cell per resource block vs. normalized distance from base station 1 (non-adaptive frequency thresholding is considered for PJP).

One of the KPI defined in ARTIST4G is the mean user throughput. Figure 4.18 can be related to this KPI just dividing the results of the CJP and PJP schemes by the number of users served (6 in each point). However, in the case of the DJP scheme, since there is a probability of outage and all the users may not be served, this method would give a lower bound.

We are now interested in defining a dynamic JP scheme encompassing different dynamic modes. To achieve this, the first step is to define under which conditions it is not possible to use each one of them. For example, the joint partial zero-forcing beamformer suffers from rank deficiency problems when trying to invert $\mathbf{Q} = \mathbf{G} + \overline{\mathbf{R}}$ for low values of the active set threshold and users located close to a base station. Based on this, it is possible to define *cooperation areas* over the cluster where the PJP scheme with a given value of the active set threshold is feasible.

Figure 4.19 shows the cooperation areas of the PJP scheme for active set threshold values of 10, 15 and 20 dB. To define each cooperation area, the area in which the PJP scheme is feasible in 90% of the channel realizations has been considered.

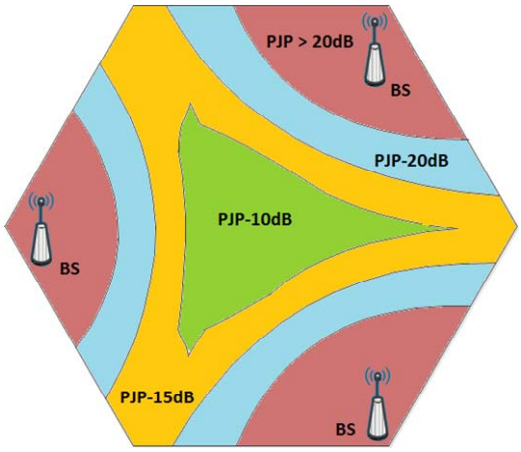

Figure 4.19: Definition of cooperation areas over a static cluster of 3 base stations for the PJP scheme with different AS thresholds (10, 15 and 20 dB).

Based on these results, it is possible to define a first version of a dynamic JP algorithm. Assume that the active set threshold value is set to 10 dB, and a user is located in the 15 dB cooperation

area. In this case, this user cannot be served with the PJP scheme and 10 dB active set threshold, and the cluster should switch to a 15 dB threshold, or use the DJP, CJP or conventional single-base transmission modes (for example, depending on other variables such as backhaul availability).

The objective is to design a truly dynamic JP scheme. This could be done, for example, using different performance metrics as input to define the switching points or operation regions of the schemes. The definition of cooperation areas for the PJP scheme presented in Figure 4.19 helps to understand where the PJP scheme can be applied, but similar results are needed for the DJP scheme. One important input for designing the dynamic JP scheme could be given by the amount of intra-cluster interference introduced by the PJP and DJP schemes. Figure 4.18 shows that the evaluated schemes can improve the average sum-rate in the cell edge, thus achieving a higher uniformity of the performance over the served area. However, users located close to a base station may benefit from conventional single base station transmission, which would contribute to increase the uniformity of the average sum-rate per cell over the considered area. In future works, the Jain Index as one of the main ARTIST4G KPI will be evaluated [ARTD51].

Currently, the active set threshold is not optimized with respect to the feedback load or service outage probability. Moreover, the active set threshold could also be optimized depending on each user conditions. For example, in frequency selective channels, the optimization could be independently performed per resource block.

The JP schemes considered as dynamic modes require strong synchronization mechanisms to ensure coherent reception at the user. One of the activities will address the impact in the dynamic JP scheme of imperfect CSI, especially the effects of non-coherent reception at the user, which will be one of the main impairments in the DJP approach. In further steps, adaptive backhaul availability will be also considered in the design of the dynamic JP scheme.

4.2.2 - Centralized/decentralized joint transmission with limited signalling information

The connection between two coordinated base stations for joint processing CoMP is assumed to be physically implemented via wired fiber lines, where at least one router has to be passed. According to the number of passed routers, the delay can be in the range of 10 ms. Note, that the 50% coherence time of 10 ms is reached at a UE speed of 7 km/h, for a mobile communication system with a center frequency of 2.6 GHz. With increasing UE, the CSIT becomes more uncorrelated with the actual channel. In these circumstances, the performance of joint transmission intensely degrades compared to a static channel. To reduce the delay for distributing CSI among base stations, directive radio links can be installed, if they are in line of sight. Compared to distributing CSI via the wired core network, no further routing is necessary and small delay times can be achieved, as they are known for inner-cell feedback. Using the same frequency spectrum for serving UEs and distributing CSI, the system interference is increased. Therefore, it might be reasonable to reduce the interference introduced by the directive radio connections. This can be achieved if CSI is more compressed as for the inner-cell feedback. In this case, every base station has a different CSIT version. For our analysis, we assume that connections of the core network are unrestricted in rate but possess high latency. Since it is mathematically equivalent with a scheme where CSIT from all base stations is collected at a central point, which computes the precoding matrices and feed them back to all base stations, we call this scheme centralized. The equivalence holds, because precoding matrices are transmitted uncompressed to the eNBs, due to the unlimited rate. This allows an abstraction from the location of the processing. The case where eNBs are connected via direct connections is called decentralized, because precoding decisions have to be done at the eNBs individually. According to the nomenclature of section 3.2 we call that case distributed once CSI exchange via direct connections leads to further compression, so that every eNB possess an individual CSI version. The tradeoff between the both mentioned schemes will be analyzed according to the time variance of the small scale fading. Both CSI distribution methods are illustrated in Figure 4.20. Basically, this evaluation compares the influence of backhaul restrictions in rate with restrictions in latency.

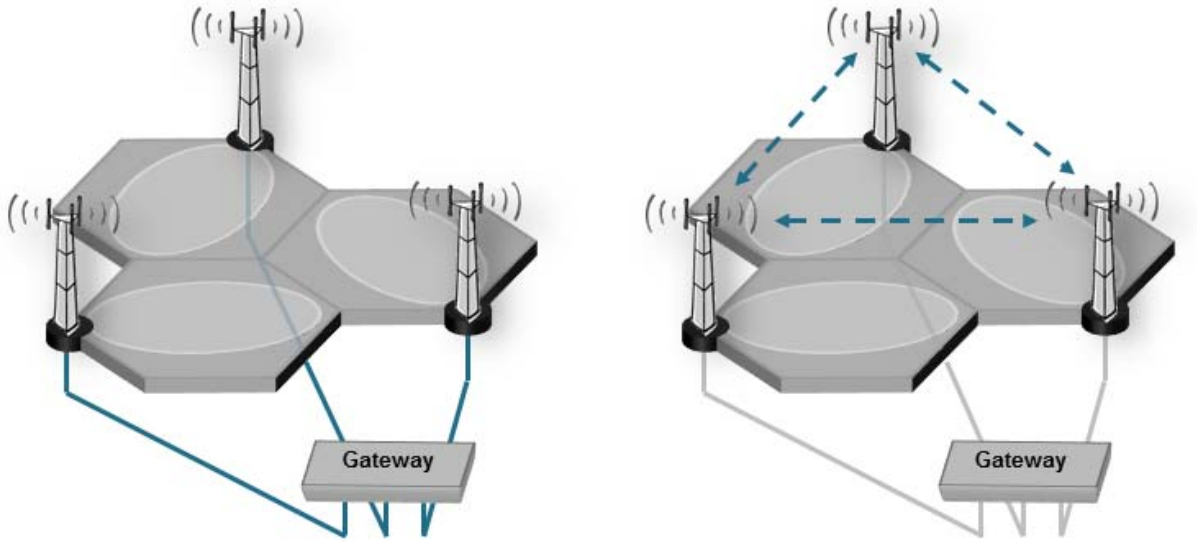

Figure 4.20: Comparison of the centralized and decentralized CSI distribution. The blue arrows describe the flow of the CSI.

System description of the innovation

The modelling of the CSI uncertainty is based on a SISO downlink transmission of one resource block. The actual data transmission is modeled afterwards for a multi-cell MU-MIMO system, where the CSIT at the eNBs is corrupted by an additive Gaussian noise term, whose variance is derived from the CSI uncertainty model. The principle closed loop including the data transmission as well as the feedback chain for making CSI available at the eNBs is illustrated in Figure 4.21.

For the modeling we consider impairments due to channel estimation, prediction, interpolation, quantization and compression.

For channel estimation an MMSE estimator is applied. The channel estimates between the scattered pilot positions are interpolated based on the knowledge of the covariance matrix

$$\mathbf{\Phi}_{\mathrm{hh}}[T] = \mathrm{E}\{\mathbf{h}[t]\mathbf{h}^{H}[t+T]\} = \sigma_{\mathrm{h}}^{2} \cdot \Pi_{t}[T] \otimes \Pi_{f}$$

of the channel $\mathbf{h}[t] \in C^{[N_C N_S \times 1]}$, where t is the index of the resource block that will be transmitted at the time this channel occure, The resource block consists of N_S symbols and N_C subcarriers. The elements of $\mathbf{h}[t]$ are Gaussian distributed with zero mean and variance σ_{h}^{2}. Furthermore,

$$[\Pi_{t}[T]]_{i,j} = J_{0}\left\{2\pi \frac{f_D}{f_S}(TN_S + j - i)\right\}$$

denotes the correlation in time and

$$\left[\Pi_{f}\right]_{i,j} = \mathrm{si}\{2\pi D \Delta F(j-i)\}$$

the correlation in frequency. Here, f_D, f_S, D and ΔF denotes the maximum Doppler frequency, the symbol rate, the maximum delay spread and the subcarrier spacing, respectively.

The channel prediction is also based on that statistical knowledge, which differs from Kalman filtering. The predictor we assume minimizes the MSE between the predicted channel and the actual channel at this time.

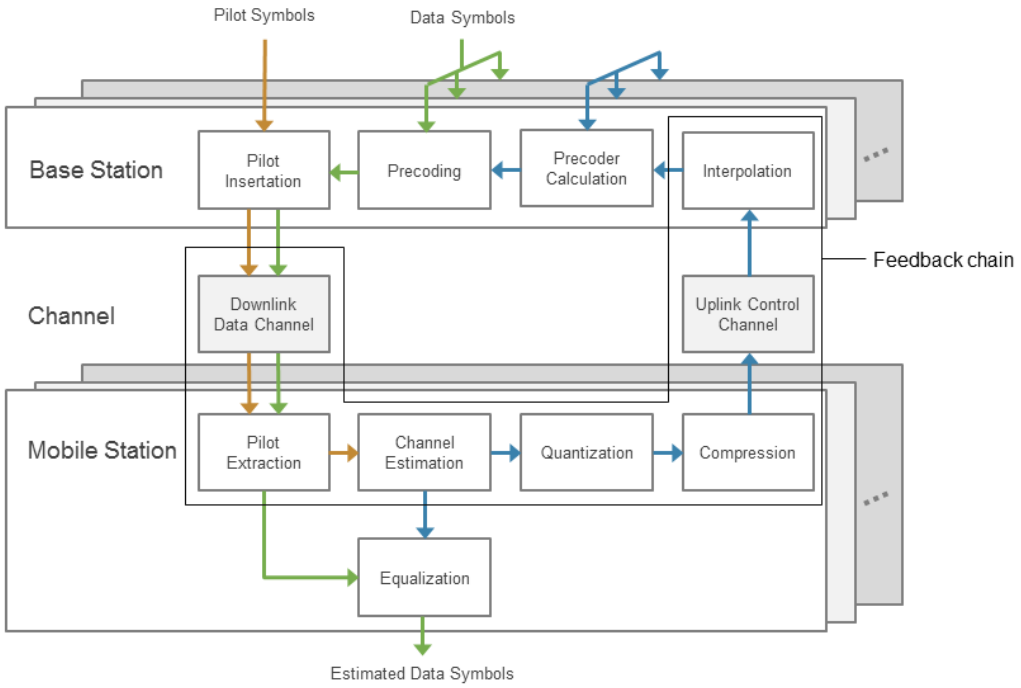

Figure 4.21: Closed loop of data transmission and CSI feedback.

The quantization with N_q bits is modelled by an additive Gaussian noise due to rate distortion theory. At the eNB side the CSI is decompressed to obtain channel knowledge for every resource element of the resource block.

The CSI uncertainty arising by the presented feedback chain can be modelled by adding a Gaussian random variable to the actual channel:

$$\hat{\mathbf{h}}[t] = \mathbf{h}[t] + \mathbf{e}[T, N_q].$$

Since $\mathbf{e}[T, N_q]$ is not uncorrelated with $\mathbf{h}[t]$ it can be split into the uncorrelated part $\tilde{\mathbf{e}}[T, N_q]$ and the correlated part $\mathbf{A}[T]\mathbf{h}[t]$, where $\mathbf{A}[T]$ is a diagonal scaling matrix. This leads to the impairment model

$$\hat{\mathbf{h}}[t] = (\mathbf{I} - \mathbf{A}[T])\mathbf{h}[t] + \tilde{\mathbf{e}}[T, N_q].$$

Both parts can be obtained by calculating the cross correlation of the predicted CSIT and the actual channel from the feedback model and the impairment model.

For applying this model to the centralized and decentralized CSI distribution the precoding matrix is calculated by different CSI versions, respectively. In the centralized scheme a higher delay T is assumed, where for the decentralized case a further CSI compression due to a smaller backhaul rate results in smaller values of N_q for the CSI of users from neighboring cells. A CSIT matrix in spatial domain of a single resource element available at eNB $n \in \{1,...,N\}$ is expressed as $\hat{\mathbf{H}}[n] = \left[\hat{\mathbf{H}}_1^T[n],...,\hat{\mathbf{H}}_M^T[n]\right]^T$, where N is the number of participating eNBs and M is the number of UEs. For every eNB n the set L_n includes the indexes of UEs assigned to eNB n. Note that a UE can only be assigned to a single eNB. CSIT available at eNB n is modeled by $\hat{\mathbf{H}}[n] = \mathbf{H} + \mathbf{E}[n]$, with $\mathbf{E}[n] = \left[\mathbf{e}_1^T[n],...,\mathbf{e}_M^T[n]\right]^T$. The impairment of CSIT obtained from inner-cell UEs is $\mathbf{e}_m[n] \sim N_C\left(0, \mathbf{\Phi}_{ee}[T, N_{q,FB}]\right)$, such from UEs of neighboring cells is

$\mathbf{e}_{\bar{m}}[n] \sim N_C\left(0, \mathbf{\Phi}_{ee}\left[T, N_{q,BH}\right]\right)$, where $m \in L_n$ and $\bar{m} \notin L_n$. For the comparison of centralized and decentralized CSI distribution the quantities T, $N_{q,FB}$ and $N_{q,BH}$ are marked with the superscript C and D, respectively. Note that due to no restriction in backhaul rate for the centralized scheme $N_{q,BH}^{C} = N_{q,FB}^{C}$.

For a first analysis a simple zero-forcing precoding scheme is used. The basic zero-forcing matrix is obtained by the moore-penrose inverse

$$\tilde{\mathbf{W}}[n] = \left[\tilde{\mathbf{W}}_1^T[n], ..., \tilde{\mathbf{W}}_N^T[n]\right]^T = \hat{\mathbf{H}}^H[n]\left(\hat{\mathbf{H}}[n]\hat{\mathbf{H}}^H[n]\right)^{-1}.$$

To obtain unit column power beamformers per eNB a scaling is executed

$$\mathbf{W}_n[n] = \frac{\tilde{\mathbf{W}}_n[n]}{\sqrt{\mathrm{dg}\left\{\mathrm{dg}\left\{\tilde{\mathbf{W}}_n^H[n]\tilde{\mathbf{W}}_n[n]\right\}\right\}}}.$$

The user power is allocated by

$$\mathbf{P} = \mathrm{blkdg}\left\{\mathbf{P}_1, ..., \mathbf{P}_N\right\},$$

where $\mathbf{P}_n$ is the diagonal power allocation matrix applied to eNB n with $\mathrm{tr}\left\{\mathbf{P}_n\right\} \leq \rho_n$ and ρ_n is the power restriction of eNB n. The transmission equation for the joint transmission results in

$$\hat{\mathbf{d}} = \mathbf{HWP}^{1/2}\mathbf{d} + \mathbf{n},$$

where $\mathbf{d}$, $\hat{\mathbf{d}}$ and $\mathbf{n} \sim N_C\left(0, \sigma_n^2\right)$ is the transmitted symbol vector, the received symbol vector and the additive Gaussian noise, respectively.

Performance results and future steps

For a first evaluation the performance of the joint processing was simulated for certain values of T, $N_{q,FB}$ and $N_{q,BH}$. A reliable assumption is a delay for centralized scheme of $T^C = 8\,ms$ and for the decentralized scheme for $T^D = 4\,ms$. The number of feedback bits for the centralized scheme is set to $N_{q,BH}^{C} = N_{q,FB}^{C} = 20\,bits$ per resource block and for the decentralized scheme $N_{q,FB}^{D} = 20\,bits$ and $N_{q,BH}^{D} = \langle 5\,bits, 10\,bits \rangle$. For a system with $N = M = 3$ and single antenna eNBs and UEs the mean achievable rate is calculated, where the achievable rate of UE k is

$$R_k = \log_2\left(1 + \frac{\left|\left[\mathbf{HWP}^{1/2}\right]_{k,k}\right|^2}{\sum_{l \neq k}\left|\left[\mathbf{HWP}^{1/2}\right]_{k,l}\right|^2 + \sigma_n^2}\right).$$

The power is equally distributed to UEs and every eNB has the same power constraint. Hence, $\mathbf{P} = \rho\mathbf{I}$. The joint transmission itself it not executed for the whole resource block but for a single resource element, where the parameters of impairment to the actual channel is obtained by averaging over the whole block.

We observe from Figure 4.22 that for user velocities greater than $7\,km/h$ the decentralized solution clearly outperforms the centralized one, even if the number of backhaul bits per resource block is 5 compared to $20\,bits$ for the centralized scheme. The results show that the CSI uncertainty is larger when routing through the high latency, high rate core network compared to low latency, low rate connections.

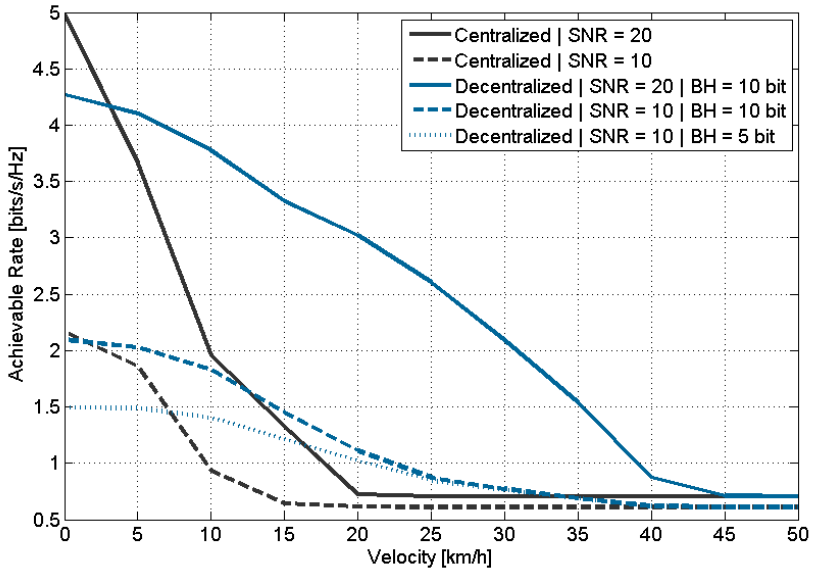

Figure 4.22: Comparison of centralized and decentralized joint transmission

The simulation parameters are chosen according to an LTE system, as shown in Table 4.7.

Table 4.7: Simulation parameters

Simulation Parameter	Value
Number of eNBs	$N = 3$
Number of eNB antennas	$N_b = 1$
Number of UEs	$M = 3$
Number of UE antennas	$M_u = 1$
Feedback delay	$T^D = 4\,ms$
Feedback + backhaul delay	$T^C = 8\,ms$
Carrier Frequency	$f_c = 2,6\,GHz$
Sub-carrier spacing	$\Delta F = 15\,kHz$
Symbol rate	$f_s = 14\,kHz$
Maximum delay spread	$D = 3\,\mu s$

We can conclude that backhaul latency limits the applicability of joint transmission CoMP, even if small user velocities are assumed (in the range of pedestrians). Hence, the application of wireless connections, possessing low latencies can enable to serve moving UEs with higher velocities. Note, that for these simulations the additional interference due to the radio base station connections is not taken into account. That is one aspect that will be investigated in the future of this project.

4.2.3 - Distributed MIMO precoding and partial data sharing

Joint processing of collaborating base stations can improve spectral efficiency as well as cell edge coverage, which leads to an enlargement in user fairness. In this contribution we consider downlink scenarios, where coordinated base stations jointly serve users at cell edge areas. For this purpose user data has to be available at every coordinated eNB (full cooperation). In this case the collaborating eNBs can be combined to a single virtual super eNB. Under the assumption that all participating transmit antennas are located at the super eNB, a joint precoding matrix can be calculated to pre-equalize the transmit symbols. Since the calculation of the precoding matrix is based on CSIT, every UE has to estimate the channels from all eNBs involved in joint transmission. Afterwards complete CSI has to be fed back to the UE specific serving eNB. The CSIT is impaired by channel estimation, quantization and delays. Introducing scattered pilot patterns, interpolation in time, frequency or space can further affect CSI quality.

Considering joint transmission of coordinated eNBs, two basic approaches can be compared. At the first scheme every eNB sends the CSIT received from its assigned UEs to a central unit. Based on the whole CSIT the central unit computes the precoding matrix and sends the respective partition of the matrix back to every eNB. This approach is called centralized. Note that limited backhaul rates can result in further CSI compression. However, equal backhaul limitations between the central unit and every eNB leads to identical precoder versions, available at the eNBs.

Since centralized approaches require a high amount of data traffic, decentralized solutions are a reasonable alternative to reduce signalling information. Considering this approach, CSIT is only exchanged between the involved eNBs. Assuming a further CSIT compression due to limited backhaul rates, every eNB holds a different version of the full CSIT. Based on the available CSIT every base station calculates its precoding matrix independently. Hence different precoding matrix versions are available at the several eNBs. In the previous section 4.2.2, it was shown that the imperfectly shared CSI had a serious impact on system performance.

Therefore, the problem is how to make the choices of precoding matrices at the various eNBs as consistent as possible. This problem is referred to as case 1 below. In case 2, we address the problem of partially sharing the user data in order to reduce the routing overhead of JP CoMP.

System description of the innovation

Case 1: Distributed MIMO precoding

We consider the problem described above of joint MIMO precoding across multiple distant cooperating base stations with different CSIT. In this case a specific feedback architecture is proposed and a robust precoding method is developed. The base stations are assumed to be sharing user data and aim at serving a group of users in a decentralized MIMO fashion. This situation is illustrated in the following Figure 4.23.

In the downlink scenario, implementation of JP CoMP requires both data and CSI to be shared by the transmitters, or to be fed back to some central processor which designs the transmission and informs the base stations of which precoding solutions shall be used. This sharing comes, however, at a cost of delay, feedback and backhaul resources. One way to reduce the delays or have a more efficient use of the backhaul is to reduce how much CSI is shared. Thus, we assume the user data is conveniently routed to all concerned transmitters, but the transmitters obtained local CSIT only (distributed optimization).

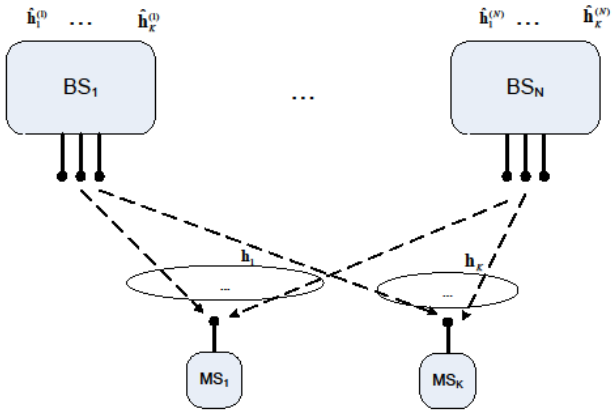

Figure 4.23: Cooperative MIMO channel with imperfect CSIT sharing setup.

The novelty of such setup resides in the fact that the finite accuracy of CSI fed back by the mobiles to the BS is taken into account and, more importantly, the fact that each of the transmitters obtains a possibly different estimate of the same global multi-user channel. Despite not sharing the same vision of the CSI, the transmitters seek to jointly act in a consistent manner in designing the precoders.

Ideally, the different transmitters would have to conciliate their views in order to design a consistent set of precoding vectors that will maximize a performance metric at the user side. This problem falls in the class of so-called Team Decision Theory problems or decentralized statistical decision making problems. More generally, in such problems, i) each decision maker has different but correlated information about the underlying uncertainty in the channel, and ii) the transmitters need to act in a coordinated manner to realize the common payoff (e.g. the average sum rate).

We describe here the key elements of our model. Full details shall be provided in the final deliverable.

We consider a set of N base stations with $N_t \geq 1$ antennas each communicating with K single-antenna mobile stations. The rate achieved at user *k* is equal to $r_k = \log_2(1+\gamma_k)$, where the SINR is function of the chosen beamforming vector at each base station.

We propose to use a new hierarchical feedback model proposed in Section 4.4.4 for obtaining the CSI. Transmitter *j* chooses the beamformer W_j based on its local CSI, and the extra statistical information it has (in the form of statistical information on the feedback quality received by the other base stations). Thus decisions at different transmitters are based on possibly different information. However, the performance (SINR, rate, Bit Error Rate for example) depends on all of these decisions. This is taken into account by a Bayesian formulation.

We define the common goal of the considered team of *N* transmitters as the maximization of the expected value of a sum utility function, the sum rate for example.

To simplify exposition of the solution to the above problem, we focus on the *K=N=2* case. The hierarchy in the knowledge (as defined by our distributed CSI model), and as a result the corresponding beamforming strategies fall into one of 3 cases:

1. Common knowledge: It corresponds to the traditional assumption under limited CSIT, where both transmitters have the same knowledge. This arises, for instance, when users are at the cell edge. This is equivalent to having centralized beamforming decisions.

2. Degraded knowledge: One of the transmitters has a better representation of both channels, and will adapt its beamforming on a finer scale than the other transmitter. Such a situation would arise, for example, if the two users being served lie in the same 'cell'.

3. Symmetric knowledge: One of the transmitters has a better representation of the channel of a given user and a worse one for the other user, with the reverse occurring at the other transmitter. This corresponds, for instance, to the base stations serving users each situated within their own 'cell', As will be detailed below one needs to jointly optimize sets of beamforming decisions at the two transmitters corresponding to a given common coarse state of channel knowledge.

   In this contribution we focus on the symmetric case as this represents the more common setup among the ones described and also the more challenging to formulate; the remaining cases can be dealt with in a similar manner. We characterize each user's quantized CSI by a pair $\mathbf{i}_1 = (i_{1,2}, i_{1,1})$ for user 1, and another $\mathbf{i}_2 = (i_{2,1}, i_{2,2})$ for user 2. The first index in each pair corresponds to the coarse knowledge (hence is shared by both users), i.e. the index of the codeword in the coarsest codebook, to which the channel is quantized, and the second index provides the missing bits to locate the finer codeword around the coarsest one. Given the structure of the distributed CSI, the beamforming matrix decisions may be parametrized in terms of these indices, so that beamforming matrix at transmitter 1, called W_1, varies with $(\mathbf{i}_1, i_{2,1})$ whereas W_2 is a function of $(i_{1,2}, \mathbf{i}_2)$.

Based on this formulation, we obtain a novel optimization problem, where the beamforming matrix at each base station is determined in a distributed manner, while minimizing the effects of non equal CSIT representation at the different base stations. The solution for this optimization problem is given in [ZG10a].

Performance results and future steps

To illustrate the gains from such a decentralized scheme, we show the average sum rates (average cell throughput) achieved for a symmetric K = N = 2, Nt = 1 channel, where Rayleigh fading is assumed and the covariance matrix of user 1's channel is given by [1 0; 0 β], that of user 2 by [β 0; 0 1], β being a simulation parameter modeling the strength of the `cross links'.

The performance is compared to that of upper and lower bound schemes. Simple upper and lower bounds to the proposed schemes correspond to joint beamforming based on the more accurate (unachievable in a distributed CSIT system) and the least accurate (achievable) CSIT, respectively. Another distributed scheme which attempts to use the local channel knowledge would be for each base station to design its transmission assuming all the other base stations share the same knowledge as itself. This is much simpler than the proposed distributed scheme, and has similar complexity to joint beamforming design based on the coarse CSIT.

The hierarchical codebooks are designed using Lloyd's algorithm: first the coarse codebook, then for each codeword in it, the corresponding finer codebook.

Figure 4.24 compares the proposed decentralized scheme to the upper and lower bounds above for $L_1(2) = L_2(1) = 2$ and $L_1(1) = L_2(2) = 6$, L indicating the number bits. We label the scheme which attempts to use local channel knowledge as if it were shared 'myopic beamforming (BF)'. Thus, the upper bound scheme would require $2(L_1(1)+L_2(2)) = 24$ bits of CSIT being shared, whereas the schemes based on distributed CSIT would require $L_1(1) + L_2(2) + L_1(2) + L_2(1) = 16$ bits. The benefit of the second layer of CSI over the coarser shared representation of the channel depends on the SNR and on the value of β. At low SNR and for β low, there is little use for the extra information.

The performance of myopic BF, even though it relies on more information than the joint beamforming relying on coarse CSI, is significantly worse, highlighting the importance of

coordinated action. For reference, we also plot the performance that would be obtained if the knowledge at transmitter j, j=1,2, were indeed common to both transmitters and joint beamforming done; clearly this yields more gain than joint beamforming based on coarse CSI.

Table 4.8: Simulation parameters

Simulation Parameter	Value
K (number of users)	2
N (number of cooperating eNBs)	2
Nt (number of antennas per eNB)	1

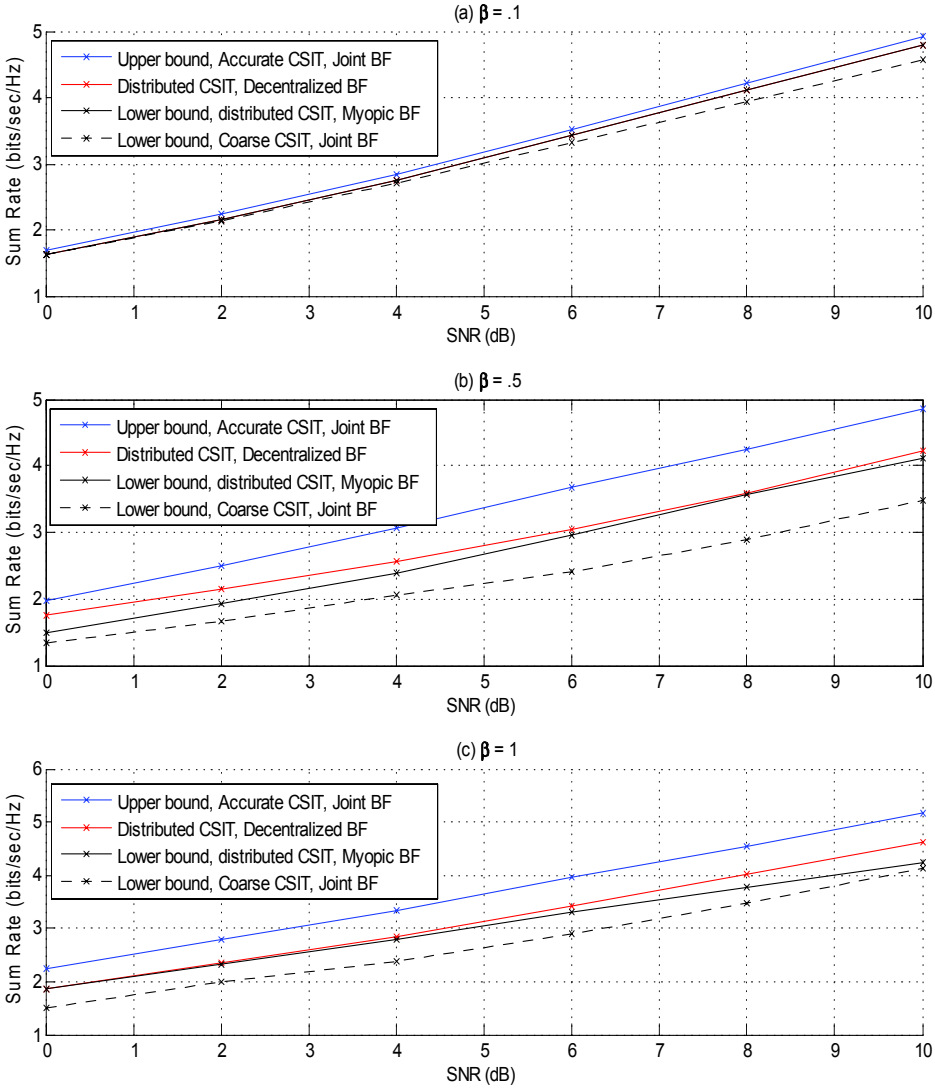

Figure 4.24: Sum Rate comparison for $L_1(2)=L_2(1)=2$, $L_1(1)=L_2(2)=6$ bits and different β.

Case 2: MIMO precoding under partial message sharing

Practical CoMP methods address cooperation in a multicell environment where base stations wish to jointly serve multiple users, under typically a constrained-capacity backhaul.

The fact that the backhaul links are constrained in their capacity is often not taken into account when evaluating the actual benefits of multi-cell MIMO precoding. In fact full MIMO cooperation requires full data sharing (i.e. the user messages are fully replicated to the multiple bases which are taking a role in the cooperative transmission). At the other extreme, not sharing the user messages would result in what information theorists call an “interference channel”.

The advantage of the no sharing case is that additional “fresh” data traffic can be pushed into the backhaul pipes instead of just using them to replicate data. But the disadvantage is that the base stations cannot apply joint MIMO precoding schemes, this limiting the over-the-air capacity.

Therefore, since data sharing comes at a cost in backhaul rates, a trade-off between sharing and not sharing emerges for finite backhaul capacity. We propose to investigate this trade-off by formulating a rate splitting problem between non shared (private to each transmitter) and shared (common) information. A preliminary study is considered to derive, for the case with the two cells and two users, the corresponding achievable rate regions, under optimal linear beamforming design for both common and private symbols. Some mathematical details are provided in [ZG10b].

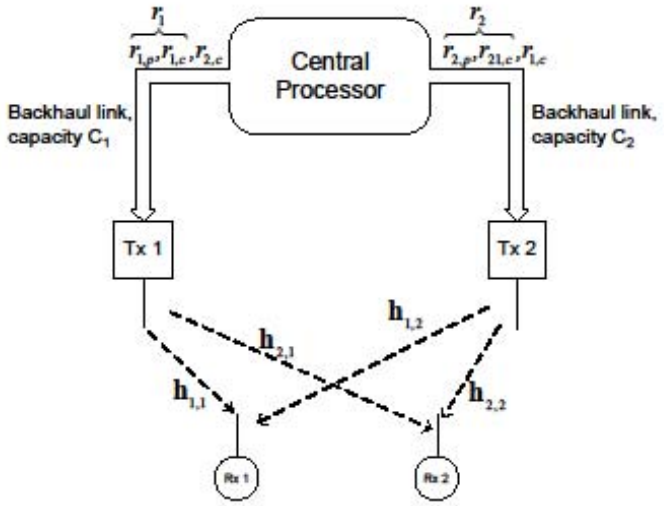

Figure 4.25: Constrained backhaul setup

In this work, we investigate the advantages of reducing the overhead related to the exchange of CSI data as well as user plane data in Joint Processing CoMP schemes. For both cases, robust forms of precoding (beamforming) are constructed. As of now such schemes are limited to cooperation clusters of two cells only, the generalization to an arbitrary number of eNBs is ongoing.

4.2.4 - Robust linear precoding with per-base-station power constraints

Joint processing CoMP schemes can enlarge the data rate for users close to the cell edge. To apply these techniques CSI has to be available at every participating eNB. Since link quality of cell edge users commonly suffers from bad SINR conditions, also CSI quality is affected due to worse channel estimation performance in this area. This problem can be attended by robust transmission techniques including statistical knowledge of the CSI uncertainty into the precoding scheme. If the impairment can be modeled as Gaussian distributed, it can be included into the

precoding scheme to alleviate the performance degradation in the high SNR regime [CJC+08] due to imperfect CSI knowledge. In comparison to single-cell MU-MIMO precoding, joint transmission comes with the additional challenge of per-base-station power constraints, since every base station is restricted to a certain transmit power. In recent studies, solutions were found, taking care of this problem [SSV+08], [VBS09]. For joint transmission CoMP, power control is an important technique. In this contribution, we compare linear precoding techniques in terms of performance and complexity. Therefore, we focus on the minimization the MSE between the estimated and the actual data symbols. This optimization affects the transmit filter (precoder) and the receive filter. Here two approaches can be distinguished. For the TxWF the overall receive filter (combination of user-wise transmit filters) is just a scaled identity matrix. If the transmit and the receive filter are jointly computed at the eNB, the signaling overhead to forward the receive filter is small, since only a scalar value has to be broadcasted to the UEs. For the second approach individual user-wise receive filter matrices are considered (according to the literature we call this scheme MMSE). This additional degree of freedom can be of major advantage if user channel possess very different attanuations. Furthermore, the separation of multiple data streams assigned to one UE can be forced at the receiver side. However, this approach comes with a high complexity, since transmit and receive filter have to be optimized in an iterative fashion.

For both approached (TxWF and MMSE) robustness according to CSI uncertainties can be achieved by including statistical knowledge of the uncertainty into the precoding scheme.The robust versions of both precoding schemes are denoted by RTxWF and RMMSE.

In this contribution, we first show performance differences of robust and non-robust schemes according to the level of the CSI uncertainty. For this, we will present how to model this uncertainty according to a cooperative network, where latency aspects are of major interest. Based on that, we want to show the limits of joint processing CoMP under realistic conditions.

In a second step we will try to find further robust mathematical formulations considering user specific receive filter matrices, with a reduced computational complexity compared to the RMMSE scheme. Furthermore, we will try to find suboptimal solutions, to achieve a trade off between performance and complexity..

System description of the innovation

We focus on downlink transmission where N eNBs jointly serve M UEs. At eNB $n = 1,...,N$ data is transmitted over N_n antennas, while UE m is equipped with M_m antennas. The resulting MIMO system consists of $N_B = \sum_n N_n$ inputs and $M_U = \sum_m M_m$ outputs, whose relation is considered by the channel coupling matrix

$$\mathbf{H} = \left[\mathbf{H}_1^T, ..., \mathbf{H}_M^T \right]^T \in \mathbb{C}^{[M_U \times N_B]},$$

where $\mathbf{H}_m \in \mathbb{C}^{[M_m \times N_B]}$ is the channel from the N eNBs to UE m. We initially assume frequency flat channels $\mathbf{H} \sim N_{\mathbb{C}}\left(0, \sigma_h^2\right)$ with uncorrelated links between all antenna elements. The L_m parallel data symbols transmitted to UE m are represented by $\mathbf{d}_m$, where $\mathbf{d} = \left[\mathbf{d}_1^T, ..., \mathbf{d}_M^T \right]^T$ includes the data symbols of all M UEs. To adapt the data symbols to the according channel conditions $\mathbf{d}$ is multiplied by the precoding matrix

$$\mathbf{B} = \left[\mathbf{B}_1^T, ..., \mathbf{B}_N^T \right],$$

where $\mathbf{B}_n$ is the precoding matrix applied at eNB n. The received data symbols at UE m are corrupted by additive white Gaussian noise $\mathbf{n} \sim N_{\mathbb{C}}\left(0, \sigma_n^2\right)$ and equalized with the receive filter $\mathbf{U}_m$. The estimated data symbols can then be expressed by

$$\hat{\mathbf{d}} = \mathbf{U}(\mathbf{HBd} + \mathbf{n}),$$

where $\mathbf{U} = \text{blkdiag}\{\mathbf{U}_1, ..., \mathbf{U}_M\}$, is a block diagonal matrix with the user-wise receive filter matrices on the diagonal.

We assume that the channel knowledge is impaired by an additive white Gaussian error term $\mathbf{E} \sim N_{\mathbb{C}}(0, \sigma_e^2)$ whose elements are uncorrelated with the actual channel $\mathbf{H}$. Since at least knowledge of the channel statistics is available at the transmitter side the CSIT should possess the same power like the actual channel. The CSIT can then be denoted by

$$\hat{\mathbf{H}} = \alpha \mathbf{H} + \mathbf{E}$$

where α results from the constraint $E\{\mathbf{H}\mathbf{H}^H\} = E\{\hat{\mathbf{H}}\hat{\mathbf{H}}^H\} = \alpha^2 E\{\mathbf{H}\mathbf{H}^H\} + E\{\mathbf{E}\mathbf{E}^H\}$.

Hence, an eNB that obtains the CSIT $\hat{\mathbf{H}}$ and knows σ_e^2 can include that knowledge into the filter design. If σ_e^2 is unknown at the transmitter side the CSIT is directly included into the design, since it is the best available knowledge of the actual channel.

Performance results and future steps

A very low complex transceiver scheme is the TxWF [JKG+02], where uniform downscaling at the receiver side is assumed, which leads to the overall receive filter $\mathbf{U} = \beta^{-1}\mathbf{I}$. Furthermore, it is assumed that knowledge of the noise power is available at the transmitter.

Optimal solutions without the above restrictions of scalar uniform receive filters can be achieved by a transformation into a Second Order Cone Program (SOCP) [SSV+08],which can be solved by standard software solvers like SEDUMI [Stu99].

If knowledge of the CSI uncertainty statistic is available, it can be included into the filter design. For the TxWF this leads to the Robust TxWF (RTxWF) [CJC+08]. Also the MMSE solution can be adapted with statistical knowledge of the CSI uncertainty [VBS09], which leads to the RMMSE.

We have simulated these four precoding schemes (TxWF, RTxWF, MMSE and RMMSE) over frequency flat channels with uncorrelated links in the spatial domain. Furthermore, no pathloss and no shadow fading was considered. The system settings are shown in Table 4.9.

Table 4.9: Simulation parameters

Simulation Parameter	Value
Number of eNBs	$N = 2$
Number of eNB antennas	$N_n = 1$
Number of UEs	$M = 2$
Number of UE antennas	$M_m = 1$

The simulation results are shown in Figure 4.26. From the curve where no CSI impairments are considered we observe that the performance difference between TxWF and MMSE is in general not very large, if pathloss and shadow fading are unconsidered. This performance gap disappears in the high SNR regime. The reason for that is the restriction of the iterative transceiver computation to a maximum number of iterations, where for a given iteration number the accuracy shrinks with increasing SNR. Note, that if no CSI impairments occur, robust and non-robust schemes possess the same performance. In the case of imperfect channel knowledge at the transmitter, the robust scheme outperforms the non-robust scheme in the high SNR regime. However, the impact of robustness is very small for the presented level of CSI uncertainty. The performance gain compared to non-robust schemes become larger with increasing CSI uncertainty. Hence, it will be of high interest, what level of uncertainty can be

considered for realistic CoMP scenarios and what are the performance gains achieved by robust precoding.

From Figure 4.27 a large gap between the simple analytical TxWF scheme and the iterative MMSE scheme can be observed. For the MMSE scheme, the complexity grows in the high SNR regime due to an increasing number of iterations, which are necessary for a certain accuracy. Because the performace gap between the two schemes is very small the TxWF would be clearly preferred, if computational complexity is an issue due to delay restrictions. As mentioned above the performance gap is assumed to be much larger if pathloss and shadow fading are considered and the MMSE scheme could become a serious option. In that case, suboptimal solutions with a reduced complexity can be of high interest.

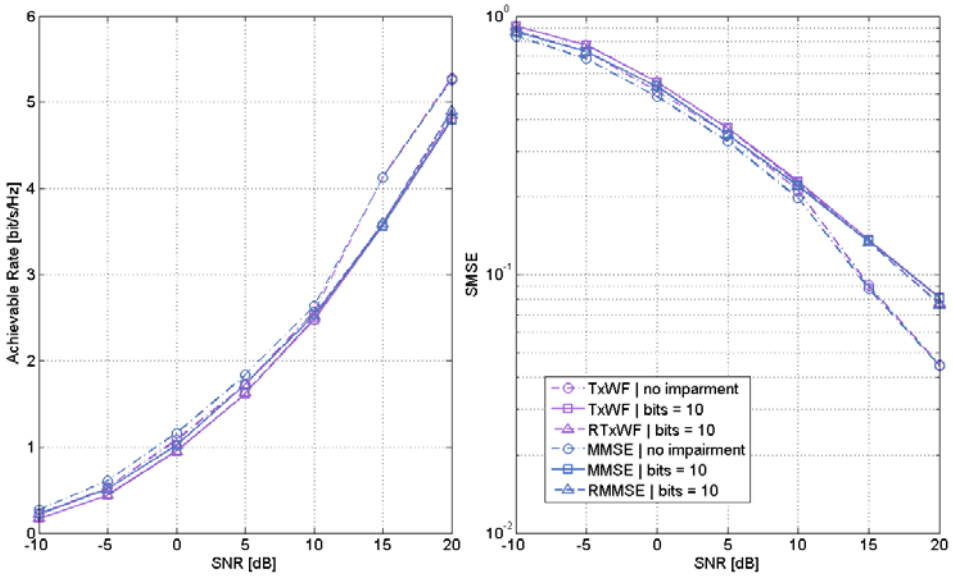

Figure 4.26: Averaged achievable user rate (left) and sum-MSE (right).

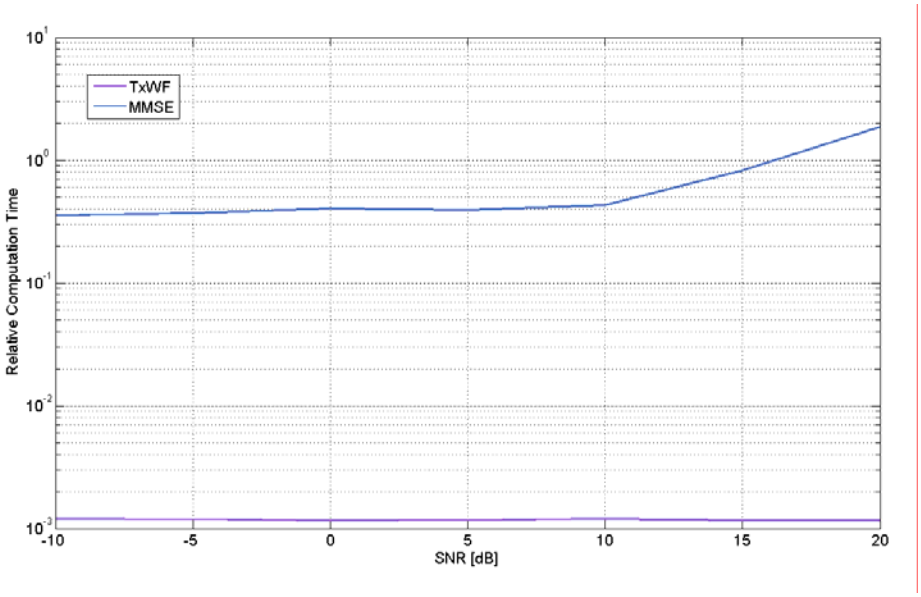

Figure 4.27: Computation time is plotted over the SNR for the presented schemse.

From our analysis we observed small performance gaps between the TxWF and the MMSE precoding scheme if the channel coefficients are assumed to be i.i.d. (no pathloss and no shadow fading is considered). In the further progress we will simulate the schemes under realistic channel conditions considering pathloss and shadow fading. Furthermore, we want to show the performance gain of the robust schemes under realistic CSI uncertainties. After that analysis we want to derive suboptimal robust MMSE schemes for reducing the computational complexity

4.2.5 - Waterfilling schemes for Zero-Forcing coordinated transmission

Interference management in cellular systems based on a frequency reuse one approach has recently been addressed by several research teams, due to its simplicity and high degree of real implementation feasibility. In [ACH07] the authors analyze several approaches for overcoming interference in MIMO cellular networks. If the interference is known by the transmitters, cooperative encoding among base stations using DPC can suppress Other-Cell Interference (OCI). In [KFV06] [FKV06] several strategies of joint processing are proposed. Interference is eliminated by jointly and coherently coordinating the transmission from the base stations in the network, assuming that base stations know all downlink signals. Besides DPC, they propose a ZF scheme that, although suboptimal, does not require the user ordering that renders DPC unrealizable.

Joint processing is similar to MU-MIMO with the main distinguishing feature being the cooperative interference cancellation. The power management is consequently more complex than in a standard MU-MIMO downlink since it involves the cooperation between several base stations in the system. Both DPC and ZF schemes provide the basis for transmission where the transmit powers for each base station antenna must be obtained. In [KFV06] [FKV06] they are solved by convex optimization to maximize the minimum transmission rate for all users and significant improvements in spectral-efficiency are shown by simulation. In [BZG+09], distributed generalizations of classical beamforming approaches are provided and a parameterisation of the beamforming vectors used to achieve the outer boundary of the achievable rate region is obtained for two multiantenna transmitters and two single-antenna receivers.

In this subsection, we focus on ZF-based joint processing schemes with the aim of maximizing the Weighted Sum Rate (WSR) of the users of multiuser OFDM systems in a downlink transmission. We derive two power allocation schemes that resemble the well-known waterfilling distribution. These schemes based on the waterfilling technique are proposed in [GSC09], but only for narrowband transmission. In this work, we extend them to the case of employing OFDM. We examine the achievable rates in a 2-user simplified scenario and the distribution of the rates obtained in a more realistic system emulating a 16-cell cellular network.

System description of the innovation

The system model assumes a joint transmission downlink scenario based on OFDM, where M base stations serve N users. Each base station has t transmit antennas and each user has r receive antennas. In scenarios, where several users are assigned to the same base station, $M \neq N$ is considered. However, in the following, the analysis will be applied to BS-user pairs, therefore the case $M = N$ will be used.

The principle of OFDM is to split a high-rate data stream into a number of lower rate streams, which are then simultaneously transmitted on a number of orthogonal subcarriers. Hence, each subcarrier experiences approximately frequency flat fading; hence each subcarrier can be dealt with regardless each others. We consider a decentralized (but not distributedly optimized) system where the whole channel is known to transmitter and receiver. We assume a linear time-invariant channel with frequency selective fading and additive Gaussian noise. Provided that the length of the cyclic prefix is chosen longer than the longest impulse response, the channel seen by each user can be decomposed into N_{OFDM} independent flat subchannels with frequency response $\mathbf{H}_k^p$ for the user k and the subchannel p.

In a joint processing scheme the transmitted signal from a particular BS may eventually arrive, depending on the propagation conditions, to a certain number of adjacent users in the cellular system that are served by other BSs. Under this assumption, the channel on each subcarrier *p* (*p* = 1...N_{OFDM}) may be modelled by a *N·r* ×*M·t* matrix $\mathbf{H}^p$ where each matrix coefficient represents the fading from each transmit antenna in the BS to each receive antenna at the user side.

The received signal model is, on the *p*-th subcarrier, as follows:

$$\mathbf{y}^p = \mathbf{H}^p \mathbf{x}^p + \mathbf{n}^p$$

where $\mathbf{y}^p$ is the received *N·r* ×1 signal vector on the *p*-th subcarrier, $\mathbf{x}^p$ is the *M·t* ×1 signal vector transmitted from all the BSs on the *p*-th subcarrier, and $\mathbf{n}^p$ is the *N·r* ×1 i.i.d complex Gaussian noise vector on the *p*-th subcarrier, with variance σ^2. If we define $\mathbf{H}_k^p$, with *k* = 1. . .*N*, as the *r* × *M·t* channel matrix seen by user *k* on the *p*-th subcarrier, then

$$\mathbf{H}^p = \left[\mathbf{H}_1^{pT}\ \mathbf{H}_2^{pT}\ \ldots \mathbf{H}_N^{pT}\right]^T$$

For this scenario we define $\mathbf{x}^p$ as follows

$$\mathbf{x}^p = \sum_{i=1}^{r} b_{1i}^p \mathbf{w}_{1i}^p + \sum_{i=1}^{r} b_{2i}^p \mathbf{w}_{2i}^p + \cdots + \sum_{i=1}^{r} b_{Ni}^p \mathbf{w}_{Ni}^p = \mathbf{W}^p \mathbf{b}^p$$

where b_{ki}^p represents the *i*-th symbol for user *k* transmitted with power P_{ki}^p on the *p*-th subcarrier, and $\mathbf{w}_{ki}^p = \left[w_{ki}^{p,1}, \ldots, w_{ki}^{p,(m-1)t+j}, \ldots, w_{ki}^{p,Mt}\right]^{\mathrm{T}}$ are the precoding vectors being $w_{ki}^{p,(m-1)t+j}$ the weight of *j*-th transmit antenna (*j* = 1...*t*) of the *m*-th base station for the *i*-th symbol of the user *k* transmitted on the *p*-th subcarrier. The precoding matrix, will be obtained under a ZF criteria as in [FKV06], to guarantee that

$$\mathbf{H}_k^p \left[\mathbf{w}_{q1}^p, \mathbf{w}_{q2}^p, \ldots, \mathbf{w}_{qr}^p\right] = \begin{cases} 0: & k \neq q \\ \mathbf{U}_k^p \mathbf{S}_k^p: & k = q \end{cases}$$

$$\left\|\mathbf{w}_{ki}^p\right\|^2 = 1, \qquad k = 1,\ldots,N;\ i = 1,\ldots,r,\ p = 1,\ldots,N_{OFDM}$$

where $\mathbf{U}_k^p$ is a unitary matrix and $\mathbf{S}_k^p = diag\left\{\left(\lambda_{k1}^p\right)^{1/2}, \left(\lambda_{k2}^p\right)^{1/2}, \ldots, \left(\lambda_{kr}^p\right)^{1/2}\right\}$ is a diagonal matrix that contains the square roots of the nonzero eigenvalues of the matrix $\mathbf{Q}_k^p \mathbf{Q}_k^{pH}$, being $\mathbf{Q}_k^p$ the part of the channel matrix $\mathbf{H}_k^p$ orthogonal to the subspace spanned by the other users' channels $\mathbf{H}_q^p$ $(q \neq k)$.

On the receiver side, each user may independently rotate the received signal and decouple the different streams. Thus, the final signal obtained by *k*-th user on *p*-th subcarrier can be expressed as

$$\tilde{\mathbf{y}}^p = \mathbf{U}_k^{pH} \mathbf{U}_k^p \mathbf{S}_k^p \mathbf{b}_k^p + \tilde{\mathbf{n}}_k^p = \begin{bmatrix} \left(\lambda_{k1}^p\right)^{1/2} b_{k1}^p \\ \vdots \\ \left(\lambda_{kr}^p\right)^{1/2} b_{kr}^p \end{bmatrix} + \tilde{\mathbf{n}}_k^p$$

Power Allocation Schemes

Under joint transmission with ZF it can be observed that the overall system is a set of parallel noninterfering channels. Therefore, in this kind of MIMO-OFDM scenario, the achievable rates per user are as follows

$$R_k = \frac{1}{N_{OFDM}} \sum_{p=1}^{N_{OFDM}} \sum_{i=1}^{r} log_2\left(1 + \frac{\lambda_{ki}^p P_{ki}^p}{\sigma^2}\right)$$

The aim will be maximize a weighted sum of the rates R_k for the set of users, where the weights $\alpha_k \in [0,1]$, $\left(\sum_{k=1}^{N} \alpha_k = 1\right)$, can be seen as indicating the priorities of the users: the closer α_k is to 1, the higher the priority given to user *k*. This requires solving an optimization problem in terms of the power P_{ki}^p allocated to the *i*-th stream of user *k*, subject to a constraint on the maximum available power for transmission from each base station P_{max}.

This problem is convex since the logarithmic function is concave in the power assignments, the addition operation preserves concavity and the power constraints are linear. Therefore it can be solved by standard convex optimization techniques [BV04]. However, closed-form solutions, even if suboptimal, would be desirable in order to reduce the computational time and resources required for the optimization. To that end, in the next subsections we examine in deep the problem and look for such kind of solutions.

In order to solve this problem, we can introduce a Lagrangian $\Lambda(\mathbf{P}, \boldsymbol{\mu})$ where **P** is the vector collecting all the powers P_{ki}^p, $k = 1, \ldots, N$, $i = 1, \ldots, r$, $p = 1, \ldots, N_{OFDM}$ and $\mu = [\mu_1, \ldots, \mu_M]$ is the vector of the Lagrange multipliers. Then the solution of the problem is given by the values of $\mathbf{P}^+$ and μ such that

$$\begin{cases} P_{ki}^p = \sigma^2\left[\dfrac{\alpha_k}{ln(2)L_{ki}^p} - \dfrac{1}{\lambda_{ki}^p}\right] \\ L_{ki}^p = -\sum_{m=1}^{M}\sum_{j=1}^{t} \mu_m \left|w_{ki}^{p,((m-1)\cdot t+j)}\right|^2 \\ \sum_{j=1}^{t}\sum_{p=1}^{N_{OFDM}}\sum_{k=1}^{N}\sum_{i=1}^{r} P_{ki}^p \left|w_{ki}^{p,((m-1)\cdot t+j)}\right|^2 = P_{max} \end{cases}$$

which resembles the well-known waterfilling distribution. However, here the waterlevel is given by $\sigma^2\alpha_k / \left(ln(2)L_{ki}^p\right)$, that is, the waterlevel is different for each symbol *i* to be transmitted to each user *k* on each subcarrier *p*. Even though the values of the waterlevels can be found again by convex optimization techniques, we still have a similar computational complexity that we would like to reduce.

By considering the most stringent of the power constraints defined in the previous subsection, we can reduce the problem to an "equivalent" base station m_0 having for each symbol transmitted to each user the precoding weights whose sum of squared values is maximum among all the BSs, that is

$$\Omega_{ki}^p = \max_{m=1\ldots M}\left(\sum_{j=1}^{t}\left|w_{ki}^{p,((m-1)\cdot t+j)}\right|^2\right)$$

Application of the Lagrange multiplier technique gives the new function whose partial derivatives, with respect to the powers P_{ki}^p, give the set of equations

$$\frac{\alpha_k}{ln(2)}\frac{\lambda_{ki}^p}{\left(1+\lambda_{ki}^p P_{ki}^p/\sigma^2\right)}+\mu\Omega_{ki}^p=0$$

Therefore the problem is equivalent to finding a constant value *K* such that, for all the power levels $P_{k\,i}^{p}$, the following equations hold

$$P_{ki}^p=\left[K\frac{\alpha_k}{\Omega_{ki}^p}-\frac{\sigma^2}{\lambda_{ki}^p}\right]^+$$

with

$$K=\frac{-\sigma^2}{ln(2)\mu}$$

where [·]+ denotes the maximum between zero and the argument. This corresponds again to a waterfilling distribution with variable waterlevel. However, for given user priorities α_k and channel realization determining λ_{ki}^p and Ω_{ki}^p, the problem reduces to finding a constant *K* that can be solved with the same algorithms that solve standard waterfilling (see for example [Cio07]).

In order to further simplify the solution to the optimization problem we may consider the fact that in a practical realization the values of Ω_{ki}^p are close to each other for all *k*, *i* and *p*. Then we can simplify the previous solution to give

$$P_{ki}^p=\left[K\frac{\alpha_k}{\Omega_{ki}^p}-\frac{\sigma^2}{\lambda_{ki}^p}\right]^+$$

which corresponds to a waterfilling distribution with the waterlevel modified only by the user priorities. In particular for equal priorities α_k = 1/*N* it corresponds to a standard waterfilling.

Performance results and future steps

In this section we compare the performance in terms of achievable rates of the proposed waterfilling (WF), modified waterfilling (MWF) and the optimum solution found by Convex Optimization (CVX). For the sake of comparison we also include the rates achieved when using a Uniform Power (UP) distribution. In this last case the power allocated to each user transmission is the same and corresponds to the maximum value that fulfils the power constraints.

A simple two-BS, two-user scenario is considered. Here we employ a simplified frequency-selective channel model with N_{path} paths and an exponential Power Delay Profile (PDP). Therefore, the channel matrix of the *n*-th path is

$$\mathbf{H}(n)=PDP(n)=\frac{e^{-\beta n}}{\left(\sum_{c=1}^{N_{path}}e^{-2\beta c}\right)^{1/2}}=\left(\frac{1-e^{-2\beta}}{1-e^{-2\beta N_{path}}}\right)^{1/2}e^{-\beta n}$$

where β is the factor which indicates the decreasing speed of the power, and $\mathbf{H}_G$ is a matrix whose entries are i.i.d. complex Gaussian random variables with zero mean and variance σ^2 = 1. Due to a high computational complexity of the CVX, we will consider an OFDM system with 8 subcarriers, but the results can be extended to more subcarriers. Hence, the channel frequency response **H** is calculated as the FFT, with length N_{OFDM}, of $\{\mathbf{H}(n)\}_{n=1}^{N_{path}}$. Here, the constraint on the maximum available power for transmission from each base station is P_{max} = 1. The simulations assumptions are summarised in Table 4.10.

Table 4.10: Simulation parameters

Simulation Parameter	Value
Channel Model	Frequency-selective channel model with an exponential power-delay profile. The factor β which indicates the decreasing speed of the power is 1 or 0.1
Number of paths	4
Number of Base Stations, *M*	2
Number of transmit antennas per BS, *t*	1, 2 or 4
Maximum available power for transmission from each BS	1W
Number of Users, *N*	2
Number of receive antennas per user, *r*	1 or 2
Number of subcarriers	8
Number of channel realizations at each position	1000
Channel Estimation	Ideal
Feedback and Control Channel Errors	None

Figure 4.28 shows the throughput as function of the number of transmit antennas per BS comparing the three different approaches and the uniform power allocation as a reference. A single carrier system is used as reference too. The number of receiver antennas is equal to 2 and two different values of b are considered. Moreover, the same priority is assigned to both users.

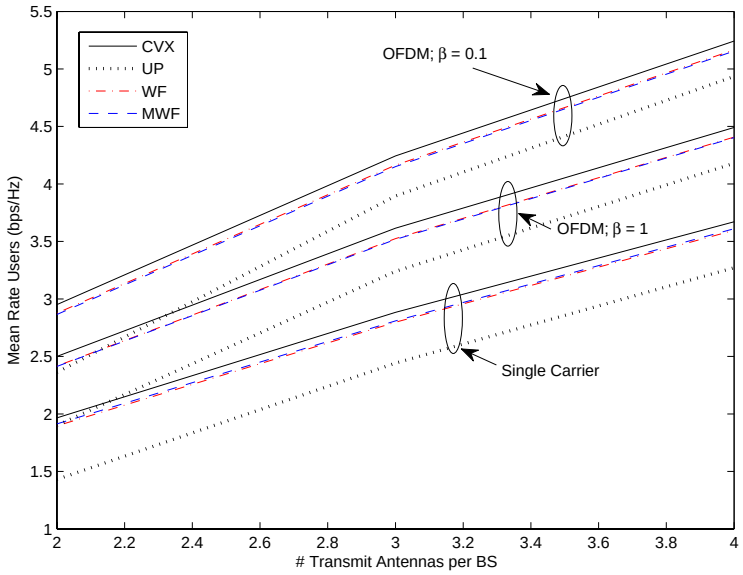

Figure 4.28: Throughput versus the number of transmit *t* antennas with OFDM (8 subcarriers), *M* = 2, *N* = 2, *r* = 2 and several values of β.

It can be seen that the gap between the mean rates obtained with WF and MWF and the optimal solution CVX is quite narrow. These rates are considerably higher than what is achieved by UP. Comparing a single carrier scheme with flat fading to an OFDM system with frequency selective fading, the increase of mean rates is quite important. So, as the channel selectivity increases, higher mean rates are achievable if the number of subcarriers used is chosen accordingly. Also, the increase of mean rates with higher values of *t* is substantial, meaning that the capabilities of the use of multiple antennas are leveraged.

On the other hand, we would like to find the boundary of the region of achievable rates for each proposed scheme. In this case the region of achievable rates on each subcarrier is a convex set in the positive quadrant and one way to describe it is to bound it by straight lines (hyperplanes), $\alpha R_1 + (1-\alpha) R_1 = B(\alpha)$, for $\alpha \in [0,1]$.

The region of achievable rates can then be written as

$$R = \left\{ (R_1, R_2) \in R_2^+ : \alpha R_1 + (1-\alpha) R_1 \le B(\alpha), \forall \alpha \in [0,1] \right\}$$

Figure 4.29 shows the mean achievable rates comparing the three algorithms. A uniform power allocation is used as reference. A value of $\beta = 0.1$ has been chosen, that means a channel with high frequency selectivity is used. Different values of the number of transmit and receive antennas are considered. As in Figure 4.28, the achievable rates obtained with WF and MWF are very close to the optimal solution CVX.

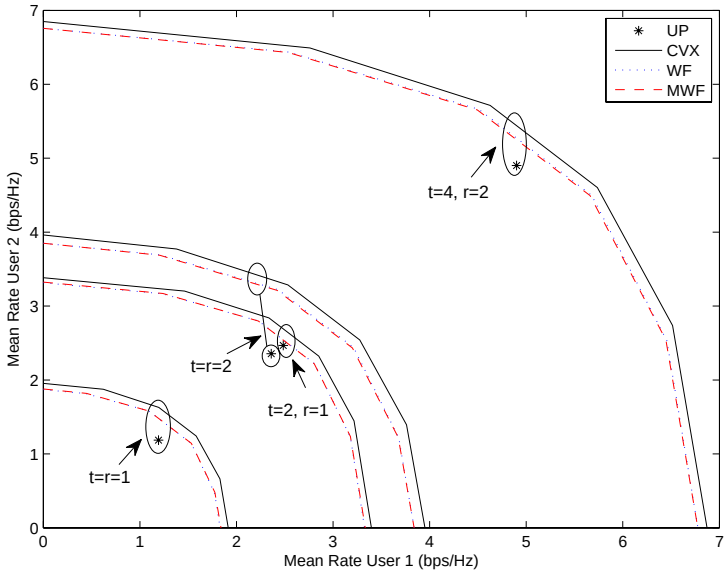

Figure 4.29: Mean achievable rates with OFDM (8 subcarriers), β = 0.1, *M* = 2, *N* = 2 and several values of the number of transmit *t* and receive *r* antennas.

In the following we provide a description of a realistic scenario to be evaluated in future steps. We set up a cellular system similar to the one in [FKV06]. It is defined by a set of *M* = 16 hexagonal cells arranged to form a torus with a BS in the center each cell. Due to propagation loss, we assume that each cell is only interfered by its first concentric ring. This is illustrated in Figure 4.30 showing one cell placed near the border of the cellular deployment (in blue) and another cell placed away from the border (in red). Users are uniformly distributed over the scenario and each user is assigned a BS following a power-received rule.

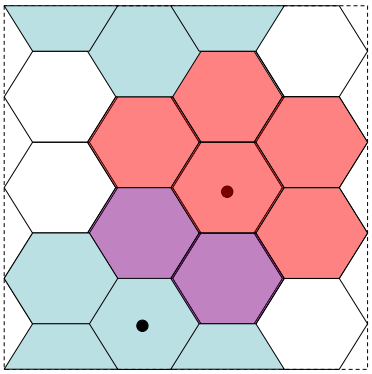

Figure 4.30: Cell deployment and interference rings.

The channel fading coefficients are obtained based on the Spatial Channel Model from 3GPP [3GPP25996]. It is an Urban Micro NLOS scenario with 4 paths where the pathloss model is based on the COST 231 Walfish-Ikegami NLOS.

The simulations assumptions are summarised in Table 4.11.

Table 4.11: Simulation parameters

Simulation Parameter	Value
Channel Model	SCM from 3GPP
Number of paths	4
Scenario	Urban Micro NLOS
Pathloss Model	COST 231 Walfish-Ikegami NLOS
BS antenna heigth	12.5 m
MS antenna heigth	1.5 m
Building height	12 m
Building to building distance	50 m
Street width	25 m
Carrier frequency	1.9 GHz
Radius of the cell	500 m
Number of Base Stations, *M*	16
Number of transmit antennas per BS, *t*	1, 2 or 4
Maximum available power for transmission from each BS	10 W
Number of Users, *N*	16
Number of receive antennas per user, *r*	1 or 2
Antenna spacing	0.5 λ (linear arrays are supposed)
Gain of the receive antenna	10.3 dBi
Number of subcarriers	8
Number of channel realizations at each position	1000
Channel Estimation	Ideal
Feedback and Control Channel Errors	None

The BS-user achievable rates will be computed by means of simulation of different channel samples. We will randomly generate the channel matrix for different signal to noise ratios. The user rates will be computed for the CVX, WF, MWF and UP power allocation strategies. For the sake of comparison, it will be also included the CVX solution using single carrier modulation.

We have extended two power optimization schemes (WF and MWF) for a ZF Coordinated Base Station Transmission downlink from narrowband to OFDM transmission. We can see that both algorithms achieve the same capabilities and are very close to the optimal solution. However, the optimum can be derived only resorting to the numerical solution of the convex optimization problem, with a heavy computational complexity, much higher than the proposed schemes of WF and MWF. Besides, the WF algorithm which has a lower complexity than MWF, reduces to the standard WF if all users have the same priority. Therefore, the proposed WF scheme is the most suitable solution for this kind of systems.

The future steps are:

- Finalization of previous simulations: realistic scenario with 16 cells (Figure 4.30).
- Realistic scenario with 64 cells with an eNB in its centre and 64 users. Each cell is interfered by its first and second concentric rings (19 eNBs).
- Channel estimation: CSI will be estimated via scattered pilot patterns in time and frequency.

4.2.6 - Coordinated beamforming for interference rejection

The proposed contribution is focused on the investigation, definition and evaluation of an interference avoidance scheme applicable at L1 able to enhance the performance of the system in terms of spectral efficiency. The research activity considers a downlink CoMP decentralized transmission technique that requires only the exchange of CSI and control over the backhaul link, without requiring any sharing of user data among the geographically separated transmission points.

In the proposed coordinated beamforming scheme for interference rejection the user data is transmitted only from the serving cell so to limit the latency/capacity requirements over the backhaul. The scheme is based on the principle that the interference generated from the serving cell towards other-cell UEs is reduced by means of an appropriate L1 precoding technique. The general principle of the proposed coordinated beamforming scheme is shown in the following Figure 4.31.

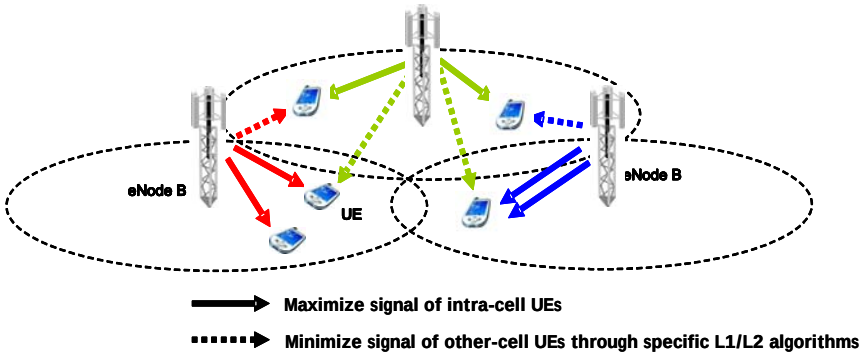

Figure 4.31: Principle of the interference control scheme.

Such interference avoidance scheme is applicable on top of different L1 MIMO transmission modes: SM SU-MIMO, Transmit Diversity (TxD) SU-MIMO, Single Cell MU-MIMO, etc. The proposed scheme, in principle, can be applied both to cells that belong to the same eNB (intra-eNB CoMP) or to cells that belong to different eNBs (inter-eNB CoMP). On top of this L1 interference rejection scheme, also Layer 2 (L2) mechanisms can be activated so to allocate the resources dynamically, as will be defined in D1.3 [ARTD13].

System description of the innovation

The coordinated beamforming scheme for interference rejection operates as follows. Each UE camps on the serving cell received with best radio quality while the inter-cell interference experienced by each UE is measured and continuously monitored. Such measure is performed at the UE by exploiting the Synchronization Signals (SS) or the Reference Signals (RS) transmitted by the different cells. Some possible examples of radio quality measures are the Reference Signal Received Quality (RSRQ), the Signal to Interference Ratio of Reference Signals (RS SINR) and the Reference Signals Received Power (RSRP). The measurements performed by the UE must be conveyed to the network in order to feed the algorithms that control the interference in the network.

In particular the UEs monitor, through the appropriate measurements, the neighbouring interfering cells identifying those that create the highest level of interference, by means of a given threshold mechanism. The basic idea behind this mechanism is that the network should set a dynamic threshold based on the radio quality measurements experienced at the UE. The following Figure 4.32 shows the concept of dynamic threshold based on the cell radio quality indicator (e.g. based on RSRP, RS SINR, RSRQ, etc.). The threshold set by the network is denoted as T. The user terminal periodically measures the quality indicator of the different cells present in the network including the serving cell and the interfering cells. The threshold T set by the network represents the minimum difference between the value of the radio quality indicator of the serving cell and the radio quality indicator of any interfering cell.

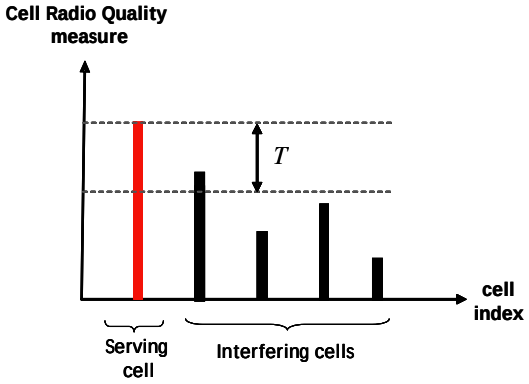

Figure 4.32: Threshold mechanism applied for interference rejection.

The cells cooperating in the interference rejection mechanism are identified and form the so called cooperating set. When the difference between the radio quality indicator of the interfering cells and the serving cell falls below the given threshold T, such interfering cell becomes a candidate cooperating cell, to be included in the cooperating set. The number of interfering cells that apply the interfering rejection scheme, and thus are being coordinated with the serving cell, is referred to as NCIC (Number of Coordinated Interfering Cells). The dimension of the NCIC is identified as a trade-off between performance and overhead, as will be detailed in the following.

Two possible approaches are foreseen for creating the cooperating set, based either on the selection of a fixed number of interfering cells for which to apply the rejection mechanism or on the selection of a variable number of interfering cells for which to apply the rejection mechanism:

The interference rejection mechanism is activated for the identified NCIC interfering cells. For the former case only one interfering cell will activate the interference rejection mechanism towards the selected other-cell UE, thus computing the beamforming weights to reduce the generated interference towards that UE. In the latter case up to NCIC interfering cells will activate the interference rejection mechanism towards the same given UE, thus computing the beamforming weights so to reduce the generated interference towards that UE. In our evaluations, the parameter NCIC has been set equal to 1, 2 and 5. As will be described in the following the beamforming weights are calculated for a given subband in order to maximize the signal received by the served UE and, simultaneously, to minimize the interference generated

towards the selected other-cell UE by placing a minimum in the antenna radiation diagram. The subbands are formed by a number M of adjacent Physical Resource Blocks (PRBs). In order to limit the impact on the same-cell served users it is also assumed that each cell may activate the interference rejection mechanism (for a considered subband) only towards a single other-cell UE. The selection of the specific other-cell UE toward which to place the minimum of the radiation diagram is determined by computing for each interfered other-cell UE the ratio between the power received from its serving cell and the power received from the *j-th* interfering cell that should activate the interference rejection mechanism. In formulas this ratio $R^{(i)}$ for the *i-th* UE can be expressed as follows

$$R^{(i)} = 10 \cdot \log_{10}\left(\frac{P_{serv}^{(i)}}{P_{j}^{(i)}}\right)$$

where $P_{serv}^{(i)}$ is the power received by the *i-th* UE from its serving cell and $P_{j}^{(i)}$ is the power received by the *i-th* UE from the *j-th* interfering cell. In the cases where over a given subband there is more than one interfered UE that exceeds the threshold T, the *j-th* cell will activate the interference rejection mechanism towards the UE for which the ratio $R^{(i)}$ is maximum.

To perform the beamforming weights' calculation, the UE feeds backs to its serving cell the CSI information, together with the cell IDs of the interfering cell(s) that is (are) generating a high level of interference by exceeding the threshold T. This CSI is relative to the radio link(s) between the interfering cell(s) and the UE. The serving cell then forwards the CSI information to the identified interfering cell(s) over the X2 interface or the S1 interface. In particular the CSI is transferred to the interfering cells over the backhaul (i.e. through the X2 interface if the cells belong to different eNBs). The number of considered interfering cells is scalable and identified as a tradeoff between performance and CSI overhead.

Based on the exchanged CSI, each interfering cell implements the L1 interference rejection scheme, that reduces the interference generated towards the identified UE, in a decentralized manner. In fact each cell performs transmit precoding based on beamforming weights calculated independently from other cells. This is done in order to balance the mitigation of interference generated on other-cell UEs and the maximization of the data rate towards the served UEs.

A suitable L1 interference rejection approach is based on Multi-User Beamforming (MU-BF) [TSS05] with the maximization of the Signal to Leakage plus Noise Ratio (SLNR) [STS07]. The challenge is to design transmit beamforming vectors for every user while limiting the co-channel interference to other-cell users. One approach is to perfectly cancel the generated interference at every user by means of zero forcing beamforming, which requires a relatively large number of transmit antennas. In our study we will consider an alternative approach based on the concept of signal leakage for designing transmit beamforming vectors in a multi-user system [STS07]. Leakage is a measure of how much signal power leaks into the other users. The performance criterion for choosing the beamforming coefficients will be based on maximizing the SLNR for all users simultaneously. Therefore the proposed criterion aims at maximizing the received desired signal power of a given user, while minimizing the overall interference power caused by this user to a properly selected user in an adjacent cell. Moreover, in contrast to the zero-forcing solution, the leakage scheme does not impose any constraint on the number of transmit/receive antennas. It further takes into account the influence of noise when designing the beamforming vectors.

We consider a downlink multi-user environment with a base station communicating with K users. In our simulations K=10 users are dropped in each cell and each user is allocated to one subband formed by M=5 adjacent PRBs. The considered system bandwidth is B=10 MHz and thus the number of available PRBs is equal to 50. The base station employs n_T transmit antennas and each user could be equipped with multiple antennas as well. Let $n_R^{(i)}$ denote the number of receive antennas at the i-th user. In our simulations $n_T = 4$ and $n_R^{(i)} = 1 \ \forall i$.

The signal received by the *i-th* UE can be expressed as:

$$\mathbf{y}_i = \mathbf{H}_i \mathbf{w}_i s_i + \sum_{j=1}^{J} \mathbf{H}_j \mathbf{w}_j s_j + \mathbf{n}_i$$

where $\mathbf{H}_i$ is the channel matrix of the *i-th* UE with respect to its serving cell and $\mathbf{w}_i$ is the corresponding precoding vector. The second term in the equation above represents the interference caused by the J adjacent interfering cells and $\mathbf{n}_i$ is the thermal noise with power σ_i^2.

We assume that the channel matrix $\mathbf{H}_j$ between the *j-th* interfering cell and the *i-th* UE can be estimated and in some way conveyed to the *j-th* cell in order to apply the interference rejection mechanism. In addition the matrix $\mathbf{H}_j$ is not required to be known by the other coordinated interfering cells. One possible way is that the UE estimates the matrix $\mathbf{H}_j$ (using for example the RS transmitted by the *j-th* cell) and feeds back the matrix through uplink signaling to its serving cell. The matrix is then forwarded by the serving cell to the *j-th* interfering cell via X2 interface. The signal to noise ratio at the input of the *i-th* receiver is equal to:

$$SINR_i = \frac{\left\| \mathbf{H}_i \mathbf{w}_i \right\|^2}{n_R^{(i)} \sigma_i^{\,2} + \sum_{j=1}^{J} \left\| \mathbf{H}_j \mathbf{w}_j \right\|^2}$$

One could use the above SINR expression as an optimization criterion for determining the beamforming vectors of the interfering cells $\mathbf{w}_j$, that would be determined by maximizing the SINR for each user i. In order to maximize the SINR of the *i-th* user it is necessary to minimize the contribution of each interfering cell by a suitable choice of the related precoding vector $\mathbf{w}_j$

$$\min_{\mathbf{w}_j} \left\| \mathbf{H}_j \mathbf{w}_j \right\|^2 \qquad \forall j = 1,..,J$$

However, the minimum outlined above is subject to the constraint that each of the J interfering cells must also serve a given user over the same transmission resources with a minimal performance degradation. One possible solution to the problem stated above is given by method described in [TSS05] and [STS07], where it is described a technique for the calculation of the precoding weights suitable in case of single cell MU-MIMO systems. In our work we have extended this concept to the case of coordinated multi-cell systems in order to minimize the interference generated towards other-cell UEs and, at the same time, continue to serve the own-cell UEs with a minimum degradation.

The concept of leakage, defined in [TSS05] and [STS07] for the single cell MU-MIMO case, has been extended to a multi-cell scenario. The leakage for the user i caused by the *j-th* interfering cell, is defined as the power that this cell transmits to its served own-cell user with respect to the total power leaked from this cell to the user i. By denoting with $\mathbf{H}_k$ the channel matrix between the *j-th* cell and its own-cell served UE *k,* over the same transmission resources used by the *i-th* UE, it is possible to define the SLNR as follows:

$$SLNR_i = \frac{\left\| \mathbf{H}_k \mathbf{w}_j \right\|^2}{n_R^{(i)} \sigma_i^{\,2} + \left\| \mathbf{H}_j \mathbf{w}_j \right\|^2}$$

The objective is to select beamforming vector $\mathbf{w}_j$ such that the above expression is maximized.

Following a similar approach as in [STS07], the weight vector used by the j-th interfering cell, that jointly maximizes the SLNR, is given by:

$$\mathbf{w}_j \propto \max.\text{eigenvector} \left\{ \left(n_R^{(i)} \sigma_i^{\,2} \mathbf{I} + \mathbf{H}_j^H \mathbf{H}_j \right)^{-1} \mathbf{H}_k^H \mathbf{H}_k \right\}$$

where the norm of $\mathbf{w}_j$ is adjusted to $\left\| \mathbf{w}_j \right\|^2 = 1$.

It should be noted that the vector that optimizes the SLNR is not optimal relative to the SINR criterion, which is the criterion that is usually used to evaluate system performance. Moreover the computational complexity of the ZF solution and the leakage-based solution are similar, namely, $O(n_T^3)$.

Performance results and future steps

The performance of the above multi cell L1 interference rejection scheme has been evaluated by means of system level computer simulations in order to assess the obtainable enhancements of spectral efficiency related to specific parameterizations of the algorithm, system configuration set-up and specific propagation scenarios. In particular the following parameterizations and assumptions were considered when running the computer system level simulations:

Table 4.12: Simulation parameters

Simulation Parameter	Value
Coordination scheme	Multi-cell Interference Rejection based on Coordinated beamforming
UE CSI reporting	Ideal (channel matrix known for each resource at the transmitter)
Cellular Layout	Hexagonal grid, 19 sites, 3 sectors per site
Simulated Link	Downlink
Deployment scenario	Urban Macrocellular (UMa)
Traffic model	Full buffer
Scheduler	Round Robin (non coordinated among different cells)
Bandwidth	10 MHz
Channel model	Spatial Channel Model (SCM)
Number of antenna elements (BS, UE)	(4, 1)
Antenna separation (BS, UE)	(λ/2, λ/2)
Link to system interface	Mutual Information Effective SINR Mapping (MIESM)
HARQ	Realistic (embedded into link level performance curves)
	8 processes - Maximum 4 transmission times
UE channel Estimation	Realistic (embedded into link level performance curves)

The performance of the Multi-cell L1 interference control scheme has been evaluated in terms of CDF of the cell throughput for the two envisioned configurations:

- Fixed number of interfering cells for which to apply the rejection mechanism (NCIC = 1);
- Variable number of interfering cells for which to apply the rejection mechanism (NCIC > 1).

In the following Figure 4.33 a set of curves, showing the performance of the scheme with a fixed number of interfering cells for which to apply the rejection mechanism, are shown for different values of thresholds T. Performance increase is highlighted with respect to the baseline system assumed to be the non coordinated LTE Release 8 system based on codebook single layer precoding (LTE transmission mode 6). Also the case in which traditional non-coordinated singe user adaptive beamforming (LTE transmission mode 7), calculated by means of SVD decomposition, is reported in the figure. It is interesting to notice the trend of performance enhancement once the threshold value is lowered from T = -3dB down to T = -12dB.

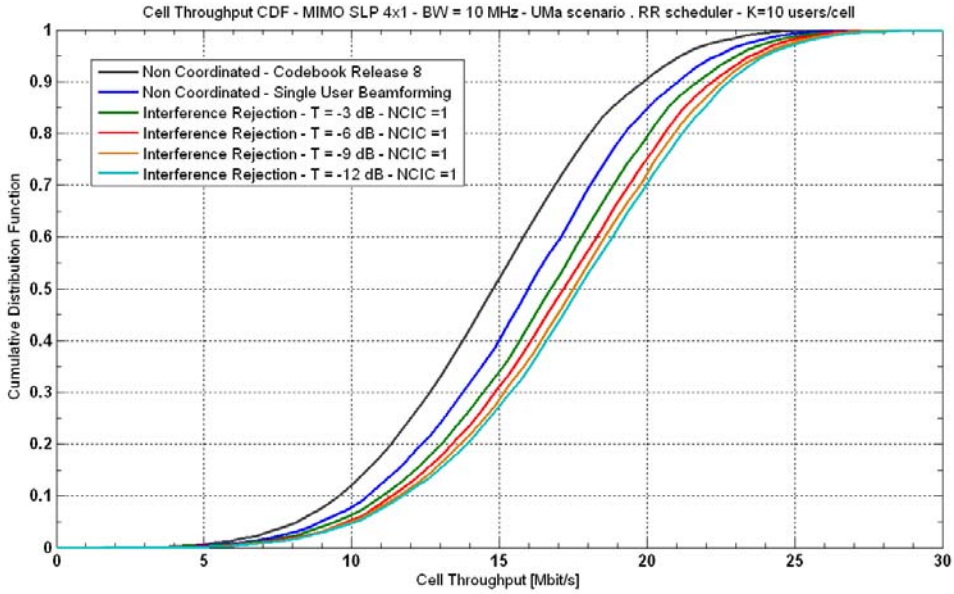

Figure 4.33: Performance of the Multi-cell L1 interference control scheme: NCIC = 1.

When switching to the scheme with variable number of interfering cells for which to apply the rejection mechanism, the performance increases significantly, as shown in the following Figure 4.34. It is though also evident from the simulation results that once NCIC exceeds 2, the increase in performance is negligible, whereas, on the contrary, the overhead and complexity, for implementing a higher NCIC value, increases. Therefore such simulation results may enable to identify a proper NCIC tradeoff value for the parameterization of the system.

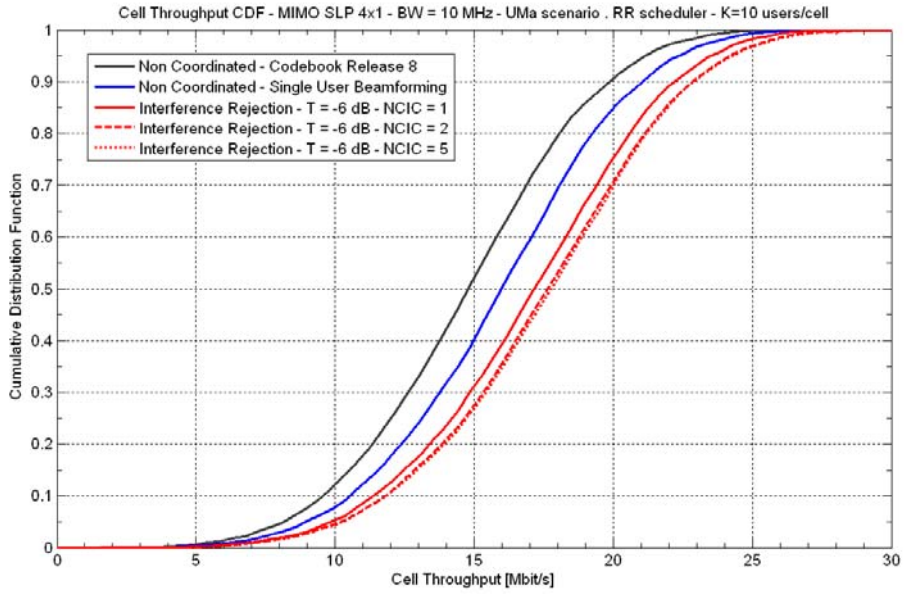

Figure 4.34: Comparison of system performance for different NCIC.

Finally simulations where run for the scheme with a variable number of interfering cells for which to apply the rejection mechanism, as shown in the following Figure 4.35. Once again a set of curves were derived, showing the performance for different values of thresholds T.

Performance increase is highlighted with respect to the baseline system assumed to be the non coordinated LTE Release 8 system based on codebook transmission. Also the case in which traditional single user adaptive beamforming, where the beamforming weights are computed by means of SVD decomposition, is reported in the figure. It is interesting to notice the trend of performance enhancement is greater than the earlier case for fixed NCIC = 1.

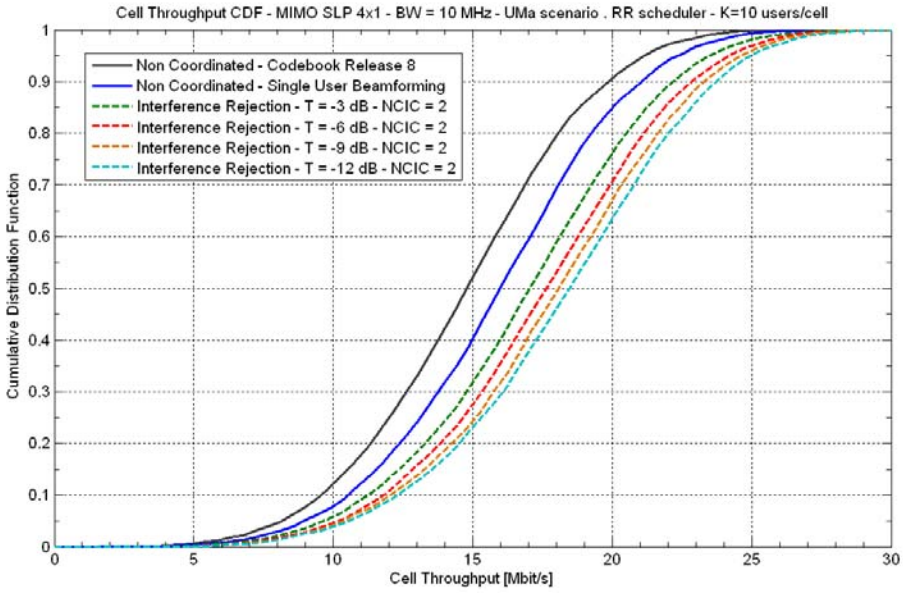

Figure 4.35: Performance of the Multi-cell L1 interference control scheme: NCIC =2.

The user throughput distribution has been evaluated by simulations and the 5-percentile of the distribution, representing the cell edge user performance, has been derived for the different schemes. The key performance indicator η representing the ratio of the average user throughput over the cell-edge user throughput has been evaluated:

$$\eta = \frac{\text{Average User Throughput}}{\text{Cell Edge User Throughput}}$$

This KPI has the interesting property to allow monitoring the performance enhancement of the system at the cell edge, where we have stressed our major interest, without losing performance of the system in average. The following Table 4.13 shows the relevant statistics for different schemes and for the baseline reference systems and the related increase in performance.

Table 4.13: Relevant statistics for the Multi-cell L1 interference control scheme.

Simulated system	Average cell throughput (50-percentile) [Mbit/s]	Average user throughput [Mbit/s]	Cell edge user throughput (5-percentile) [Mbit/s]	η
LTE R8 codebook	14.8	1.48	0.22	6.7
Adaptive beamforming	15.9	1.59	0.29	5.5
Interf. Coord. - T=-6 dB – NCIC = 1	17.2	1.72	0.35	4.9
Interf. Coord. - T=-6 dB – NCIC = 2	17.6	1.76	0.37	4.8
Interf. Coord. - T=-6 dB – NCIC = 5	17.8	1.78	0.374	4.8

The preliminary system performance of the multi-cell L1 interference control scheme has been presented in terms of CDF of the cell throughput for the two presented configurations base on fixed and variable number of interfering cells for which to apply the rejection mechanism. The scheme is based on a variable threshold value that enables to identify potential candidates to be included in the CoMP cooperating set. An appropriate beamforming design is defined for the NCIC cells to reject the interference in a coordinated manner among the cooperating set.

Performance results have been shown for different values of the threshold and the KPI identifying the ratio that monitors the performance enhancement of the system at the cell edge has been shown for the different schemes.

Future work will be performed in the direction of evaluating the overhead introduced in the system by this scheme and the impact of such overhead on the system design leading to a proper tradeoff in terms of parameterization. Additional MIMO transmission modes will be evaluated also in different propagation scenarios and alternative types of CSI reporting will be considered depending on the complexity/accuracy tradeoff adopted in the system.

4.3 - Advanced 3D Beamforming

The adaptive beamforming technology already found a wider distribution some years ago in the context of the evolving WiMAX systems. As an advanced base station feature, it has proven to be able to reduce inter-cell interference through concentrating the transmitted energy towards the user rather than distributing it more equally over the whole cell. At the same time, this technology also became part of other upcoming communication standards like LTE and LTE-advanced.

Beamforming leads to a different statistic of the inter-cell interference characterized by lower mean interference power but increased variance. Depending on the deployment scenario, substantial gains in coverage and cell edge throughput can be achieved.

However, until today beamforming is restricted to control only the horizontal base station antenna pattern. One typical antenna array used for beamforming is a four-element vertically polarized antenna array with half-wavelength element spacing. In vertical direction these arrays have a narrow Half Power Beam Width (HPBW) of few degrees and are adjusted with a fixed downtilt. The main lobe of the vertical antenna pattern points to the ground somewhere inside the cell, so that the cell edge UEs are already outside the main lobe. On the other hand, the fixed vertical antenna gain at the cell edge leads to interference, even if only UEs in the inner part of the cell are served.

At this point, it becomes obvious that an appropriate adjustment of the vertical beam pattern depending on the served user location and on a per resource basis has a potential to further improve the performance of cellular systems. Within ARTIST4G this potential is analyzed. The basic impact of vertical beamforming on interference in typical multi-cell environment is investigated, as well as the combination with horizontal beamforming. This advanced 3D beamforming will be considered first only on physical layer, i.e. without any coordination of resource allocation between base stations. Later [ARTD13] also beam coordination between base stations, using the additional degree of freedom for scheduling, will be taken into account.

4.3.1 - UE-specific horizontal and vertical beamsteering

Today, various different types of eNB antenna systems are in use: single omnidirectional antennas, half-wavelength spaced linear arrays for beamforming, or multiple cross-polarized antennas arranged in arrays or deployed separately. A common characteristic of all of them is the fact that the vertical beam pattern has a relatively narrow HPBW and its angular direction or downtilt is fixed. Recently, antennas with the capability to change the downtilt under operating conditions have become available [And10]. But also for those antennas the adjustment of the downtilt is slow and intended for long-term adaptation according to e.g. traffic load changes. As a consequence, the interference caused at the cell edge is constant, even if only UEs in the inner part of the cell are served.

Further, since the vertical beam pattern has only a small HPBW, the maximum gain is achieved only for a small region within the cell, where the center of the beam touches the ground, depending on downtilt, cell size and eNB height above ground.

These disadvantages of conventional antenna systems can be overcome by antenna arrays with the capability of a full dynamic beamsteering in both horizontal and vertical direction on a per UE basis. Consequently, each UE can be served with a downtilt corresponding to its current location in the cell. Such novel antenna arrays are currently being developed.

The use of pure horizontal beamforming or precoding techniques already showed that interference avoidance can be achieved by appropriate beam coordination [ALUD10]. Advanced 3D beamforming now exploits the additional degrees of freedom given by the combined capabilities of horizontal and vertical beamsteering. If users within the cell could be served with an antenna pattern with larger downtilt, the interference at the cell edge is highly reduced.

In the following subsections different implementation options for the vertical beamsteering are investigated. First, the basic impact of the vertical beamsteering, in combination with a fixed horizontal sector antenna pattern, i.e. the pure downtilt adaptation, is analyzed. Then the combined effects of horizontal and vertical beamsteering are evaluated. The influence of vertical HPBW and cell size on these results is shown. The spectral efficiency, the cell coverage and the cell edge throughput are the relevant metrics taken into account.

System description of the innovation

For the investigations of the 3D beamforming capabilities a hexagonal cell structure with three 120° cells per site and frequency reuse 1 is assumed. The design of the antenna pattern itself and the selection of an appropriate downtilt on per UE basis have the following objectives:

- Maximize the signal strength at the location of the desired user.
- Minimize the mutual interference between adjacent cells, since current cellular radio systems are mainly interference limited.

To achieve the best possible overall performance, a trade-off between these two objectives has to be found. The application of a steeper downtilt for terminals close to the eNB is expected to lead to a decrease of the mutual interference between neighbouring cells. Both cell edge UEs and UEs close to the eNB should benefit from such a transmission scheme. On the one hand, the system parameters can be tuned in order to achieve a preferably high spectral efficiency, but on the other hand also an optimization with respect to cell coverage is possible.

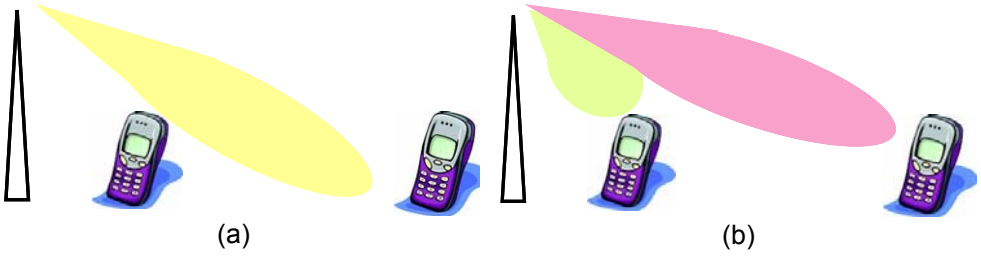

Figure 4.36: Fixed downtilt (a) and vertical beamsteering (b).

In a first investigation, the focus is on the potential and the impacts of modifying only the downtilt on a per UE basis according to the location of the UEs, as shown in Figure 4.36. For this study we use a vertical antenna pattern with fixed shape and a HPBW of 10° as defined in [3GPP36814], which is rotated according to the applied downtilt. In horizontal direction a fixed sector pattern with a HPBW of 65° is utilized. Further, for this first analysis, a pure Line of Sight (LOS) relation between transmitter and receiver is assumed, i.e. the channel is frequency flat. All UEs get the same amount of radio resources.

In a second approach the combination of horizontal and vertical beamsteering is analyzed, using a 4-element half-wavelength spaced antenna array with a resulting horizontal beamwidth of about 30°. In this scenario the vertical HPBW of 6.5° and an Inter-Site Distance (ISD) of 500m according to the 3GPP case 1 scenario [ARTD51] are applied.

The simulation setup used for these studies covers the following different realization options for vertical downtilt adaptation:

- One fixed downtilt for the entire cell, i.e. no adaptation is done (baseline for comparison)
- Two different fixed downtilts with an appropriate assignment of the UE to one of these downtilts. The cell is divided into two areas of the same size in radial direction. If the UE is located in the inner area (near the eNB) the "near downtilt (near DT)" is applied, else the "far downtilt (far DT)" is applied.
- Main lobe steered directly to the UE
    - Without limitation of downtilt, i.e. exact steering for all UEs in the cell. In this case the desired user signal is maximized, but UEs close to the cell border may cause severe interference in the adjacent cell.

- With a limitation of the lowest possible downtilt. Such a limitation avoids too much interference in neighbouring cells by excluding the case where the main lobe is steered directly towards the cell border. However, cell edge UEs cannot exploit the maximal signal strength in the main lobe anymore.

In all cases no specific coordination of the scheduling has been taken into account yet, so that the gain is achieved only due to the statistical effect of dynamic downtilt adaptation compared to the conventional case, where a fixed downtilt is applied independent from the location of the UEs in the cell. This effect becomes directly obvious if we assume a UE close to the eNB. It will be served with a comparatively steep downtilt. Besides the signal maximization of this particular UE, the level of interference caused in neighbouring cells with this transmission will be considerably reduced, i.e. the SINR in both cells will be increased. In the neighbouring cell, in particular the cell edge UEs will benefit from this effect. In all considered cases we presume that the eNB has exact knowledge of the current location of its connected UEs.

Performance results and future steps

In the following, system simulation results for the different abovementioned scenarios and realization options are presented. The utilized key performance indicators are defined according to [ARTD51] as long as not indicated differently.

Impact of vertical downtilt variation

Firstly, the scenario with pure downtilt adaptation but without additional horizontal beamforming is considered. In this case, the ISD is 500m and the vertical HPBW is 10°. Table 4.14 summarizes the main system parameters used for these simulations.

The achieved performance in terms of spectral efficiency and cell coverage is shown in Figure 4.37 and Figure 4.38, respectively. Cell coverage is defined as the percentage of the cell area that exhibits an expected SINR of at least -5dB. For the realization option ‘one fixed downtilt’, the values of near and far downtilt are identical. The performance of exact vertical main lobe steering with and without downtilt limitation is included as well for comparison. For these curves, the x-axis of the diagrams is meaningless.

Table 4.14: Main system parameters

Simulation Parameter	Value
Channel Model	Line of Sight, 3D antenna model
ISD	500m
Velocity	not modelled
eNB antenna	Sector antenna
UE antenna	1 antenna
Channel estimation	Ideal
System bandwidth	10 MHz
Duplex method	FDD
Traffic model	Full buffer
Number of cells	57 (19 sites with 3 cells each)
Number of UEs per cell	10

The black shaded lines in Figure 4.37 and Figure 4.38 (indicated “Single Downtilt”) represent the realization option ‘one fixed downtilt’. Both spectral efficiency and coverage reach their respective maximal values in the range of 15°-16°. This corresponds to the downtilt of 15° which is recommended in [3GPP36814] for the given environment. The spectral efficiency can be slightly improved if the two different fixed downtilts 17° in the near area and 15° in the far area are applied (orange curve). However, the same combination of two fixed downtilts achieves a significant higher coverage than the best suited single downtilt (98% instead of 93°). The fact

that primarily the coverage increases implies that in particular cell edge UEs benefit from this operation mode. The reason for the higher expected SINR is mainly the avoidance of mutual interference rather than a maximization of the desired user signal. Further combinations of near and far downtilt are included in Figure 4.37 and Figure 4.38 for comparison.

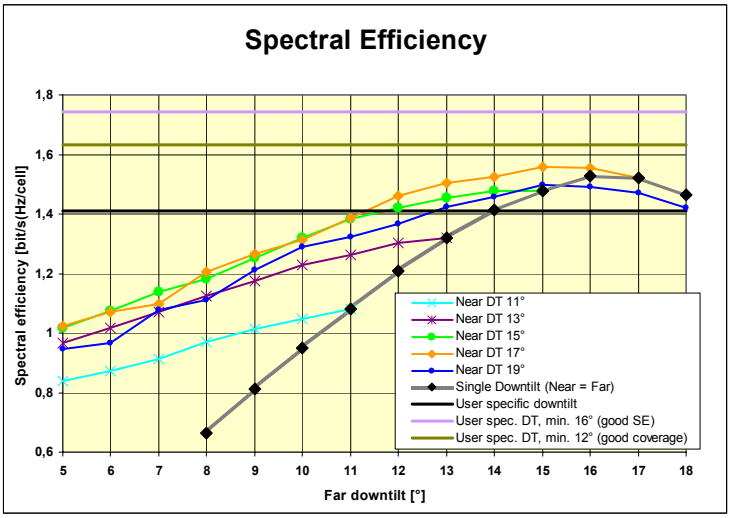

Figure 4.37: Spectral efficiency for different realization options of a transmission system with dynamic downtilt adaptation

Now we compare the performance that can be achieved with fixed downtilts with the alternative realization option, where the vertical main lobe is directed exactly towards the UE, firstly without any limitation. This case is represented by the solid black curves. Obviously, the spectral efficiency falls clearly behind appropriate fixed downtilt combinations. The reason for this behaviour is the high mutual interference caused by UEs close to the cell border that are served with extremely flat beam also covering big parts of the adjacent cell. To overcome this drawback, we now introduce the downtilt limitation, i.e. the applied downtilt must not be smaller than a given value. A limit at 16° yields the overall maximal spectral efficency (14% relative gain compared to baseline). The best cell coverage for this operation mode can be achieved with a slightly smaller limitation at 12°. In Figure 4.37 and Figure 4.38 these cases are represented by the flat olive and purple curves. It is important to note that with respect to coverage, exact steering doesn't outperform the best combination of fixed near and far downtilt. In contrast to the fixed downtilt scenario, exact vertical steering primarily boosts the strength of the desired user signal. The significantly higher performance in terms of spectral efficiency implies that mainly UEs in the near area benefit from exact steering.

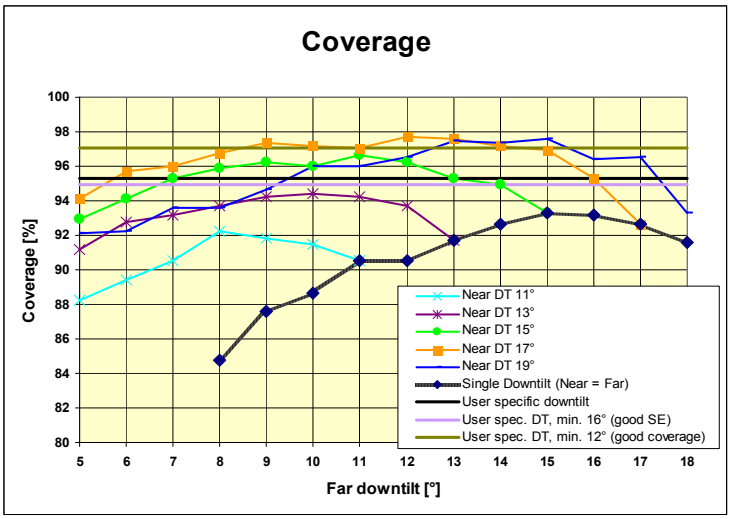

Figure 4.38: Cell coverage for different realization options of a transmission system with dynamic downtilt adaptation

Combination of horizontal and vertical beamforming

Now the combination of vertical beamforming in combination with horizontal beamforming is analyzed. In the following Table 4.15 the main system parameters used for the simulations are given.

Table 4.15: Main system parameters

Simulation Parameter	Value
Channel Model	3GPP case 1 (SCME), 3D antenna model
ISD	500m / 1732m
Velocity	3 km/h
eNB antenna	4 antennas, 0.5 λ spacing
UE antenna	1 antenna
Channel estimation	Ideal
System bandwidth	10 MHz
Duplex method	FDD
Traffic model	Full buffer
Number of cells	21 (7 sites with 3 cells each), wrap around
Number of UEs per cell	15

Figure 4.39 shows the spectral efficiency for the different realization options of the vertical downtilt for an ISD of 500m. In contrast to the previous study, a HPBW of 6.5° is applied. For the case of two fixed downtilts (Figure 4.39), for several values of near area downtilt the far area downtilt is varying from 0 up to 24°. The optimum spectral efficiency with two fixed downtilts is achieved for near area downtilt of 13 – 15°. The spectral efficiency is the same as for one fixed downtilt of 15°. Also results for exact steering to the UEs are given. Here the x-axis indicates the limitation angle of the downtilt. A gain of about 20% for a limitation to 12° is achieved. The reason for this smaller limitation angle compared to the previously mentioned optimum at 16° for spectral efficiency is the impact of the smaller vertical beam width. This indicates that the gain in spectral efficiency results from increased performance of UEs in the inner area. The 5%-ile shown in

Figure 4.40 supports this view. It has its maximum around 10-12° downtilt for the exact steering limitation, and also the two fixed downtilt cases with 13° and 15° near area downtilt reach the exact steering curve and are above the single downtilt case. When increasing the downtilt limitation or the far downtilt above 13° the 5%-ile throughput almost vanishes. This is a clear indication that we can trade off cell edge throughput with overall spectral efficiency.

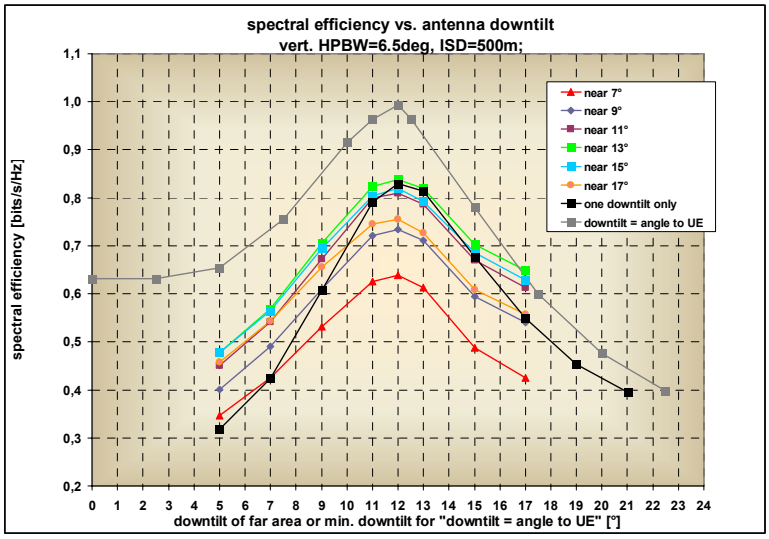

Figure 4.39: Spectral Efficiency for ISD = 500 m

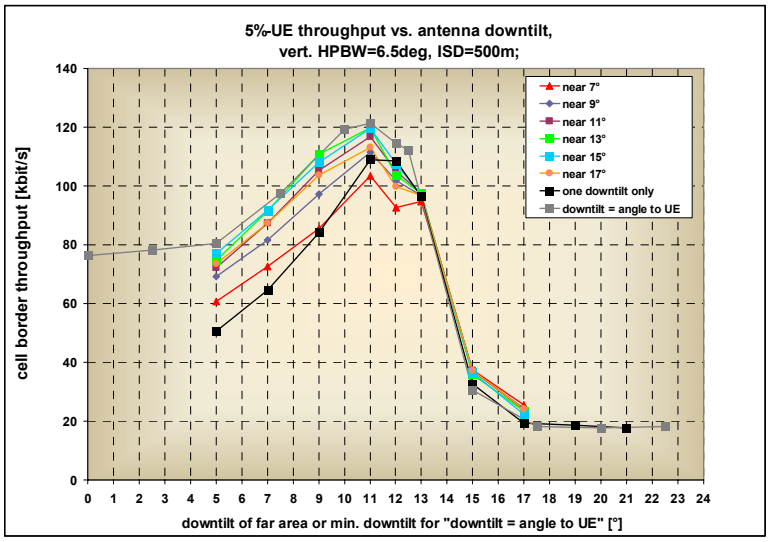

Figure 4.40: 5%-ile throughput for ISD = 500m

The results presented for the first scenario clarify that already pure dynamic downtilt adaptation without horizontal beamforming or precoding and without any kind of coordination allows for a system optimization. However, according to the envisaged performance metric, different realization options and parameter settings seem appropriate. For a preferably high spectral efficiency, exact steering with a possibly strict limitation constraint is the best choice. Also the cell coverage is then better as the baseline. If the aim is a high coverage, then two fixed downtilts is the better solution. However, this comes along with only a marginal improvement of the spectral efficiency. In both cases, the visible overall gains origin from different effects, and in the end also different areas in the cell benefit from them. The reason for the boosted spectral efficiency in case of exact steering to the UE is mainly a better quality of the desired user signal

for UEs close to the base station. The case of two fixed downtilts exhibiting high cell coverage primarily profits by reduced interference at the cell border.

Also the scenario with combined horizontal and vertical beamforming shows that mainly UEs in the inner area of the cell benefit from statistical gains in overall spectral efficiency due to downtilt parameter settings. With pure statistical effects of vertical beamforming the cell edge UEs can gain only performance at cost of overall spectral efficiency. Increase of cell size leads to smaller optimum downtilt angles and reduced gains. In all cases exact beam steering to the UEs gives best performance in terms of spectral efficiency. With downtilt limitation, or even with a suitable combination of near and far area downtilt, the performance tradeoff between cell edge and overall throughput can be influenced.

Up to now, no specific interference avoiding scheduling has been taken into account. Significant gain improvement is expected from horizontal and vertical beam coordination between adjacent cells. Related concepts and results will be part of WP1 Task 1.2 and will be presented in deliverable D1.3 [ARTD13]. Also alternative channel models [CL08], which tend to be more realistic than the geometrical 3GPP 3D antenna model, will be introduced and evaluated. Verification by measurements seems feasible within the scope of WP6.

4.4 - Enablers: channel estimation & feedback design

Channel Estimation (CE) and feedback for novel broadband systems like 3GPP LTE Release 8, 9 or 10 already have reached a high level of maturity, providing very high accuracy of CSI and powerful feedback schemes like the mullti granular codebook design. Typical performance loss for e.g. closed loop MIMO transmission due to real compared to ideal CSI estimation and PMI feedback can be kept within a few dB.

There is a common understanding in the community that CoMP as a complex topic needs further evaluation and 3GPP has for that reason started a new CoMP Study Item (SI) for future releases like LTE Release 11, 12 or even higher. In this document, it is assumed that CoMP and specifically joint processing CoMP are just at the beginning of its evolution and in the future, significantly higher performance gains might be achieved than derived from current simple schemes like intra-site network-centric cooperation. From a standardization point of view, channel estimation as well as feedback optimizations will be in the focus of any advances towards CoMP. From a previous CoMP SI it is well known that CoMP gains can easily collapse in case of realistic CE as well as feedback with realistic overhead assumptions. Therefore, the design of CE and feedback might decide about the future of CoMP as such and can be seen as one of the most important enablers of any advanced precoding solution. Note that feedback design is strongly related to CE and therefore both should be investigated in common. The main issue for CSI feedback is to find an optimum trade off between overhead and achievable DL precoding performance. Depending on the application scenario, different feedback schemes might be selected. In the end the feedback design has to be matched to the CSI estimation accuracy as well as the achievable system level performance gains, i.e. precoding, channel estimation and feedback have to be designed together.

In this section, several topics related to channel estimation and prediction as well as feedback design are discussed: In Section 4.4.1 the problem of simultaneous prediction of channels to multiple sites is investigated based on real measurement data whereas in Section 4.4.2 a prediction approach based on 3D models of the environment and accurate UE feedback of its position is discussed. In Section 4.4.3 a generic feedback compression method is presented and evaluated whereas in Section 4.4.4 hierarchical feedback matched to the relevance of a specific channel to the applied CoMP scheme is proposed. In Section 4.4.5,several approaches for future work with ARTIST4G on feedback compression are outlined.

4.4.1 - Prediction of multi-site MIMO channels for CoMP

Various CoMP schemes require channel quality information at the transmitter for scheme selection, scheduling and transmit parameter optimization. An important type of measurement is the simultaneous estimation of fading channels from several geographically dispersed antennas, to one UE antenna. Such measurements are required to answer questions such as:

- Which of these transmitters contribute enough average received power so that adding them to a joint coherent transmission would be useful? Would the alternative use of these resources for transmission to other users create significant interference for the present UE? (*CoMP scheme selection*.)
- Given the selection of a CoMP scheme, which time-frequency resource blocks in the time-and frequency selective channels would be most useful in a transmission to the present UE? Which ones could instead be used by other transmissions without creating undue interference? (Input to *scheduling decisions*, for example interference avoidance scheduling for a cluster of cells that each uses fixed grid-of-beams beamforming.)
- What is the appropriate modulation and coding for the time-frequency-spatial transmission resources that are scheduled for the UE? (*Link adaptation*).

Answering these questions requires channel estimates with a higher time-frequency resolution than obtained from the multi-site channel power measurements that are now used for handover decisions. Furthermore, due to transmission delays and computational delays, the relevant estimates need to be *prediction estimates.*

The results presented below represent a subset of results from an investigation of the limits of performance of channel prediction in a multi-site environment. Although uplink CoMP is an important problem, it is easier than the downlink problem from a channel prediction perspective. We therefore concentrate on the OFDMA downlinks of possible future FDD LTE versions. We here focus on at scenario that should not be completely unrealistic in a CoMP setting: Prediction at pedestrian velocities (up to 10 km/h) in the 2.7 GHz band, mainly assuming that the required prediction horizon (due to feedback, computation- and communication delays) is 5 ms.

There are many questions that could be posed, but we have here focused of two questions:

1. ***How well can the weakest channel be predicted, when predicting multiple channels simultaneously?*** Downlink channels from different sites will in general have very different average received power. This is a new challenge, as compared to prediction of MIMO channels in single cells. The weakest channel will be hardest to predict, and this will pose problems for CoMP schemes that need prediction estimates of their short-term fading.. If, for example, one site provides a weak channel, then adding that site to a joint downlink transmission scheme might create only small benefits. If that channel is furthermore hard to predict, then the advantages might disappear altogether. A second example: If the channel from a site will be weak, that site could transmit to other users, since this would create low interference. But the confidence in such a conclusion would depend on the quality of the channel prediction on which it is based.
2. ***Can prediction of channels from multiple sites be based on pilot position reuse (overlapping pilots)?*** Simultaneous accurate prediction of fading broadband channels from multiple antennas at multiple sites could potentially require an unrealistically large overhead due to the known pilot symbols that are used for the channel estimation. If antennas/beams at several sites can simultaneously send pilots at the same time-frequency positions, then the CoMP-relevant prediction could potentially be performed at a pilot overhead that is not larger than for present single-cell downlink channel estimation. This technique is called overlapping pilots, and it has been investigated earlier for adaptive OFDMA uplinks in [SA05],[AS07a] and [AS07b].

It is valuable to base such investigations on actual measured channels rather than on standardized channel models, since the process of channel modelling might neglect properties that are important for the questions at hand. The present investigations utilize measured multi-site single-antenna channel data, used by permission of Ericsson AB. Future investigations are planned to collect additional multi-antenna multi-site channel measurements within WP6 of Artist4G, and use them in continued evaluations.

The investigation in this section is based on prediction using Kalman estimators that use previous channel measurements and which estimate several subcarriers in parallel. A radical alternative to such schemes, based on measuring the radio environment in advance, is presented in Section 4.4.2.

Measurements and system description of the innovation

The used measurement data set at Uppsala University was originally collected by Ericsson Research in December 2008 in the Stockholm suburb Kista [MSK+09], [LMF10].The measurements consist of up to 480 seconds long channel data series, denoted *routes*, of a 3-by-4 MIMO-OFDM channel, although here we will only study one of the receiving Antenna Elements (AE). A route is divided into a maximum of 90000 slots of 5.33 ms each. The slots, in turn, are divided into 8 frames of 667 μs each. For each transmitting AE, measurements were taken only during one frame in each slot. The frame consists of 9 OFDM symbols, and an OFDM symbol has 66.7 μs for data and 7.41 μs for the cyclic prefix, the latter of which was removed after reception. The cyclic prefix admits a difference in propagation path lengths of just above 2 km. The OFDM symbol duration of 66.7 μs gives a subcarrier bandwidth of 15 kHz, which is the same as in the LTE standard.

The three transmitting antennas were connected to the transmitting equipment through optical fibre cables, each several hundred meters long, and distributed in a triangular pattern across the suburb, see Figure 4.42. The four receiving AEs were mounted on the roof of the measuring

vehicle. Short channel snapshots were collected once per slot (5.33 ms). A snapshot is 1296 samples long (excluding cyclic prefix) and sampled at 19.44 MHz in the baseband, hence representing 66.7 μs. To avoid inter-carrier interference, the three channels sampled at each receiving AE used separate dedicated frames in the slot. The transmissions used known pilot symbols only, over spectrum in the 2.7 GHz band that was allocated to LTE, but was unused at the time and thus free of interference. The experiments yielded high-quality estimates of radio channels that we here consider to be noiseless.

Because of the sparse sampling, the raw channels will be interpolated in this study, both in time and in frequency. Interpolation by 2D-DFT, then zero padding, then 2D-IDFT is used, meaning that the interpolated channel matches the original exactly at the sampling points, and that no frequency information is added. The upsampling factor in frequency is either one or three, giving a spacing between measured subcarriers of 45 kHz or 15 kHz. In time, a factor of 25 or 75 is used. The highest speed of the measurement vehicle during a measurement campaign was about 30 km/h. Here we wish to investigate prediction performance for UEs moving at pedestrian velocities. We therefore work under the pretension that the velocity is a third of what it actually was during measurement. Taking this into consideration, an upsampling factor of 3x25=75 corresponds to a situation where the channel would have been sampled once every 5330/25=213 μs and the UE velocity would have been 1/3 of the actual velocity. A sampling time of 213 μs roughly corresponds to the duration of three OFDM symbols in LTE. An upsampling factor of 25 corresponds to a separation of 9 LTE symbols.

Figure 4.41 and Figure 4.42 display the travelled route, the corresponding received power levels from the three sites, and the subset of the data and locations that are used for our present investigations. In the whole data set, the signal from the weakest of the three base stations is mostly 20-40 dB below that of the strongest base station. To focus the investigation on the range of most interest, the encircled part of the time history/path is being used. The differences in received power are mostly within 15 dB within this data subset. At this location, the measurement vehicle is driving at approximately 15-20 km/h. This corresponds to 5-6 km/h in our subsampled measurements. White noise of known power is added to the channel samples during this interval. This noise represents interference at the pilot positions, noise, inter-carrier interference and the analog-to-digital conversion noise. The resulting SNR is defined as the sum of signal powers from the three base stations divided by the noise power. It is measured over one-second intervals. Four different noise intensities are added to the data series, to cover a range of reasonable SNRs. The resulting noisy data series form the basis of our investigations.

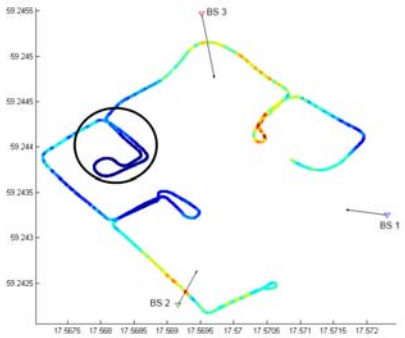

Figure 4.41: Traveled path (latitude and longitude) of received power from three single-antenna sites (BS1-BS3), highlighting the measurements used here.

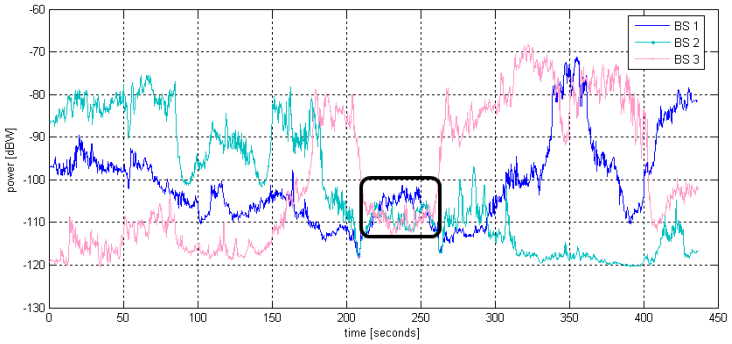

Figure 4.42: Time history of received power from three single-antenna sites (BS1-BS3), highlighting the measurements used here.

We use a state space representation to model the multiple fading channels. This enables the use of prior information about, and measured estimates of, the fading characteristics. A Kalman filter calculates the channel predictions. For increased prediction performance, one can measure multiple parallel subcarriers. Given a reasonably correct channel model, the Kalman filter will combine these measurements in an optimal manner so that measurement noise is suppressed. In this investigation, we measure four parallel subcarriers. The frequency correlation of the channel is represented by a correlation matrix, which is estimated separately. Flat fading results in the best noise suppression through averaging.

The time dynamics of the channels is described by autoregressive (AR) models, with separate modeling of each fading downlink channel. Here we use AR model order 4, which is adequate for most situations. In this investigation we are interested in limits-of-performance, so the AR model parameters are estimated based on noise-free data. They are updated with 1-second intervals, using the first 70 ms of each second for AR model estimation.

The numerical complexity of a Kalman filter is usually high. In the present context however, special matrix structures can be used that considerably reduce the numerical complexity as compared to a general Kalman filter [Aro11].

The Figure below shows an example of the performance obtained by such a Kalman prediction scheme when the Doppler spectrum is flat up to the maximal Doppler frequency. The performance is expressed in terms of the normalized complex channel mean square prediction error (NMSE) of an estimate h_{est} of a channel h, $E|h- h_{est}|^2/E|h|^2$. It is shown as a function of the SNR and of the required prediction horizon, scaled in carrier wavelengths λ. The here investigated 5 ms horizon in a 2.7 GHz channel corresponds to approximately 0.08λ at 6 km/h. Apart from the SNR and the prediction horizon, the prediction performance is highly dependent on the Doppler spectrum of the fading environment. A “peaky” spectrum results in a more easily predicted channel than the exemplified flat spectrum.

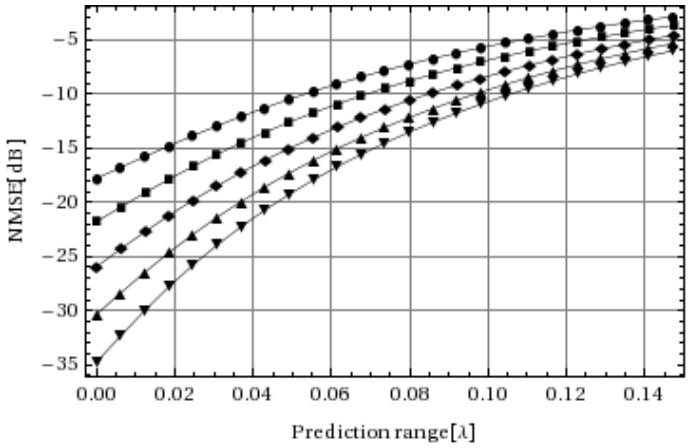

Figure 4.43: Example of attainable channel prediction performance for a channel with flat Doppler spectrum and flat fading over 4 subcarriers. Normalized mean square prediction error (NMSE) for the complex channel as a function of the prediction range scaled in wavelengths and the SNR 0, 5, 10, 15, 20 and 25dB for top to bottom curves. Results for velocity 2 m/s, 2.66 GHz carrier, Kalman predictor with 4 subcarriers, 9x1 pilot pattern.

Performance results and future steps

We turn to the first of our main questions: How well can the weakest channel be predicted, when three channels from different sites are predicted simultaneously?

Figure 4.44 and Figure 4.45 show the resulting measured prediction NMSE performance statistics from different perspectives. To visualize the large data set, we have in Figure 4.44 made a simplification. Based on earlier results on optimized link adaptation and scheduling performance based on prediction estimates of channels [WIND24],[SFT+05][SSO+07], we have used an NMSE of 0.10-0.15, corresponding to -10 to -8 dB, to indicate acceptable prediction performance. For link adaptation in SISO links, an NMSE better than this will cause only a rather small deterioration of the throughput and of multiuser scheduling gains, as compared to having perfect channel knowledge [SFT+05], [SSO+07].

This NMSE limit just represents a very preliminary performance indicator. Different CoMP schemes will require different channel estimation accuracies, some larger and some smaller than prediction NMSE of -8 to -10 dB for the weakest channel. For example, in preliminary investigations, we have found joint linear precoding designed to attain zero-forcing multi-user MIMO transmission to require considerably more accurate channel estimates for all involved channels. On the other hand, interference avoidance scheduling decisions that are based on predictions that a given frequency range of a fading channel will be very weak, might be useful even when the predictions have much larger errors.

The performance has been investigated for different pilot patterns, using overlapping pilots, with 11% pilot overhead. One pattern (3x3) places pilots on every third subcarrier and every third OFDM symbol. The other (9x1) places pilots on all subcarriers of every 9:th OFDM symbol, thus having a lower sampling rate with respect to time and a higher rate with respect to frequency. The best results are here obtained for the 9x1 pattern. This indicates that closely spaced sampling in frequency is more worthwhile than very high temporal sampling rates for these frequency-selective outdoor channels and low UE velocities. For the -8 dB limit (lower right-hand subfigure), good results are almost always obtained as long as the SNR of the weakest channel is at least 2 dB and the power of the weakest channel is less than -10 dB below that of the strongest channel. A -10 dB NMSE limit requires the SNR of the weakest channel to be above 7 dB. It has been very hard to estimate channels that are weaker than -15 dB relative to the strongest channel with adequate accuracy at reasonable SNR levels.

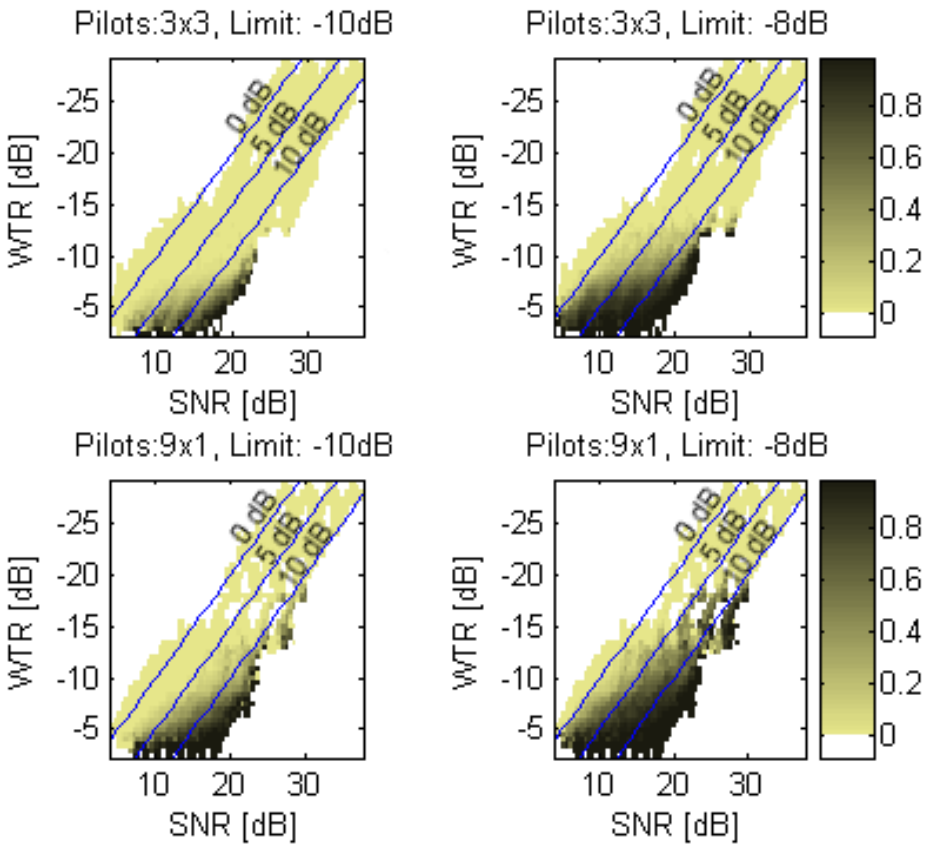

Figure 4.44: Statistics for obtaining "good enough" channel predictions. Results for two NMSE limits: -10 dB (left) and -8 dB (right) and for two pilot patterns: a 3 x 3 grid (top) and every 9:th OFDM symbol filled with pilots (bottom). The results show the percentage of cases where the weakest channel is predicted with NMSE below the limit as a function of the SNR (sum of signal powers/noise power) and of the average power of the weakest channel relative to that of the strongest channel (WTR). The diagonal lines indicate SNR 0, 5 and 10 dB for the weakest channel.

Figure 4.45 shows the same total statistics in the form of histograms of the obtained prediction NMSEs. The NMSEs are locally calculated at each pilot carrying subcarrier and averaged over one second in time. We have also added results for a denser pilot pattern (3x1), where each third OFDM symbol is filled with pilots, with (unrealistic) 33% pilot overhead. This improves the statistics by about 2 dB NMSE, a small improvement that could of course never motivate such an increase in pilot overhead. Additional insights and results can be found in [Ole10].

We now turn to the second question, what is lost by using overlapping pilots? A comparison of the results in Figure 4.45 and Figure 4.46 provides some insights. Figure 4.46 shows the same type of statistics as Figure 4.45, except that we have here used separate pilot positions for each of the three downlinks. This would increase the total pilot overhead fraction from 11% to 33% for the 9x1 and the 3x3 pattern and from 33% to 100% for the 3x1 pattern. The performance would then be improved by only around 1-2 dB NMSE for the 9x1 and 3x1 patterns. The improvement is larger, 3 dB, for the 3x3 pattern. This can again be explained by the significant frequency-selectivity of the channels. For flat-fading channels, the use of overlapping pilots would result in no performance penalty at all. For the pilot patterns that are densely sampled with respect to frequency (9x1 and 3x1), there is a small 1-2 dB performance degradation due to each channel being frequency-varying in a different way from the other two channels. For the pattern with sparse frequency sampling (3x3), this effect is increased to result in a 3 dB loss.

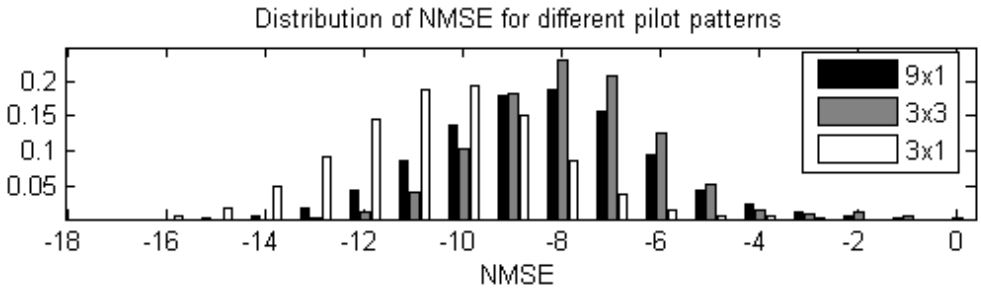

Figure 4.45: Results for overlapping pilots from three sites. Normalized prediction mean square error statistics for the weakest of the three channels, for three pilot patterns: 9 x 1 and 3 x 3 as in the figure above, plus a very dense pattern (3 x 1), with pilots on every 3:rd OFDM symbol.

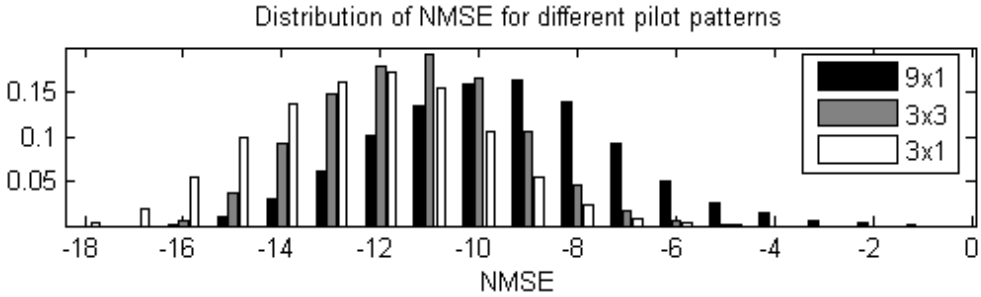

Figure 4.46: Results for separate pilot patterns used for the transmissions from the three sites. Conditions are otherwise as in the figure above.

This section has described an investigation of the performance of channel prediction of the weakest of three simultaneously predicted channels in FDD OFDMA downlinks. The weakest channel has the worst SINR, and will for that reason be hardest to predict. The measured performance for predictions approximately 0.1 wavelengths ahead, relevant for pedestrian velocities at 2.7 GHz has allowed us to draw the following two preliminary conclusions:

1. Under the described conditions, it is mostly possible to predict a channel that is not more than 10 dB weaker than the strongest channel with normalized mean square prediction error < -8 dB. But it appears very hard to estimate the weakest channel if it is more than 15 dB weaker than the strongest one, in reasonable SNR ranges. This is, in a sense, positive for joint transmission CoMP schemes since joint transmission provides the highest potential gains in scenarios with almost equal channel SNRs. But this preliminary conclusion is mainly negative. Situations where the difference between channel powers is so small will be rather rare in most propagation environments. This is due to the strong distance dependence of the received power. The large disparity of received powers is illustrated by Figure 4.42 for our utilized measurement set.
2. Joint estimation of channels from several base stations can be based on overlapping pilots from the base stations. This is positive for CoMP schemes, since it implies that the required pilot overhead need not be higher than for single-cell channel prediction.

Corresponding investigations would be interesting for multi-antenna sites and for TDD systems.

In further work along these lines, more precise descriptions of the channel prediction accuracies required by different CoMP schemes will be needed.

4.4.2 - Advanced channel prediction

Advanced JP CoMP schemes have higher requirements regarding JP CoMP precoding accuracy and – as a consequence – regarding CE quality. Quite a number of results - from extended link level simulation [ZMS+09], SL simulations [3GPP-R1100855], [3GPP-R1000936] to measurements in real world CoMP testbeds [JFJ+10] – indicate the importance of accurate and timely available CSI for proper precoding.

As radio channels are time variant the CSI outdating leads to a mismatch of the precoding and the radio channel conditions and as a result in according performance degradations. One natural direction of research is to minimize the feedback delay as far as possible, e.g. by optimum aligning of RSs and feedback channels, minimizing backhaul delays or processing times. Another option is advanced channel prediction which offers a way to avoid the problem of feedback delay and has been evaluated for quite some time. Auto correlation based methods like Wiener filtering or Kalman [GA08], [UNI10] based schemes are known to work well for short prediction ranges. The main idea is to observe the radio channel for a certain time, estimate correlations in time and/or frequency and to calculate the most probable further evolution of the radio channel [WMM+05], [PW09], [PW10], [WMZ05], [WMM05], see also the approach in Section 4.4.1 .Unfortunately, these approaches have some well known limitations. Apart from a limited prediction horizon, another limitation is that these methods fail in case of birth and death of new multipath components. As simple example take a street crossing, where channel conditions might change completely. In that case observation of the past channel evolution is not sufficient for CSI prediction. For that reason here the so called model based channel prediction will be analyzed, which will use Building Vector Data Maps (BVDM) plus location information within a BVDM to reconstruct radio channels by ray tracing algorithms.

This new approach – at least with respect to feedback minimization or CSI prediction - will be analyzed theoretically for measured real world scenarios in combination with Matlab link level simulations and a ray tracing tool using the above mentioned BVDM for the measured scenario.

System description of the innovation

The main goal of the innovation *model based channel prediction* is to extend the prediction range of well known state of the art prediction algorithms like Wiener or Kalman filtering and as a second independent issue to reduce the overall feedback overhead. The main concept as explained in detail below is to reduce feedback by parameterized compression techniques, where the main parameter is the location of an UE within an artificial model of the surrounding of an eNB. The model itself could be a BVDM of the surrounding of the eNB, which might be constantly updated based on UE feedback. Under the assumption that UE and eNB have exactly the same BVDM available the eNB will be able to fully reconstruct the wideband and frequency selective radio channel from the location information. If additionally a so called moving vector will be fed back describing the movement of the UE within the BVDM even a channel prediction will be possible, helping to overcome the above described CSI outdating issue.

Typical channel models like the Spatial Channel Model Extended (SCME) [BSG+05] are snapshot based models, which derive small scale fading by evolution within one certain large scale fading condition or for one location. Therefore birth and death of multipath components (MPC) within one scenario are not included in such models, but are expected to be essential for CSI prediction in real world scenarios. Therefore it is intended to analyze the proposed concept based on real world channel measurements as being already conducted with the NSN LTE demonstration testbed in Munich, exactly for this purpose.

The proposed concept is at least from the current point of view expected to be quite challenging with respect to accuracy of the channel model reflecting the real world scenario. Another challenge is to really estimate the best fitting UE location, i.e. the matching of UE channel measurements with the best fitting location in the BVDM model. Ray tracing simulations - as potentially the ultimate solution - still require immense processing power and storage capacity not yet available at UEs or eNBs, but this should change in the more far off future due to Moore's law. It is even so that the expected increase in UE and eNB capabilities is a motivation to search for effective methods to make use of it for improved radio performance. Note there is

no direct link between increasing processing capabilities and cellular radio performance, which is mainly defined by Shannon.

The main idea of model based CSI prediction as described above is to feedback an accurate 3D UE position instead of frequency selective CSI, e.g. per PRB as done for conventional systems like LTE Release 8. It includes several steps that will be described in turn:

As a starting point eNBs broadcast or multicast their local 3D BVDMs as a combination of measured pre-stored data and adaptive corrections regularly, e.g. within minutes or hours to all UEs. Possible required adaptations are found based on UE reports of actual channel conditions and take care of opened or closed windows, varying foliage conditions for different seasons, parking cars, new construction sites and so on. All UEs receive and store their local BVDMs. While UEs move they may add further BVDMs from other eNBs, thereby enlarging their overall view of their environment. Broadcasting of BVDMs can be done slowly, while the UE moves from one eNB to the next. As future radio systems will provide broadband data rates the relative overhead for broadcasting of this information is expected to be small even so the absolute amount of data might be relatively large. Alternatively, similar to navigation systems these 3D building vector data might be also downloaded into the UE in advance, e.g. from a CD or over an internet connection. One can think also of a background push service. In addition the eNBs broadcast continuously Common Reference Signals (CRS) or more importantly CSI RSs as in conventional LTE Release 8 or higher systems allowing UEs estimation of CSI evolution over time for all relevant channel components.

As a second step, the UE performs positioning within the BVDM based on GPS localization and channel matching. The accurate estimation of the UE position relative to the BVDM has to be available within a fraction of a wavelength of the RF frequency and is one of the first challenges of the proposed scheme. In case of a 2.6 GHz frequency the wavelength λ is just 0.11m. If the maximum phase error should be smaller than e.g. 5° this will require a location accuracy of less than 0.0016m or 1.6mm. GPS based location will be typically worse than that and other well known location algorithms are even less accurate. It is proposed to combine GPS based localization with a ray tracing based method using the 3D vector building data. Based on GPS the UE places itself in an area of the BVDM, e.g. with an accuracy of $1 \times 1 m^2$ or better. The UE compares the CRS based CSI estimation with that of a ray traced artificial CSI estimation and determines the best fitting location within the $1 \times 1 m^2$ area for which the Mean Square Error (MSE) between estimated and calculated Channel Impulse Response (CIR) is minimized. Note for the calculation the UE has to include its known effective antenna pattern. One simple option is to perform a ray tracing on a grid of possible locations and select in the end that one with the smallest deviation between measured and artificially generated CIR. This might lead for a fine grid to a large processing overhead. Smarter would be a direct calculation of the most probable location based on the main MPCs of the CIR, its relative delay and its delay variation over time. Since there might be ambiguities for noisy channel estimates, tracking over longer distances looks promising.

In a third step, the UE reports to the eNB instead of CSI values itself the best fitting UE 3D position within the BVDM as calculated above. Additionally the UE reports the best fitting moving vector, containing its estimated speed and direction, derived from the CSI evolution over the past or from a navigation tool, allowing the eNB to do CSI prediction for a very large prediction horizon compared to conventional solutions. Nearby located obstacles and specifically moving persons might lead to additional relatively fast fluctuating shadowing effects, which are difficult to model and lead to deviations of the location based CSI estimate with that of the really measured CSI. For that reason, it is proposed to send additionally delta CSI information ΔCSI concerning e.g. moving objects not included in the basic BVDM or any other inaccuracies of the model. The eNB might use this information to correct its reconstructed CIR as well as for updating and adapting its BVDM map to the current channel conditions.

After reception of the 3D location information the eNB in the fourth step is able to reconstruct the wideband CSI based on the UE location within the BVDM plus the delta CSI information ΔCSI.

In case there has been fed back additionally a moving vector $\mathbf{v}_m$ the eNB can predict in the fifth step the movement of the UE within the BVDM, at least for some time – allowing to reconstruct the wideband CSI for any required time instant.

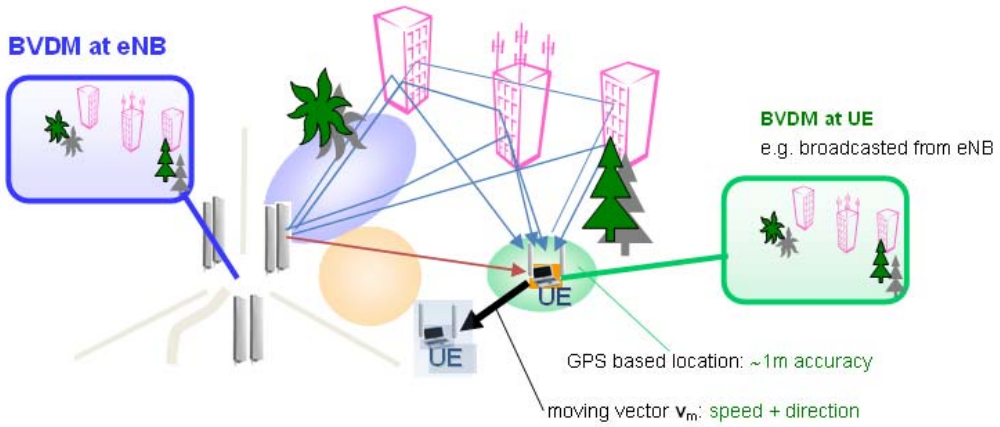

Figure 4.47: Illustration of model based channel prediction

Model based channel prediction has at least theoretically some very nice benefits. Due to the high complexity of the concept these benefits are for the time being more like promises and will be listed in the following:

For high number of channel components and high frequency selectivity as assumed for the cell edge due to a lower probability of line-of-sight conditions compared to cell center, a significant reduction in feedback rate R can be expected. The main reason is the 'parameterized' compression scheme allowing the reconstruction of wideband radio channels with a single location value. Theoretically it would be even possible to use a single value for all channel components from all cooperating eNBs. Assuming for example a RF frequency f_C = 2.6GHz leading to a wavelength of λ=0.11m and a maximum phase error φ_{max}<5° one needs a geometrical resolution of less than 1mm. For a GPS based location accuracy of 1m one needs 10bit resolution in each geometrical direction. In addition the CoMP is typically restricted to nomadic users with a speed lower than v=3.6kmh. The resulting feedback rate might be in that case as low as:

- 3-dim feedback rate: R_{3D} = 3 x 10bit = 30bit/ms = 30kbit/s
- With moving vector over 10-100mm: R_{opt} = 2 x 30kbit/s / 100 / α ≤ 600 bit/s

The value α <1 might decrease overhead further by applying further compression techniques on the location information like e.g. tracking solutions.

Moreover, model-based prediction can offer an increased CSI prediction horizon over Wiener filtering or the subspace concept. These conventional methods are based on estimation of the covariance matrix for the time variant channel impulse response based on observations of previous channel conditions at different time instants. For prediction, constant large scale parameters have to be assumed, which will be not the case e.g. for street crossings etc. Model based channel prediction allows even prediction of birth and death of MPCs. Note nearby moving objects are still a challenge as they will be typically not part of the BVDM model and have therefore to be reported as delta CSI (see above).

Figure 4.48 contains the main building blocks of model based channel prediction, i.e. the generation of the BVDM model, the positioning of the UE within the BVDM, feedback (FB) of the location and reconstruction of the according CSI. Each of the steps has some related issues requiring further evaluation (blue text in figure) like finding accurate and at the same time limited size BVDM models or analysis of the stability of real world radio channels, being a very important prerequisite for the proposed scheme. Note with stability we mean here low to moderate time variance of the radio channel for fixed receiver locations resulting in same CSI whenever an UE is located at the same position. The time variant part of a specific deployment scenario is naturally not predictable, therefore one has to rely on a certain channel stability over some reasonable period of time. UE positioning within a BVDM should be done by combing a rough Global Positioning System (GPS) localization with an accurate CSI estimation. Critical

might be specifically ambiguities of channel estimates leading to a certain misalignment probability, which might be even higher in combination with phase noise, timing instabilities, frequency drifts, inaccurate channel estimation, etc.

The above mentioned time variant part of a scenario is inherently unpredictable and motivates a low rate feedback channel for ΔCSI information, for which appropriate estimation, feedback and signalling schemes have to be developed. In the end most interesting will be to find out the achievable CSI estimation and prediction capability of model based channel prediction.

As mentioned above the full blown concept is seen as a long term research topic. Therefore it will be of great interest to find suitable combinations of conventional techniques with first steps of model based channel prediction, being more easily implementable.

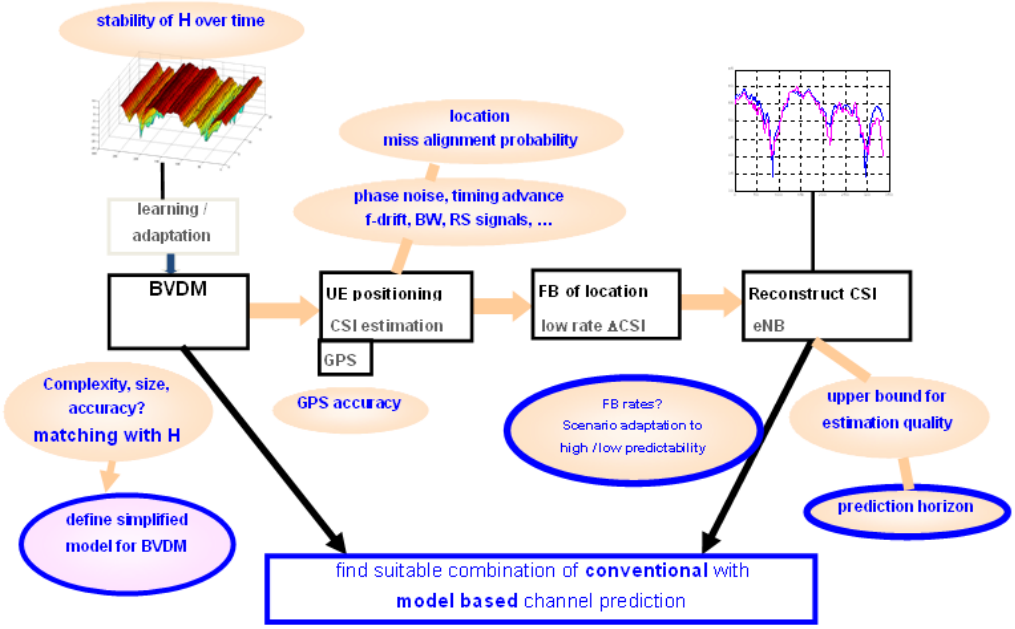

Figure 4.48: Main steps of model based channel prediction and areas of research.

Performance results and future steps

Performance analysis is and will be done based on measurements and a ray tracing simulation for the same scenario. The final goal is to achieve the best possible alignment between measurements and prediction based on the ray tracing tool.

The measurement environment itself at the campus from NSN in Munich is illustrated in Figure 4.49 including a site with 3 sectors, where only sector 2 is active. A van contains the LTE UE, having the cross polarized AE at the top of the van.

The AEs of the UE have been moved according to the routes at bottom right of Figure 4.49, i.e. for route 1 from left to right over 50cm with a step size of 2cm. Further routes 3, 5 and 6 are 2, 4 and 6cm apart of the first line with a lower number of measurements points. Interesting are routes 2 and 4, which are just the reverse paths of route 1 and 3. This allows estimating the stability of the radio channel.

The overall LTE system is a 2x2 MIMO system at RF frequency 2.6GHz. The CSI is measured based over a bandwidth of 33MHz or 2048 subcarrier, where every 6th subcarrier carries a reference signal. The resulting measurements are four dimensional channel matrices **H**(1,1,336,33), where the first two elements indicate the Tx- and Rx antenna, the third element the 336 estimates from the reference signals and the last entry is for the number of repeated measurements at one certain location.

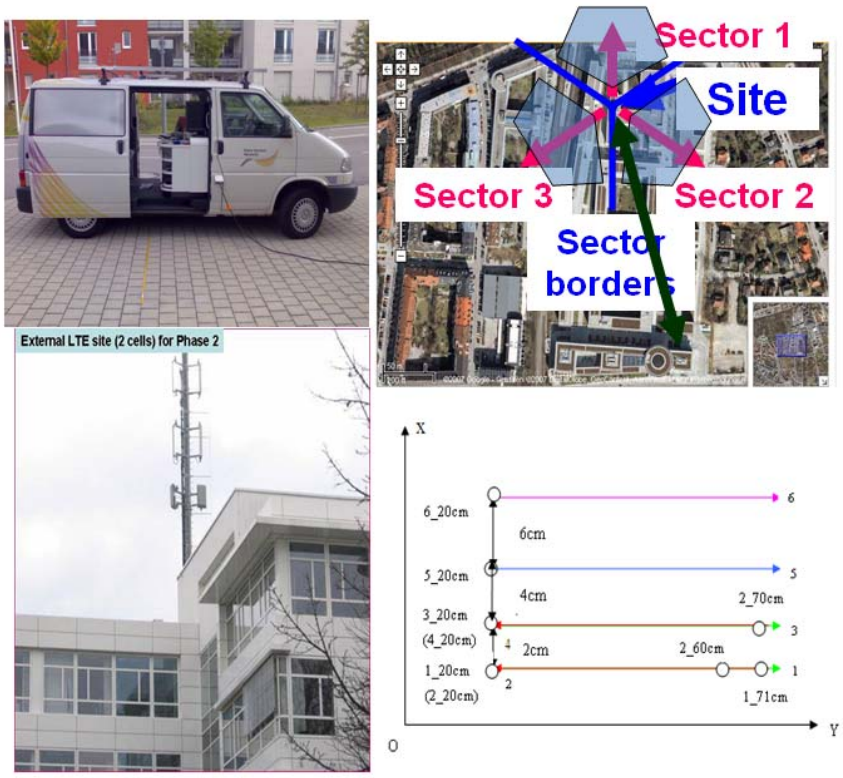

Figure 4.49: Setup of measurement with LTE demonstration system. Bottom right: paths 1 to 6 for movement of receive antennas at UE side.

Evaluation of the measurements has already started and some of the available results are given below. Note due to discontinuous measurements the time alignment per measurement varies by some time samples making extensive pre-processing of the data necessary for proper realignment.

As the stability of the radio channel conditions for one scenario are the basis of model based channel prediction, this issue has been addressed as a first issue. In Figure 4.50 the Channel Transfer Function (CTF) for location loc_1 has been measured at beginning of route 1 and at end of route 2 with a time difference of about 40 minitues in between. The visible high degree of similarity is very encouraging as it proves the validity of the whole concept. Remember the basis is a stable radio channel for fixed locations (large coherence time for a fixed receiver location), while for a moving UE the channel will be time variant. At the right side the evolution over 4 locations with about 30 measurements per location indicates that parasitic effects might easily lead to some degradations of the channel estimation. Note here for each location a new measurement had been started. For continuous measurements the visible artefacts might be avoidable.

Besides stability of the radio channel itself for one location additionally a smooth evolution of the radio channel for a moving UE has to be ensured, at least in areas without birth or death of new MPCs. Otherwise evaluation of channel estimates would be extremely difficult. Figure 4.51 contains further evaluation results, on the left side for one location and at right side for the movements along route 1. The CTF indicates a smooth evolution as requested above. At the same time prediction of MPCs over time looks still challenging requiring more analysis. Beside measurement artefacts as visible form Figure 4.51 a further reason of the varying strength of MPCs can be explained by the superposition of many reflections within one single tap of the CIR.

Further evaluation of the evolution of the CIR for the channel on route 1 can be found in Figure 4.52. Specifically interesting is the evolution for the top 5 taps (bottom, left) over location 1-20 to location 1_70, i.e. over a distance of 50cm corresponding to about 500ms in case of an UE

moving with about 3.6kmh. Up to location 1_50 there seems to be a straight prediction feasible, while at that point the radio channel seems to change, which is conventionally unpredictable. In case of model based channel prediction it is at least theoretically possible to predict this variation as well, which is one of the main promises of this technique. As a very simple model see bottom right a CIR for two different time instances t_1 and t_2 illustrating the birth (or death) of a new MPC.

The final goal is doing prediction based on BVDM models in combination with some form of ray-tracing. For ray-tracing there are only preliminary results available illustrated in Figure 4.53 giving some first hints. Promising is that there is a certain similarity of main characteristics for the measured and ray traced CIRs, e.g. with respect to power of main MPCs, length of the CIR etc.

For a detailed comparison it is necessary to take care exactly of the antenna polarizations, filtering, matching of routes and locations, variation of reflection coefficients etc., which will be the main focus of the coming analysis.

A further important topic will be the required accuracy of the BVDM map, which is for the time being very simple. It will be important to find out what are the limitations for such simplified BVDMs.

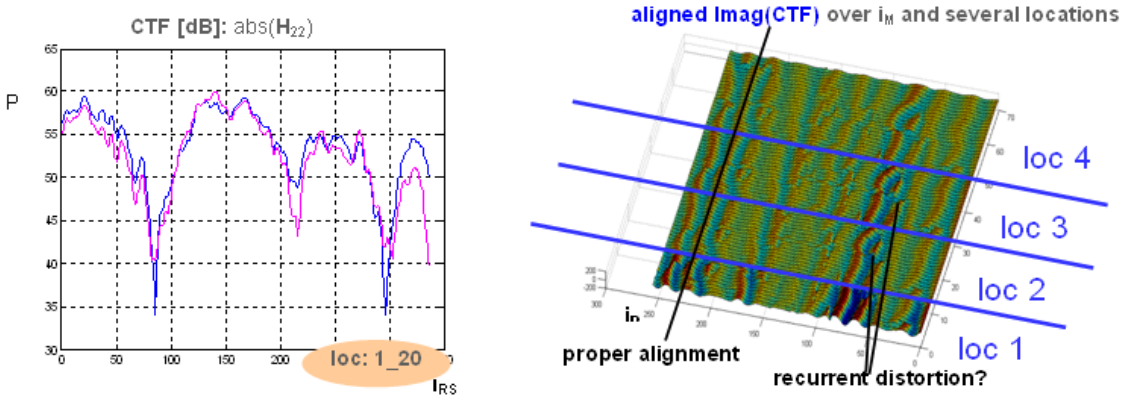

Figure 4.50: Measurement of CTF stability, time difference between measurements T>40 min (left); channel evolution from location loc_1 to 4 with about 30 measurements per location (right).

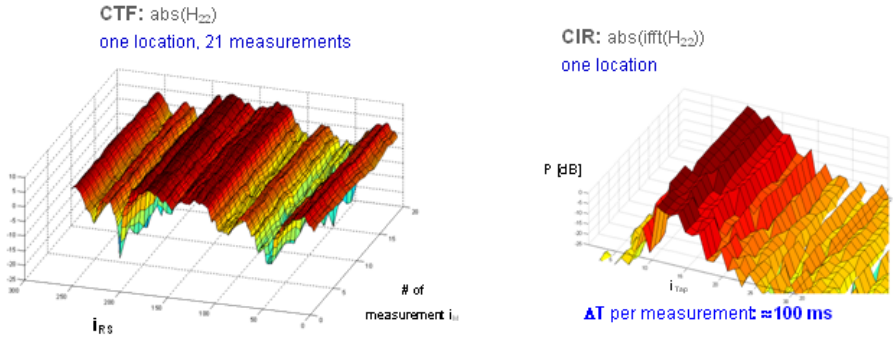

Figure 4.51: Measurement of channel stability for single location (left) and of channel evolution (right). Top CTF in frequency domain and bottom CIR in time domain.

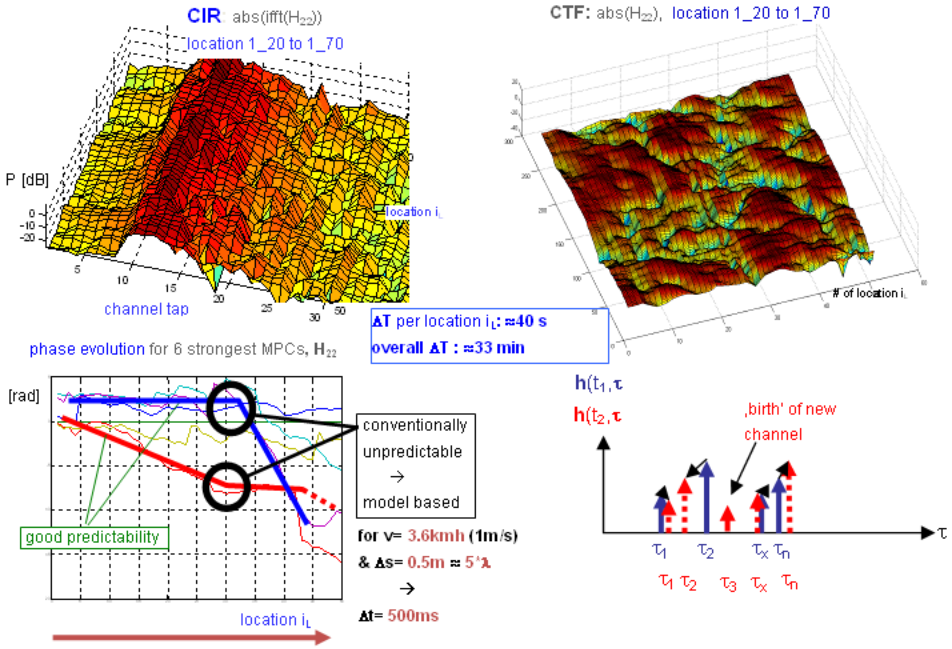

Figure 4.52: Evolution of multi path components over location 1_20 to 1_70 and general MPC model (bottom, left). Thin lines: measured phase of MPC; bold lines: potential prediction

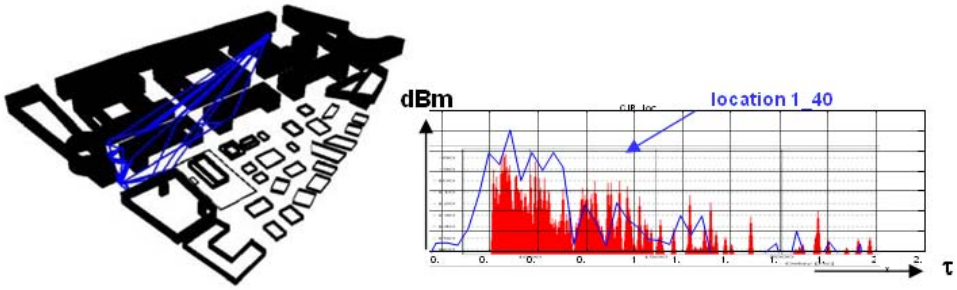

Figure 4.53: First comparison of raytracing and measurement results based on BVDM.

CSI outdating and feedback overhead for wideband radio channels are a serious issue for the implementation of powerful JP CoMP systems.

Model based channel prediction has theoretically and ideally a very high potential to increase the channel prediction horizon as well as to significantly reduce the feedback overhead. By feeding back a location within a known BVDM and reconstruction of the full wideband frequency selective radio channel from a single location value within the BVDM very low feedback rates would be possible. Under the assumption of a very accurate BVDM reflecting the reality with only minor deviations even birth and death of multipath components might be predictable in the future, but this is expected to be a long term research topic. High accuracy of BVDMs is probably related to high memory requirements as well as according high processing complexity as indicated by currently available ray tracing tools. Deriving reduced complexity models for certain sublocations of certain scenario is therefore one important research area.

For the time being first intermediate steps have to verify fundamental questions to get a better understanding what might be possible in reality. Of specific interest are currently smooth ways of combining more conventional CSI prediction like Wiener filtering with the model based approach with the goal to improve the prediction horizon and the prediction quality.

Several specific challenges of model based channel prediction have been partly addressed or will have to be addressed in the future. Among them is the stability of the radio channel which itself is a fundamental issue of the concept as strong time fluctuations would make any model based scheme impossible. Fortunately first real world measurements indicated at least reasonable mid term stability of the radio channel, but more analysis of the measurement results will be needed in the future. A second challenge is the localization of UEs in a BVDM which requires finding the best fitting location for reconstruction of the radio channel. There had been some general activities in this area, but for a better understanding more ray tracing simulations for the measured scenario have to be done. The development of a low complexity BVDM model is seen as a future research topic. The goal is to minimize complexity without loosing too much performance. Moreover, a more detailed measurement procedure will have to be developed and the best usage of reference signals will have to be re-evaluated. The most challenging task is from a current point of view to find the best matching of the BVDM based ray tracing with the measured radio channels, i.e. with reality and to really improve the prediction horizon of the new scheme.

As soon as a working scheme has been found which really has superior performance over more conventional techniques one has to think about necessary adaptations allowing standardization within 3GPP, at least of some simplified schemes. This is not a trivial task as channel prediction might have issues with testing, robustness against feedback errors, incompatibility with existing SU- and MU-MIMO schemes etc.

4.4.3 - Feedback compression

As shown in many reports, employment of Adaptive Modulation and Coding (AMC), along with scheduling, leads to spectral efficiency improvement in wireless communication systems. With AMC, the scheduler employs the CQI to:

1) schedule a user with appropriate Channel Quality (CQ), with the constraint that the quality-of-service requirements is fulfilled, and
2) assign a proper modulation scheme so that the throughput is maximized.

This technique, normally called multiuser diversity, can be considered as a method for providing selection diversity between users and, consequently, channel fading mitigation in wireless networks.

Theoretically, in order to capture multiuser diversity, it is essential for all users to estimate and report their momentary CQI, e.g. SINR, during the transmission. However, the signalling overhead resulting from sending the feedback may be so large that it can make the whole system impractical [EO07]. Hence, there is a tradeoff between the system performance and the spectrum resource that is considered for the channel quality feedback. Therefore, it is necessary not only to implement efficient feedback compression techniques but also to employ appropriate data transmission schemes exploiting the feedback information in the best way.

System description of the innovation and performance results

Practical feedback compression schemes: preliminary results

Figure 4.54 shows the block diagram of a typical scheme considered for feedback compression in downlink. In order to design an efficient feedback compression algorithm, both the time and frequency-domain dependencies must be considered. Depending on delay spread and the Doppler effect, the SNR values of adjacent resource blocks in time and frequency are highly correlated, and an appropriate approach must exploit these two kinds of correlations. In order to exploit the correlation in time, sub-sampling [EO07] or differential coding [3GPP-R1062772] procedures have been introduced. On the other hand, the frequency-domain correlation is processed using different transform coding methods, among which the DCT and Haar transform have shown the best performances [ME10]. Below, the current research on single-link CQ feedback compression for frequency-selective channels is introduced. The ongoing research aims to extend this work to various CoMP scenarios. In section 4.4.4, a particular multi-base hierarchical scheme for feedback of the more complete CSI to be used for multi-base cooperative MIMO precoding is proposed, in which a broadcast channel is assumed for the feedback to the cooperating base stations, so far with no explicit considerations of the correlations in frequency-selective channels. In contrast to the work below, since a broadcast feedback channel is assumed in section 4.4.4, the feedback bit allocation is constrained by the multiple receivers' decoding capabilities of the common broadcast feedback channel.

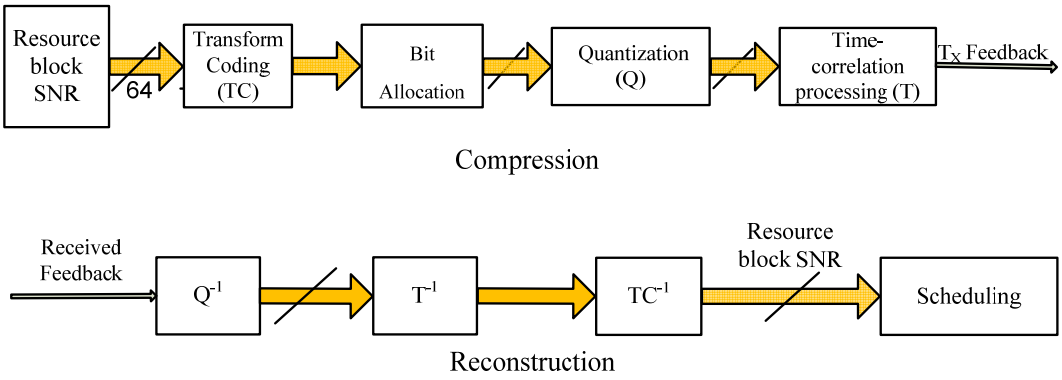

Figure 4.54: Diagram of the feedback encoding and decoding approach. The resource block-SNR values are processed by DCT, Haar transform, etc. at TC and then, bit allocation is applied using one of the, e.g., Lowest *M*, *M* significant average, *M* significant instantaneous, uniform, *Zonal sampling*-based or optimal bit allocation method explained in the following. Then, based on the selected source distribution approach, the transformed values are quantized using standard quantizers. Finally, sub-sampling or differential coding is performed at the last block which exploits the time-domain correlations. The process is inverted at the decoder.

As shown by theory and simulations [3GPP-R1062575], [3GPP-R1051334], [3GPP-R1070368], [3GPP-R1063086], one of the most important modules of an efficient feedback compression scheme is the bit allocation block in which the available bits considered for representing the CQ are distributed between suitable resource blocks. Based on the required efficiency and complexity, there are a number of candidates for bit allocation:

1) **Lowest *M***: This scheme basically allocates all the available bits to the lowest indexed M coefficients of the input, e.g. SNR values of a time slot in different frequencies, and no bits at all to the rest of the coefficients. It is a simple procedure which requires no additional bit mapping [3GPP-R1062575], [3GPP-R1051334], [3GPP-R1070368], [3GPP-R1063086].
2) ***M* significant**: In this technique, the *M* most significant coefficients of the input, e.g. *M* input coefficients with the highest average or with the highest momentary absolute

value, are sent. The selected resource blocks can be considered to be fixed or variant in different time slots; in the case called "*M* significant average" the suitable resource blocks are selected based on their average values and so, the same elements are fed back in different time slots. Therefore, there is no need to use bit mapping procedure. On the other hand, in the second case, named as "*M* significant instantaneous," different resource blocks are considered at each time slot based on their corresponding absolute values. Hence, the bit rate is increased by bit mapping procedure required for indicating the momentary selected indexes [3GPP-R1062575], [3GPP-R1051334], [3GPP-R1070368], [3GPP-R1063086].

3) **Uniform and Zonal sampling**: In the method named "uniform bit allocation" transmission bits are uniformly distributed between all resource blocks while the second technique assigns the available bits to different resource blocks based on the *Zonal sampling* procedure [Say06]. This is a simple and efficient technique which distributes the bits based on the resource blocks variances. Starting from the element with highest variance, one bit is given to the highest-variance component and then its variance is divided by 4. This procedure continues until all available bits are distributed.
4) **Proposed Optimal bit allocation**: Although *Zonal sampling* is a very simple and efficient bit allocation procedure, it is based on some assumptions, such as having infinite number of bits, which are not valid in practice. The bit allocation algorithm proposed in the following, which we call optimal bit allocation, can outperform *Zonal sampling* in the sense of reproduction error reduction [ME10].

Algorithm 1 Proposed Optimal bit allocation algorithm

I. Considering the error variances to be the coefficients initial variances, assign the first bit to the highest variance coefficient.
II. Recalculate the error variances according to

$$\delta_i^2 = E\left((x_i - y_i)^2\right)$$

in which y_i's are the outputs of the Max-Lloyd quantizer, designed for the *i*-th coefficient having n_i number of bits, in response to inputs x_i's.

III. Find the coefficient in which adding the next bit results in maximum reproduction error reduction. Increase its number of bits by 1.
IV. Go to II and continue the process until all available bits are distributed.

Although the algorithm is illustrated for MSE criterion, it can be adapted for other metrics such as throughput as well. For each component a scalar quantizer is designed based on its available number of bits and according to the standard Lloyd algorithm. Finally, Table 4.16 summarizes the number of bits required for different configurations of the system. In this table, *M* is the number of resource blocks in Lowest *M*, *M* significant average or *M* significant instantaneous methods, *N* is the total number of resource blocks, *b* is the number of bits considered for each resource block in Lowest *M*, *M* significant average or *M* significant instantaneous techniques and *C* denotes the total number of bits considered for *Zonal sampling*-based or optimal bit allocation methods. Finally, it should be mentioned that feedback compression has been one of the interesting topics of 3GPP project where the results can be found mainly in [3GPP-R1062575], [3GPP-R1051334], [3GPP-R1070368], [3GPP-R1063086].

Table 4.16: Feedback overhead of different bit allocation methods

Lowest M	$M \times b$

M Significant Average	$M \times b$
M Significant Instantaneous	$M \times b + \left\lceil \log_2 \binom{N}{M} \right\rceil$
Uniform Bit Allocation	$N \times b$
Zonal Sampling Bit Allocation	C
Optimal Bit Allocation	C

Figure 4.55 shows the performance of these methods for a simple wireless channel model. Here, a Rayleigh fading channel with Clarke's (Jakes') Doppler spectrum is simulated in which we have

$$S_c(f) = F[R_c(\tau)] = \begin{cases} \frac{1}{\pi f_D} \frac{1}{\sqrt{1-\left(f/f_D\right)^2}}, & |f| \le f_D \\ 0, \quad otherwise \end{cases}$$

where $S_c(f)$ and $R_c(\tau)$ are the spectral density and autocorrelation functions of the channel $c(t)$ band-limited to f_D (Doppler frequency). In the simulations, a three-tap channel is utilized [Stu96]. Also,

$$E_r = 10\log_{10}\left(1+\frac{\beta}{\delta}\right)$$

is used for demonstrating the reproduction error in which β is the power of the error and δ denotes the original signal power. As we see combination of DCT and the proposed algorithm shows the best performance, minimizing the reproduction error for a given number of feedback bits (For more details about the theoretical and simulation results, the readers are referred to [ME10]). These results target the system level KPI relate to minimizing the control channel overhead, as defined in [ARTD51.]

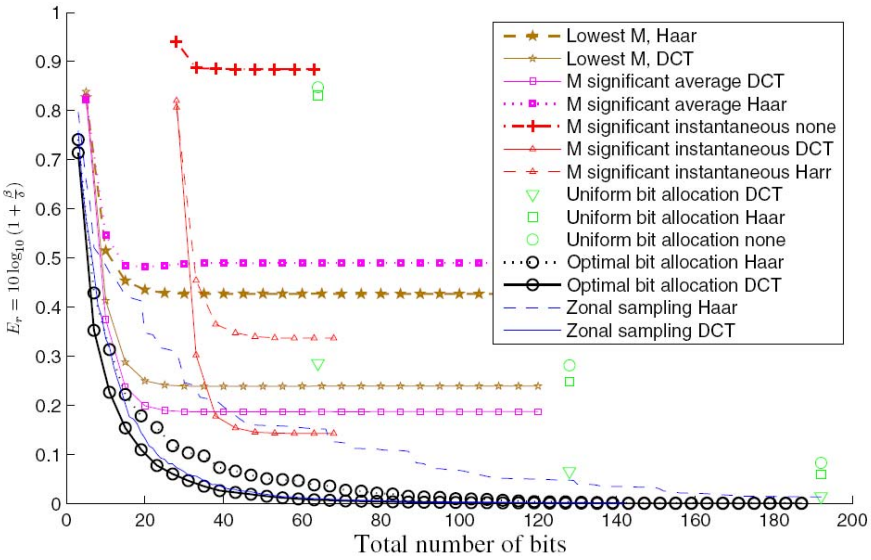

Figure 4.55: Reproduction error in different configurations of the compression system. The five lowest resource blocks have been considered in the Lowest M approaches.

In this section we have described an optimal bit allocation scheme for CQ feedback under a finite feedback rate constraint. Efficient feedback compression is important in order to minimize

the control channel overhead in adaptive transmission systems. The proposed algorithm is shown to minimize the reproduction error of the feedback signal compared to state-of-the-art for a frequency-selective channel in a single-link scenario.

In general, cooperative networks can be modelled as spectrum sharing channels in which different users communicate within the same spectrum resource. Figure 4.56 shows a general spectrum sharing network for two users, while the number of users can be easily extended to any arbitrary number.

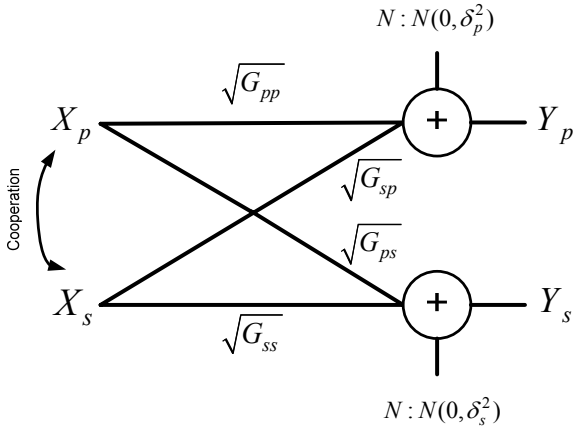

Figure 4.56: Spectrum sharing network. The users communicate within the same spectrum resource.

Within the model depicted in Figure 4.56, various aspects of the network can be modelled. The channels between different terminals can be different, and there will be different quality-of service requirements and level of cooperation. For each scenario, the required amount of CSI feedback will be different, and the optimal way of providing the feedback will also likely be different (ARQ- or CSI-based schemes can be mentioned as examples here). Our long-term plans include theoretical studies of required feedback to optimize system throughput, and, under various constraints as discussed above, develop optimal feedback schemes.

4.4.4 - Hierarchical feedback for multicell cooperative MIMO precoding

One of the distinctive features of interference avoidance techniques which are implemented at the transmit side (e.g. the eNB on the downlink) is the requirement that some form of channel knowledge is fed back from the receivers to the transmitters (CSIT feedback). The CSIT-carrying feedback rates are typically very limited and the feedback resource must be wisely utilized to best represent the most relevant components of the wireless propagation channel.

Such a problem is addressed in the above section 4.4.3. This also gives rise to a number of works addressing this problem by designing filters which are robust to partial knowledge of the channel state information. Here we are now interested in how different eNB could be provided with just the right amount of CSI accuracy, function of their distance from the considered users.

The distinguishing feature of CSIT feedback for JP CoMP is that the CSIT for a user belonging to a given cell n must be made available not only to the eNB for that cell but to all other eNB belonging to the same cooperation cluster. This exchange of information across cells can be envisioned in two distinct ways: (i) the current LTE compliant approach consists in feeding back the CSIT to the serving eNB alone, then asking each eNB to transmit over backhaul links (e.g. X2) the CSIT to the other cooperating eNB, (ii) a more efficient (but currently not standard compliant) approach consists in asking the UE to feedback the CSIT to all listening eNBs, whether being the serving eNB or just a cooperating eNB. This second approach exploits the "broadcast nature" of the wireless propagation channel, ensuring the CSIT is *simultaneously* feedback *and* shared across cooperating cells in just one shot.

In both of these scenarios, it is envisioned that the level of CSIT accuracy that a given cooperating eNB obtains about a given UE shall depend on the distance between them.

Therefore it is expected that the serving eNB shall obtain a more accurate version of the UE's CSIT compared with the CSIT estimate obtained at another more distant (yet cooperating) cell.

Consequently, two problems arise, currently untreated in the literature:

- Designing proper precoding methods that are robust to this lack of accuracy and importantly to the lack of uniformity in the accuracy level across eNBs. This point is addressed in one of the contributions in Chapter 4.2.
- Enabling some structure in the CSIT feedback, so that, even though a given eNB may not know exactly the CSIT available at another eNB, it can still make informed guesses about it, based on some statistical parameters (distance between the UE and the various eNB for instance).

System description of the innovation

The innovation here addressed the second point above. The technique is referred to as Hierarchical Feedback and a special multicell beamforming (JP CoMP) technique is developed to deal with this form of feedback in 4.2.3.

Channel estimation

Before the channel can be actually fed back to the infrastructure side, the channel coefficients must be estimated at the user side. If the users are to estimate efficiently the channels from multiple cell sites, this calls for novel channel estimation techniques in terms of, for instance, how to design the pilots.

Additionally channel estimation can be enhanced by a prediction scheme which exploits the correlation structure of the propagation channel. This can be used to relax backhaul requirements in terms of CSI information exchange between the cooperating cell sites.

CSIT hierarchical feedback

Under the cooperative multi-cell MIMO precoding setup, there is a need for mobiles to feedback their CSI to the base stations engaged in downlink cooperation. The classical approaches assume that the same (possibly finite) CSI is available at all base stations. We investigate a more efficient feedback framework where closer bases are given more precise CSI than more distant ones. We study the application of so-called "hierarchical feedback" schemes to this problem.

In hierarchical feedback, the feedback is generated from a codebook which allow for multilevel representation of the same CSIT. It is also assumed that the user terminal broadcast their feedback signal to all surrounding base stations. Thus, base stations (including non-home cell) decode the feedback directly from what they hear from the mobile. Furthermore hierarchical feedback design allows to explicitly relate the feedback information decoded by different base stations. For example the home base station would decode the fine level of CSIT while a more distant base station may just decode a coarser version of the same CSIT. The advantage of the hierarchical structure in the feedback codebook is that the the home base gains some knowledge of the instantaneous CSIT decoded by other base stations and can use this for the purpose of robust precoding and beamforming.

Thus each user quantizes his channel using a hierarchical codebook, leading to different transmitters (base stations) knowing its channel up to different levels of said codebook.

Base stations could further exchange information about:

- Each user's channel statistics,
- The hierarchy in their knowledge.

These vary at a much slower rate than the instantaneous channel knowledge.

For user k, k = 1, …, K, we define a degrees of accuracy mapping:

$$L_k : \{1,...,N\} \to \{0, l_{k,\max}\},$$

which maps each transmitter to the number of bits it can decode from user *k*'s feedback information, in other words, to its level of knowledge in that user's hierarchical codebook. $l_{k,\max}$ corresponds to the most accurate level (the hierarchical codebook has $2^{l_{k,\max}}$ codewords), whereas 0 bits means only statistical knowledge of the channel. Thus transmitter *j* can decode quantized $\mathbf{h}_k$ up to level $L_k(j)$ yielding estimate $\hat{\mathbf{h}}_k^{(j)}$. One interesting advantage of this hierarchical information structure is that, if $L_k(j_1) > L_k(j_2)$, then transmitter j_1 knows exactly what is known by transmitter j_2, in addition to its own estimate. On the other hand, transmitter j_2 does not know precisely what is decoded by transmitter j_1. However, it does know that $\hat{\mathbf{h}}_k^{(j_1)}$ must belong to the subset of codewords located in the Voronoi region centered at $\hat{\mathbf{h}}_k^{(j_2)}$. This is illustrated in Figure 4.57 where $L_k^{-1}(l)$ denotes the inverse of accuracy mapping l and gives the set of users (if any) which decode the feedback information of user k with accuracy level l.

At this point each cooperating eNB knows either exactly the CSIT available at the other cooperating eNB or at least it knows a small subset of possible candidates. From this it is possible to develop an optimal Bayesian scheme for designing the precoders at each eNB, in a fully distributed way (see 4.3.2).

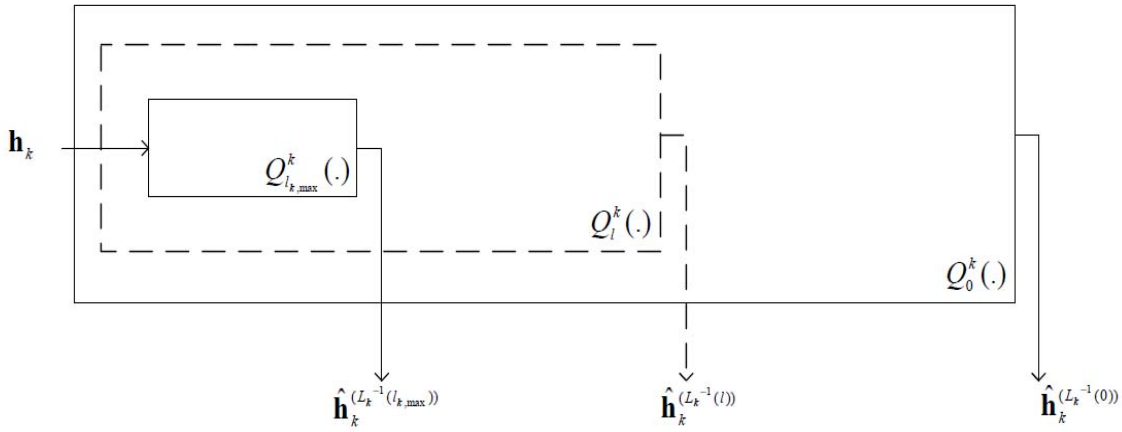

Figure 4.57: Distributed hierarchical CSI model

The principle of hierarchical feedback was introducted for the first time. This form of quantization of the channel information allows for a distributed precoding design across the cooperating eNB which takes into account the lack of uniformity in the CSIT available at all eNB. Performance results are reported in the beamforming design section.

4.4.5 - Advanced feedback compression schemes

LTE Advanced as the next evolutionary step in 3GPP standardization will increase the number of possible eNB/UE antennas from 4/2 to 8/4 and has as one goal the optimization of the overall MU-MIMO scheme, including an optimized feedback design. Studies so far indicate that moderate enhancements to the codebook design should be sufficient so that the current way forward is for implicit feedback only. To improve performance with moderate feedback rates, tracking, adaptive or downloadable codebooks have been proposed.

Tracking codebooks have advantages in case of low mobility where differences between subsequent reports might be small so that by feeding back only the delta reports simultaneously high accuracy as well as low overhead is achievable. Even if technically interesting tracking codebooks are not well accepted in standardization fora due to error propagation for such schemes. Feedback reports are not self-contained meaning that two or more reports have to be combined to get the full information. Perfect synchronization between transmitter and receiver is

required to differentiate between a first and a tracking report. In case of codebook based tracking there is a further challenge: even small changes in the channel conditions will generally lead to a completely different codebook entry so that delta reporting is not directly possible [KZH10] [HZH08]. For UE implementation feedback processing will have to be done over several reports, something which is often seen as a drawback. The same might be true regarding testability.

Downloadable codebooks have been proposed to adapt the feedback to different scenarios like different antenna configurations. While such a solution would be very flexible it leads to a more complex system design. Standardization effort can be expected to be high as codebooks will have to be defined for each individual scenario. In addition testability of such a scheme looks difficult.

Promising, at least for MU-MIMO, are the so called multi granular codebooks which are the combination - i.e. multiplication - of a wideband codebook $\mathbf{W_1}$ with a codebook $\mathbf{W_2}$ adapting to short term CSI variations [3GPP-R1100852].

This has many similarities with the so called effective channel concept as it has been proposed in [JTW+08]. For the effective channel concept a semi-static wideband precoding per eNB and individual post coding per UE is being assumed. The goal is to reduce the number of channel components, which have to be reported, to the number of transmitted data streams. So short term CSI is only reported per effective channel component.

System description of the innovation

In combination with the activities for CSI estimation it is planned to compare different approaches for compression of CSI feedback. In addition, a framework including minimum overhead for CQI reporting should be derived. This is important as in case of rank adaptation several CQI reports for each rank should be avoided.

The following schemes should be investigated, at least on a high level basis: First, lossless compression of the quantized channel state information ideally reduces overhead without any performance loss, but might be in reality very sensitive to feedback errors. Therefore higher coding rates might be required. In addition, lossless compression ratios might vary, while typically a constant feedback container size is much more favourable in real systems. So matching of variable feedback packets into fixed size containers has to be investigated.

Due to low mobility assumption, tracking solutions are still of high interest despite the above mentioned challenges. So it is worth to analyze possible solutions of this second type for, e.g., self contained tracking solutions or at least robust fallback modes in case of feedback errors.

As a third alternative, multi granular codebooks or the more flexible effective channel concept can be taken as starting point for investigations of possible enhancements over LTE Advanced feedback. One interesting question will be whether explicit or implicit feedback for inter site CSI should be used and whether there is a need for amplitude information.

As a promising but challenging fourth alternative, feedback in combination with CSI prediction will be analyzed. Based on some real world channel measurements a first assessment of the model based CSI prediction has been done (see Section 4.4.2) and will be continued.

Moreover, intended precoding solutions as well as the required precoding accuracy will affect other questions like the required frequency selectivity of the CSI feedback, leading to the trade off overhead versus precoding performance.

Performance results and future steps

While there has been some first analysis of tracking solutions or for lossless compression techniques, optimization of feedback is seen to be strongly related to the envisaged channel estimation scheme. Hence work concentrated so far on model based channel prediction. Feedback optimizations will be evaluated in detail in a later stage of the project.

The goal of this innovation is to provide a suitable feedback scheme for advanced CoMP schemes like JP, combining low overhead with most accurate CSI information at transmitter side. The investigations and comparisons will be done based on analytical analysis of promising

concepts, based on link level simulations and where needed also on some light system level simulations. Measurements and ray tracing simulations done for channel estimation in the chapter above will be used as well for deriving the most powerful and reliable feedback scheme.

More detailed analysis is planned only for the most promising concepts. Main focus will lie on feedback reduction in combination with model based channel prediction as introduced in the previous chapter.

5 - Conclusions and next steps

Techniques for interference avoidance lie at the core of ARTIST4G innovation. The progress made so far within the project and reported in the form of the above contributions illustrates both how rich and challenging this research area is. During the first year of the project, several diverse avenues were explored that relate to the key components leading to interference avoidance from the transmitter side. These avenues relate to i) improved methods for multi-user MIMO beamforming in the single cell context (on which is based the generalized form of multi-cell beamforming), ii), new methods for the multi-user multi-cell MIMO beamforming, either with JP CoMP or with coordinated beamforming, iii) fundamental beamforming design (independent of the single user, multi-user, or multi-cell context of application) with the concept of 3D beamforming, and iv) enabling technologies such as channel prediction and estimation and feedback design.

For single-cell multiuser MIMO schemes based on LTE Release 8, the performance of precoding and MCS adaptation was analysed. System level simulations revealed that gains are achievable if the inter user interference could be controlled in a better way as it is the case with the implicit CQI/PMI/RI reporting defined in [3GPP36213]. CSI based feedback together with SLR based precoding and the impact of the feedback quantization on the performance will be investigated next. Three different schemes of the succession for transmit and receive filter design were evaluated in terms of data transmission performance. It was shown that a joint design outperforms a distributed design. However, this approach came with the highest amount of signaling information. In further investigations, an adequate metric shall be found that combines both aspects for a fair comparison between the three schemes. For a double Alamouti scheme in SC-FDMA, the MU performance suffered with respect to the SU case if MMSE detection was applied, which is suboptimal in reducing the interference between the two Alamouti streams. In order to improve the MU performance, more complex detectors are needed and this is left for future investigations. Time Reversal was applied to simple MIMO schemes for HeNBs. It was found that in a building where the HeNB is deployed in the corridor, MIMO brings a gain in spectral efficiency due to the high angular spread in rooms around the corridor. The next steps include a comparison of the proposed scheme with ZF and SVD, in terms of spectral efficiency, complexity, robustness and the extension to Multi-User and Multi-Cell transmission with coordinated femtos.

For multicell multiuser MIMO schemes, the contributions have been in three main areas. First the problem of beamforming design for JP CoMP was addressed, with a comparison of state of the art methods in linear beamforming techniques under realistic system level assumptions. Several improvements were provided in the form of either robust or distributed designs which alleviate the need for accurate exchange of information across the cooperating base stations. The sensitivity of JP CoMP beamforming methods to feedback error and delays was analyzed. Second, power control schemes were considered, in conjunction with the beamforming design problem. Power control for the frequency selective channel considered the allocation of power across subcarriers over the cooperating eNBs. A waterfilling based technique was proposed. Finally, a form of cooperation based on coordinated beamforming was presented, which aims at coordinating the beam from interfering cells to mitigate interference. In this case cooperation benefits are obtained without the need for user data exchange. The next steps include a comparison of the cost-benefits of coordinated beamforming versus JP CoMP and the development of robust JP CoMP schemes which easily generalize to a larger cooperation cluster. Finally, good candidates for field trial implementation should be identified.

For the advanced 3D beamforming, it has been shown that dynamic downtilt adaptation per UE, either with sectorized or beamformed horizontal antenna pattern, can improve system performance. The detailed analysis of the achieved results showed that there is a potential for further increase of spectral efficiency and cell edge performance with coordinated scheduling exploiting the additional degree of freedom due to vertical beamforming. Related concepts and results will be part of WP1 Task 1.2 and will be presented in deliverable D1.3 [ARTD13]. But also more detailed insight into real world channel characteristics, compared to the 3GPP 3D antenna model, is required. Therefore, WP1 will discuss the simulation results and deployment

assumptions with WP6. The results of related lab and field trials planned in WP 6 will be compared with the results from WP1 for further verification of the 3D beamforming concepts.

As enabling technologies, channel estimation and feedback design were identified. Two approaches of advanced channel estimation and prediction have been investigated. In the first contribution, the requirement to estimate or predict channels to multiple sites simultaneously for application in a CoMP scheme has been investigated based on measurements. It was concluded that in scenarios with close-to-equal channel qualities to several sites, channel estimation accuracy was well above the required threshold and therefore CoMP schemes will not break down due to bad channel estimates. The second contribution investigated model-based channel prediction based on 3D maps of the environment and accurate position feedback of the UE. Initial measurements to validate working assumptions necessary for this approach were presented and confirmed the viability of this method. Moreover, three contributions were presented that are related to feedback design. In the first investigation, an algorithm for optimal bit allocation on a transform coding scheme was proposed, evaluated and shown to be superior to other methods. The second contribution proposed the concept of hierarchical feedback where channels to remote base stations are fed back with less accuracy than channels to close base stations because the required accuracy of the channel information necessary at the transmitters is assumed to be higher if the channel has higher quality. The third contribution contained some proposals for future work on feedback design within later stages of this project.

Given the diverse nature of the contributions made in the above areas, choices will be made in the next phase of the project to determine the innovations that show promise and those which are suitable for a real-life implementation test. The challenge ahead lies in the construction of a complete interference avoidance scheme which will combine the above progress in basic beamforming design with some of the new approaches in the MU-MIMO and multi-cell coordination/ JP CoMP, together with the selection of a suitable feedback architecture. The aim of this construction will be to show good performance, robustness, ability for distributed implementation when possible, and reasonable feedback overhead.

6 - References

[3GPP-R1051334] 3GPP, Motorola, “CQI feedback scheme for EUTRA”, R1-051334.

[3GPP-R1062575] 3GPP, LG Electronics, “Further analysis on DCT based CQI reporting scheme”, R1-062575.

[3GPP-R1062772] 3GPP, NEC, “Compressed CQI reporting scheme”, R1-062772.

[3GPP-R1063086] 3GPP, Huawei, “Overhead reduction of best-M based CQI reporting”, R1-063086.

[3GPP-R1063179] 3GPP, Alcatel, “Performance Evaluations of STBC/SFBC Schemes in E-UTRA Uplink”, R1-063179.

[3GPP-R1070368] 3GPP, Huawei, “System level comparison of best-M and DCT-based CQI compression schemes”, R1-070368.

[3GPP-R1090777] 3GPP, Alcatel-Lucent, "UE PMI feedback signalling for user pairing/ coordination", R1-090777.

[3GPP-R1100852] 3GPP, Ericsson and ST-Ericson, “PMI-based Multi-granular Feedback for SU/MU-MIMO Operation”, R1-100852.

[3GPP-R1100855] 3GPP, Ericsson and ST-Ericsson, “Performance evaluation of intrasite DL CoMP”, R1-100855.

[3GPP-R1100936] 3GPP, Alcatel-Lucent Shanghai Bell, Alcatel-Lucent, “CoMP JT in FDD downlink”, R1-100936.

[3GPP-R1103419] 3GPP, Alcatel-Lucent, Alcatel-Lucent Shanghai Bell, CATT, Ericsson, Huawei, LG Electronics, Marvell, M. Electric, Motorola, Nokia, Nokia-Siemens-Networks, N. DOCOMO, Panasonic, Qualcomm, Samsung, Sharp, ST-Ericsson, Texas Instrument, and ZTE, “Way-forward on CSI Feedback Design for Rel-10 DL MIMO", R1-103419.

[3GPP25996] 3GPP TR 25.996, “Spatial channel model for Multiple Input Multiple Output (MIMO) simulations”.

[3GPP36814] 3GPP TR 36.814, “Evolved Universal Terrestrial Radio Access Network (E-UTRAN); Further advancements for E-UTRA physical layer aspects”, Release 9.

[3GPP36211-R8] 3GPP TS 36.211, “E-UTRA Physical Channels and Modulation”, Release 8.

[3GPP36213-R8] 3GPP TS 36.213, “E-UTRA Physical Layer Procedures“, Release 8.

[3GPP36211] 3GPP TS 36.211, “E-UTRA Physical Channels and Modulation”, Release 9.

[3GPP36213] 3GPP TS 36.213, “E-UTRA Physical Layer Procedures”, Release 9.

[ACH07] J.G. Andrews, Wan Choi, and Robert W. Heath Jr., “Overcoming Interference in Spatial Multiplexing MIMO Cellular Networks”, IEEE Wireless Communications, Vol. 14, No. 6, pp. 95–104, Dec 2007.

[Ala98] S.M. Alamouti, “A Simple Transmit Diversity Technique for Wireless Communications,” IEEE Journal on Select Areas in Communications, vol. 16, no. 8, October 1998.

[ALUD10] “Co-Scheduling”, Alcatel-Lucent contribution to EASY-C Public Workshop April 16, 2010

[And10] Andrew (A CommScope Company), "SmartBeam: 3° of freedom”, http://www.commscope.com/andrew/eng/aboutus/index.html, 2010

[Aro11] D. Aronsson, MIMO OFDM Estimation and Prediction with Optimal Filters, PhD Thesis, Department of Engineering Sciences, Uppsala University, February 2011.

[ARTD11] D1.1 - “Definitions and architecture requirements for supporting interference avoidance techniques”, ARTIST4G technical deliverable, August 2010.

[ARTD13] D1.3 - “Innovative scheduling and cross-layer design techniques for interference avoidance”, ARTIST4G technical deliverable to appear, 2011.

[ARTD51] D5.1 - "Scenarios, Key Performance Indicators and Evaluation Methodology for Advanced Cellular Systems", ARTIST4G technical deliverable, June 2010.

[ARTD61] D6.1 - “First Feedback on Implementation Aspects Connected to the Selected Innovations”, ARTIST4G technical deliverable to appear, 2011.

[AS07a] D. Aronsson and M. Sternad, “Kalman predictor design for frequency-adaptive scheduling of FDD OFDMA uplinks”, IEEE Conference on Personal, Indoor and Mobile Radio Communications, PIMRC, Athens, Greece, September 2007.

[AS07b] D. Aronsson and M. Sternad, “OFDMA uplink channel prediction to enable frequency-adaptive multiuser scheduling”, European Signal Processing Conference Eusipco, Poznan, Poland, September 2007.

[BSG+05] D.S. Baum, J. Salo, G.D. Galdo, M. Milojevic, P. Kyösti, and J. Hansen, "An Interim Channel Model for Beyond-3G Systems," IEEE Vehicular Technology Conference 2005 Spring, Stockholm: 2005.

[BSX+10] C. Botella, T. Svensson, X. Xu, and H. Zhang, “On the performance of joint processing schemes over the cluster area,” Proc. IEEE Vehicular Technology Conference-spring, 2010.

[BV04] S. Boyd, L. Vandenberghe, “Convex Optimization”, Cambridge Univesity Press, NY, USA, 2004.

[BZG+09] E. Björnson, R. Zakhour, D. Gesbert, B. Ottersten, “Distributed Multicell and Multiantenna Precoding: Characterization and Performance Evaluation”, IEEE Global Communications Conference (GLOBECOM 2009), Honolulu, Hawaii, Dec. 2009.

[Cos83] M. Costa, "Writing on dirty paper," IEEE Transactions on Information Theory, vol. 29, 1983, pp. 439-441.

[CBS06] C. Ciochina, F. Buda and H. Sari, “An Analysis of OFDM Peak Power Reduction Techniques for WiMAX Systems,” ICC’06, Istanbul, Turkey, June 2006.

[CCM+09] C. Ciochina, D. Castelain, D. Mottier and H. Sari, “New PAPR-Preserving Mapping Methods for Single-Carrier FDMA with Space-Frequency Block Codes,” IEEE Transactions on Wireless Communications, vol. 8, issue 10, pp. 5176-5186, Oct. 2009.

[Cio07] J.M. Cioffi, “Advanced Digital Communications, EE379c”, Stanford University Course Notes, http://www.stanford.edu/class/ee379c, 2007.

[CJC+08] Castro, P.M.; Joham, M.; Castedo, L.; Utschick, W.; "Robust MMSE linear precoding for Multiuser MISO systems with limited feedback and channel prediction," Personal, Indoor and Mobile Radio Communications, 2008. PIMRC 2008. IEEE 19th International Symposium on, vol., no., pp.1-5, 15-18 Sept. 2008

[CL08] D. Chizhik, J. Ling, "Propagation over clutter: Physical Stochastic Model," IEEE Trans. on Antennas and Propagation, Vol.56, No.4, April 2008

[CS03] G. Caire and S. Shamai, "On the achievable throughput of a multiantenna Gaussian broadcast channel," IEEE Transactions on Information Theory, vol. 49, 2003, pp. 1691-1706.

[EO07] T. Eriksson and T. Ottosson, “Compression of feedback in adaptive OFDM-based systems using scheduling,” Communications Letters, IEEE, vol. 11, no. 11, pp. 859–861, Nov. 2007.

[EVH+04] Emami, M.; Vu, M.; Hansen, J.; Paulraj, A.J.; Papanicolaou, G.; "Matched filtering with rate back-off for low complexity communications in very large delay spread channels"Signals, Systems and Computers, 2004. Conference Record of the Thirty-Eighth Asilomar Conference on Volume 1, 7-10 Nov. 2004 Page(s):218 - 222 Vol.1 Digital Object Identifier 10.1109/ACSSC.2004.1399123

[FKV06] G.J. Foschini, K. Karakayali, R.A. Valenzuela, “Coordinating multiple antenna cellular networks to achieve enormous spectral efficiency”, IEEE Proceedings Communications, Vol. 153, No. 4, pp. 548–555, Aug. 2006.

[GA08] M. Grewal and A. Andrews, Kalman Filtering Theory and Practice Using MATLAB, John Wiley & Sons, 2008.

[GSC09] A. García Armada, M. Sánchez Fernández, and R. Corvaja, “Waterfilling Schemes for Zero-Forcing Coordinated Base Station Transmission”, IEEE Global Communications Conference (GLOBECOM 2009), Honolulu, Hawaii, Dec. 2009.

[HKR97] P. Hoeher, S. Kaiser, and P. Robertson, Two-dimensional pilot-symbol-aided channel estimation by Wiener filtering, in Proc. IEEE International Conference on Acoustics, Speech, and Signal Processing (ICASSP), Munich, Germany, Apr. 1997, pp. 1845-1848.

[Hot03] A. Hottinen, “Multiuser scheduling with matrix approximation,” IEEE International Symposium on Signal Processing and Information Technology ISSPIT 2003, Darmstadt, Germany, 14-17 Dec. 2003.

[HZH08] K. Jee Hyun, W. Zirwas, and M. Haardt, "Adaptive Codebooks for Efficient Feedback Reduction in Cooperative Antenna Systems," IEEE Global Telecommunications Conference, 2008.

[JFJ+10] V. Jungnickel, A. Forck, S. Jaeckel, F. Bauermeister, S. Schffermller, S. Schubert, S. Wahls, L. Thiele, T. Haustein, H. Droste, G. Kadel, "Cell-Edge Trials using Coordinated Multi-Point Transmission in the Downlink, Proc. 3rd International Workshop on Wireless Distributed Networks (WDN), Istanbul, Turkey, Sep, 2010.

[JG04] S. Jafar and A. Goldsmith, “PhantomNet: exploring optimal multicellular multiple antenna systems,” EURASIP Journal on Applied Signal Processing, vol. 5, pp. 591-604, 2004.

[Jin06] N. Jindal, "A feedback reduction technique for MIMO broadcast channels," 2006 IEEE International Symposium on Information, 2006, pp. 2699-2703.

[JKG+02] Joham, M.; Kusume, K.; Gzara, M.H.; Utschick, W.; Nossek, J.A.; "Transmit Wiener filter for the downlink of TDDDS-CDMA systems," Spread Spectrum Techniques and Applications, 2002 IEEE Seventh International Symposium on , vol.1, no., pp. 9- 13 vol.1, 2002

[JTW+08] V. Jungnickel, L. Thiele, T. Wirth, M. Schellmann, V. Venkatkumar, and T. Haustein, "Feedback Design for Multiuser MIMO Systems," 13th International OFDM-Workshop, 2008.

[JUN05] Joham, M.; Utschick, W.; Nossek, J.A., "Linear transmit processing in MIMO communications systems," Signal Processing, IEEE Transactions on, vol.53, no.8, pp. 2700- 2712, Aug. 2005

[KFV06] M.K. Karakayali, G.J. Foschini, R.A. Valenzuela, “Network coordination for spectrally efficient communications in cellular systems”, IEEE Wireless Communications, Vol. 13, No. 4, pp. 56–61, Aug. 2006.

[KO02] Klang, G.; Ottersten, B., "Space-time interference rejection cancellation in transmit diversity systems [cancellation read combining]," Wireless Personal Multimedia Communications, 2002. The 5th International Symposium on , vol.2, no., pp. 706- 710 vol.2, 27-30 Oct. 2002

[KZH10] J. Kim, W. Zirwas, and M. Haardt, "Efficient Feedback via supspace based channel quantization for distributed cooperative antenna systems with temporally-correlated channels," submitted to EURASIP special issue MIMO Transmission with limited feedback.

[LBS+10] T.R. Lakshmana, C. Botella, T. Svensson, X. Xu, J. Li, and X. Chen, “Partial joint processing for frequency selective channels,” Proc. IEEE Vehicular Technology Conference-fall, 2010.

[LMF10] B.K. Lau, J. Medbo and J. Furuskog, “Downlink cooperative MIMO in urban macrocell environments”. 2010 IEEE International Symposium on Antennas and Propagation (ARSURSI).

[LX08] Z. Li and X.-G. Xia, “PAPR reduction for repetition space-timefrequency coded MIMO-OFDM systems using Chu sequences,” IEEE Trans. on Wireless Commun., vol. 7, no. 4, pp. 1195–1202, Apr. 2008.

[ME10] B. Makki, T. Eriksson, “Efficient Channel Quality Feedback Signaling Using Transform Coding and Bit Allocation,” Proc. IEEE Vehicular Technology Conference-spring, 2010.

[MF08] P. Marsch and G. Fettweis, "A direct solution for rate balancing in MIMO broadcast channels with per-base-station power constraints," in Proceedings of the 7th International ITG Conference on Source and Channel Coding, January, 2008.

[MK10] J. Mundarath and J. Kotecha, "Optimal receive array beamforming for non-collaborative MIMO space division multiple access," IEEE Transactions on Communications, vol. 58, 2010, pp. 218-227.

[MLG06] H. G. Myung, J. Lim, and D. J. Goodman, “Single Carrier FDMA for Uplink Wireless Transmission”, IEEE Vehicular Technology Magazine, vol. 3, no. 1, Sep. 2006, pp. 30-38.

[MSK+09] J. Medbo, I. Slomina, A. Kangas, and J. Furuskog, ”Propagation channel impact on LTE positioning accuracy – A study based on real measurements of observed time difference of arrival”. IEEE Personal, Indoor and Mobile Radio Communications (PIMRC) 2009, Sept. 13-16, 2009, Tokyo, Japan.

[Ole10] R. Abildgaard Olesen, “Channel Estimation for Coordinated Multipoint Transmission”, Master of Science Thesis, Department of Engineering Sciences, Uppsala University, Dec. 2010.

[PBG+04] G. Piñero, C. Botella, A. González, M. de Diego, N. Cardona, “Downlink power control and beamforming for a cooperative wireless system,” Proc. IEEE International Symposium on Personal, Indoor and Mobile Radio Communications, 2004.

[PBG+10] A. Papadogiannis, H. J. Bang, D. Gesbert, and E. Hardouin, “Efficient selective feedback design for multicell cooperative networks,” to be published in IEEE Transactions on Vehicular Technology, 2010.

[PW09] N. Palleit and T. Weber, "Obtaining transmitter side channel state information in MIMO FDD systems," IEEE 20th International Symposium on Personal, Indoor and Mobile Radio Communications, IEEE, 2009, pp. 2439-2443.

[PW10] N. Palleit and T. Weber, "Frequency prediction of the channel transfer function in multiple antenna systems," International ITG Workshop on Smart Antennas , IEEE, 2010, pp. 244-250.

[SA05] M. Sternad and D. Aronsson, ”Channel estimation and prediction for adaptive OFDMA/TDMA uplinks based on overlapping pilots”, IEEE

International Conference on Acoustics, Speech and Signal Processing, ICASSP, Philadelphia, USA, March 19-23 2005.

[Say06] K. Sayood, Introduction to Data Compression. Morgan Kaufmann Publishers, 3rd ed., 2006.

[SFT+05] M. Sternad, S. Falahati, T. Svensson, and D. Aronsson, ”Adaptive TDMA/OFDMA for wide-area coverage and vehicular velocities”, IST Mobile and Vehicular Communication Summit, Dresden, June 19-23, 2005.

[SGH08] H. Skjevling, D. Gesbert, A. Hjørungnes, “Low-complexity distributed multibase transmission and scheduling,” EURASIP Journal on Advances in Signal Processing, 2008.

[SKH+08] S. Shim, J.-S. Kwak, R.W. Heath, Jr., and J.G. Andrews, “Block Diagonalization for Multi-User MIMO with Other-Cell Interference”, IEEE Transactions on Wireless Communications, Vol. 7, No. 7, pp. 2671–2681, July 2008.

[SKJ94] H. Sari, G. Karam, and I. Jeanclaude, “Frequency-domain equalization of mobile radio and terrestrial broadcast channels,” in GLOBECOM ’94, Dec. 1994.

[SSJ+05] Schubert, M.; Shuying Shi; Jorswieck, E.A.; Boche, H., "Downlink Sum-MSE Transceiver Optimization for Linear Multi-User MIMO Systems," Signals, Systems and Computers, 2005. Conference Record of the Thirty-Ninth Asilomar Conference on , vol., no., pp. 1424- 1428, October 28 - November 1, 2005

[SSO+07] M. Sternad, T. Svensson, T. Ottosson, A. Ahlén, A. Svensson and A. Brunstrom, ”Towards systems beyond 3G based on adaptive OFDMA transmission”, Proceedings of the IEEE, vol. 95, no. 12, pp. 2432-2455, December 2007.

[SSV+08] S. Shi, M. Schubert, N. Vucic, and H. Boche, "MMSE Optimization with per-base-station power constraints for network MIMO systems," IEEE International Conference on Communications, IEEE, 2008, pp. 4106-4110.

[STS07] M. Sadek, A. Tarighat, and A. Sayed, "A Leakage-Based Precoding Scheme for Downlink Multi-User MIMO Channels," IEEE Transactions on Wireless Communications, 2007.

[Stu96] G. L. Stuber, Principles of Mobile Communication. Kluwer Academic Publishers, 1996.

[Stu99] J. F. Sturm, “Using SeDuMi 1.02, a MATLAB tool for optimization over symmetric cones,” Optim. Methods Softw., vol. 11–12, pp. 625–653, 1999.

[TCJ07] A. Tolli, M. Codreanu, and M. Juntti, "Minimum SINR Maximization for Multiuser MIMO Downlink with Per BS Power Constraints," Wireless Communications and Networking Conference, 2007. WCNC 2007, 2007, pp. 1144-1149.

[Tel00] J. Tellado, Multicarrier Modulation with Low Peak to Average Power Applications to xDSL and Broadband Wireless, Boston/ Dordrecht/ London: Kluwer Academic Publishers, 2000.

[TJC99] V. Tarokh, H. Jafarkhani, and A.R. Calderbank, “Space-Time Block Codes from Orthogonal Design,” IEEE Transactions on Information Theory, vol. 45, pp. 1456-1467, July 1999.

[TSS05] A. Tarighat, M. Sadek, and A. Sayed, "A Multi User Beamforming Scheme for Downlink MIMO Channels Based on Maximizing Signal-to-Leakage Ratios," IEEE International Conference on Acoustics, Speech, and Signal Processing, IEEE, 2005.

[TV05] D. Tse and P. Viswanath, Fundamentals of Wireless Communication, Cambridge University Press, 2005.

[UNI10] University of North Carolina at Chapel Hill, "The Kalman Filter," www.cs.unc.edu/~welch/kalman/.

[UVR+08] C. Ubeda Castellanos, D. Villa, C. Rosa, K. Pedersen, F. Calabrese, P. Michaelsen, and J. Michel, "Performance of Uplink Fractional Power Control in UTRAN LTE," IEEE Vehicular Technology Conference, IEEE, 2008, pp. 2517-2521.

[VBS09] Vucic, N.; Boche, H.; Shuying Shi; "Robust Transceiver Optimization in Downlink Multiuser MIMO Systems," Signal Processing, IEEE Transactions on , vol.57, no.9, pp.3576-3587, Sept. 2009

[WG00] Z. Wang and G. Giannakis, “Wireless multicarrier communications,” Signal Processing Magazine, IEEE, vol. 17, no. 3, pp. 29–48, May 2000.

[WMZ05] T. Weber, M. Meurer, and W. Zirwas, "Improved Channel Estimation Exploiting Long Term channel properties," ICT, 2005.

[WIN2D112] IST-4-027756 WINNER II, Deliverable D1.1.2, “WINNER II channel models: Part I channel models,” September 2007.

[WIND24] D2.4: Assessment of adaptive transmission technologies. (Ed. S. Falahati) IST-2003-507581 WINNER, February 2005.

[WMM+05] T. Weber, I. Maniatis, M. Meurer, and W. Zirwas, "Performance Investigation of Improved Channel Estimation Exploiting Long Term Channel Properties," Conference on Multi-Carrier Spread Spectrum Technologies, 2005.

[WWK+09] X. Wei, T. Weber, A. Kuhne, and A. Klein, “Joint transmission with imperfect partial channel state information,” Proc. IEEE Vehicular Technology Conference-spring, 2009.

[WWRF08] W. W. R. Forum, Ed., Technologies for the Wireless Future. John Wiley& Sons, Ltd, 2008, vol. 3.

[ZD04] H. Zhang and H. Dai, “Cochannel interference mitigation and cooperative processing in downlink multicell multiuser MIMO networks,” EURASIP Journal on Wireless Communications and Networking, vol. 2, pp. 222-235, 2004.

[ZG10a] R. Zakhour, D. Gesbert, “Team decision for the cooperative MIMO channel with imperfect CSIT sharing”, Invited Paper, The Information Theory and Applications (ITA) Workshop, San Diego CA., February 2010.

[ZG10b] R. Zakhour, D. Gesbert, “On the value of data sharing in constrained-backhaul network MIMO”, In proc. of the International Zurich Seminar on Communications, Zurich, March 2010.

[ZL06] Danhua Zhang; Jianhua Lu, "Joint Transceiver Design Using Linear Processing for Downlink Multiuser MIMO Systems," Communications, 2006. APCC '06. Asia-Pacific Conference on, vol., no., pp.1-5, Aug. 2006

[ZMS+09] W. Zirwas, W. Mennerich, M. Schubert, L. Thiele, V. Jungnickel, and E. Schulz, "Cooperative transmission schemes," Long Term Evolution: 3GPP LTE radio and cellular technology, B. Furht and S.A. Ahson, Auerbach Publications, 2009, pp. 213-263.

List of acronyms and abbreviations

3GPP	3rd Generation Partnership Project
AE	Antenna Element
AMC	Adaptive Modulation and Coding
AR	Auto Regressive
ARQ	Automatic Repeat request
ARTIST4G	Advanced Radio Interface Technologies for 4G SysTems
BER	Bit Error Rate
BLAST	Bell Labs Layered Space-Time
BS	Base Station
BVDM	Building Vector Data Map
CCN	Central Coordination Node
CDF	Cumulative Distribution Function
CE	Channel Estimation
CIR	Channel Impulse Response
CJP	Centralized Joint Processing
CoMP	Coordinated Multi Point
CP	Cyclic Prefix
CQ	Channel Quality
CQI	Channel Quality Indicator
CRS	Common Reference Signal
CS/CB	Coordinated Scheduling / Coordinated Beamforming
CSI	Channel State Information
CSIR	Channel State Information at the Receiver
CSIT	Channel State Information at the Transmitter
CTF	Channel Transfer Function
CVX	Convex Optimization
D-BLAST	Diagonal-BLAST
DCW	Double Codeword
DD	Distributed Design
DDD	Dependent Distributed Design
DFT	Discrete Fourier Transform
DJP	Distributed Joint Processing
DL	DownLink
DoA	Direction of Arrival
DPC	Dirty Paper Coding
DT	Down Tilt
ECSI	Effective Channel State Information
ECSIT	Effective Channel State Information at the Transmitter
eNB	enhanced Node B
FB	Feedback
FDD	Frequency Division Duplex

FEC	Forward Error Correction
FER	Frame Error Rate
GPS	Global Positioning System
HARQ	Hybrid Automatic Repeat Request
HeNB	Home eNB
HPA	High Power Amplifier
HPBW	Half Power Beam Width
IDD	Independent Distributed Design
IDFT	Inverse Discrete Fourier Transform
ISD	Inter-Site Distance
JD	Joint Design
JP	Joint Processing
KPI	Key Performance Indicator
L1	Layer 1
L2	Layer 2
LOS	Line of Sight
LTE	Long Term Evolution
LTE-A	LTE Advanced
MC	Multi Carrier
MCS	Modulation and Coding Scheme
MIESM	Mutual Information Effective SINR Mapping
MIMO	Multiple-Input Multiple-Output
MMSE	Minimum Mean Square Error
MPC	Multipath Components
MRC	Maximum Ratio Combining
MS	Mobile Station
MSE	Mean Square Error
MU	Multi User
MU-BF	Multi-User Beamforming
MU-MIMO	Multi User Multiple-Input Multiple-Output
MU-MISO	Multi User Multiple-Input Single-Output
MWF	Modified Waterfilling
NCIC	Number of Coordinated Interfering Cells
NMSE	Normalized complex channel Mean Square prediction Error
OCI	Other-Cell Interference
OFDM	Orthogonal Frequency Division Multiplexing
OFDMA	Orthogonal Frequency Division Multiple Access
PAPR	Peak to Average Power Ratio
PDP	Power Delay Profile
PJP	Partial Joint Processing
PMI	Precoding Matrix Index
PRB	Physical Resource Block
QAM	Quadrature Amplitude Modulation
QPSK	Quadrature Phase Shift Keying
RAN	Radio Access Network

RI	Rank Indicator
RMMSE	Robust MMSE
RS	Reference Signal
RS SINR	Signal to Interference Ratio of Reference Signal
RSRP	Reference Symbol Received Power
RSRQ	Reference Signal Received Quality
RTxWF	Robust TxWF
SC	Single Carrier
SC FDMA	Single Carrier Frequency Division Multiple Access
SC SFBC	Single Carrier Space-Frequency Block Code
SCM	Spatial Channel Model
SCME	Spatial Channel Model Extended
SCW	Single Codeword
SDMA	Space Division Multiple Access
SFBC	Space-Frequency Block Code
SFR	Soft Frequency Reuse
SI	Study Item
SINR	Signal to Interference and Noise Ratio
SISO	Single-Input Single-Output
SLNR	Signal to Leakage plus Noise Ratio
SLR	Signal to Leakage Ratio
SM	Spatial Multiplexing
SMSE	Sum Mean Square Error
SOCP	Second Order Cone Program
SS	Synchronization Signal
STBC	Space-Time Block Code
STTD	Space Time Transmit Diversity
SU	Single User
SU-MIMO	Single User Multiple-Input Multiple-Output
SVD	Singular Value Decomposition
TDD	Time Division Duplex
TxD	Transmit Diversity
TxWF	Transmit Wiener Filter
UE	User Equipment
UL	UpLink
UMTS	Universal Mobile Telecommunications System
UP	Uniform Power
V-BLAST	Vertical-BLAST
WF	Waterfilling
WLAN	Wireless Local Area Network
WP1	Work Package 1
WSR	Weighted Sum Rate
ZF	Zero Forcing